Performance Improvements for Kinesthetic Haptic Devices through Series Actuation Approaches

by

Megh Vipul Doshi

A dissertation submitted in partial fulfillment of
the requirements for the degree of

Doctor of Philosophy

(Mechanical Engineering)

at the

UNIVERSITY OF WISCONSIN–MADISON

2025

Date of final oral examination: 05/19/2025

The dissertation is approved by the following members of the Final Oral Committee:

Michael Zinn, Professor, Mechanical Engineering
Peter Adamczyk, Associate Professor, Mechanical Engineering
Lei Zhou, Assistant Professor, Mechanical Engineering
Wei Wang, Assistant Professor, Mechanical Engineering
Giri Venkataramanan, Professor, Electrical And Computer Engineering

To my parents, Vipul and Raksha and my sister Riddhi

ACKNOWLEDGMENTS

I would like to first acknowledge my parents Vipul and Raksha Doshi along with my grandparents Jayantilal and Dhanlakshmi Doshi who intentionally or unintentionally fostered me to be inquisitive and helped grow my interest in science and engineering throughout my youth. You gave me the space to try things out without much fear of failure. I want to thank my sister Dr. Riddhi Doshi, who saved me from perhaps being a medical(real) doctor and paved the way for me to make my own decisions. Also to Riddhi and her husband Dr. Jai Juvekar for supporting me in my hard times through life and through graduate school because of all their love and support. I would like to thank my 'parents in Madison', my uncle and aunt Chirag and Sarika Gandhi, they made me feel like I always had a home in Madison to go back to. I would also like to thank my Aunt Geeta Parikh and my cousin Kunal Parikh, thanks to whom I did not have to worry as much about my family back home while I was engrossed in research.

I want to thank my various mentors through my life starting with high school, particularly Mr. Joaquim Augustine, my high school English teacher who enouraged me to realize my full potential, think outside the box and helped me through some tough times emotionally. I also want to thank Mr. Jim Matthew Kochitty, although my interactions with him were brief, but he was the first person to successfully make me really understand the beauty of physics and kinematics in high school, and perhaps the reason I followed through with a PhD in robotics.

I have had several key mentors and experiences in my time as an undergraduate. I would like to thank Mr. Ketan Shah for letting me use his lab to conduct my research during my yearly trips back home to India and also being an inspiration in doing things right through the years. I would like to thank a few professors at my undergraduate university who

helped me wet my feet in the waters of research - Dr. Sunil Karamchandani who gave me the opportunity to author my first research paper and work on a variety of different projects, Dr. Amit Deshmukh - for being a great encouragement for any and all projects I did, however random, and Mr. Tushar Sawant and Dr. Aarti Ambekar for their support through my time in undergrad. I would also like to thank my seniors in my college BAJA team, Omkar Parkar for being a proponent of pushing the envelope in the innovations we tried to bring and Ashish Rai for taking on an electrical engineer onto a team full of mechanical engineers and giving me the support to grow.

I came to Madison, hoping to do a PhD in Computer Architecture, but ended up with one in Robotics. I would like to thank some friends who made my early life in graduate school and the COVID-19 Pandemic tolerable - Sid Raghavan, Ananya J. and Munjaal Bhatt(remote). On joining the REACH Lab, the guidance and mentorship of both Mike Hagenow early on in my PhD and Patrick Dills throughout my PhD was invaluable, I would not be where I am without your influence. I would also like to thank Bolun Zhang for always being available to talk to and being a supportive voice through my PhD.

The mentorship, friendship and guidance of my advisor Mike Zinn cannot be understated. As said by many before me in the REACH Lab "you get a PhD in Robotics and in life". I never thought I would be sad or emotional when I finish my PhD, but Mike has been the best advisor I could have asked for, I will truly miss working with him. He took me into his lab after I showed up at his office with almost no knowledge of robotics and mentored me into the engineer I am today. He showed me both through his actions and words how to build an inspiring engineering career, how to be a mentor, and how to be a well-rounded person in life. Although I have always been drawn to science and engineering, I doubt I would have continued down the path to a PhD without his support and

encouragement.

Other mentors of note include Peter Adamczyk who has always been available to give advice on research and life as well, Lei Zhou who helped me with my job search, Michael Wehner, who was a great collaborator during his time here, and Bilge Mutlu, who gave me an opportunity on the NASA ULI project, I would not have nearly gotten as much exposure as I did without it. Additionally, I appreciate the time of Wei Wang and Giri Venkataramanan who round out my committee. I have had many teachers and professors over my grad school career, but the notable ones include Erick Oberstar, Eric Hoffman, Dan Negrut, Sonny Nimtsyoungskul, and of course Mike Zinn. Thank you.

Lastly, but not the least by any measure, I would like to thank my friends, both long distance and in person, in no specific order of importance - Yash Wani, for always being available to talk about any problem and help me solve it - technical or otherwise - no matter what, Stutee Oza, Suyash Ail, Suhrid Subramaniam for always being cheerleaders and an emotional support from afar, Pooja Jha, Maitri Fafadia, Niti Doshi and Sachin Patel for checking in on me and making sure I am alive, Sahil Kamath for his solidarity in sufferring and his jokes through the years, Dipul Chawla for making me feel at home in the Mechanical Engineering department, Asmit Nayak - for being the most a great roommate and friend through the years, Jeneel Kachhadiya for always being there in times of need. I also want to thank Arturo Gamboa Gonzales and Jack Stonecipher for their company during the last years of my PhD.

CONTENTS

LIST OF TABLES

LIST OF FIGURES

ABSTRACT

Kinesthetic haptic devices face persistent challenges in simultaneously achieving high stiffness rendering, low apparent inertia, and large operational workspaces—limitations that stem from fundamental tradeoffs in actuation technology. This dissertation investigates novel series actuation approaches to overcome these constraints. We explore a frequency-partitioned series admittance actuation strategy that combines high - bandwidth, low-amplitude actuators with low-bandwidth, large- amplitude actuators, demonstrating a 50% reduction in minimum stable rendered inertia and significantly increased rendering bandwidth. We also develop a series actuation framework for workspace expansion of impedance-based haptic devices that maintains rendering quality across extended operational volumes, addressing the workspace limitations of high-fidelity force feedback systems. Additionally, we present a handheld kinesthetic haptic device with coupled bidirectional input, demonstrating comparable performance to grounded interfaces in trajectory tracking tasks. Through systematic experimental evaluation, analytical modeling, and user studies, we establish performance boundaries and practical implementation considerations for these approaches. The insights gained from this research extend beyond haptic interfaces to robotics and physical human-machine interaction systems where high-quality force exchange is critical. This work provides both practical implementations and theoretical frameworks that expand the performance capabilities of kinesthetic haptic devices without requiring complex mechanical designs or control strategies.

1 INTRODUCTION

Haptic technology has developed from a specialized research area into a key component in human-computer interaction (HCI) and human-robot interaction (HRI) systems. Haptic interfaces function as bidirectional connections between humans and digital or remote environments, converting touch into computational input and output. These devices enable users to interact with virtual objects, control remote systems, and receive force feedback, changing how we interact across fields including medical simulation, teleoperation, virtual/augmented reality, and robotics. A central challenge in haptic interaction is accurately reproducing physical properties—such as stiffness, texture, weight, and inertia—while maintaining system stability and transparency. This challenge is especially significant in kinesthetic haptic devices, which provide force feedback rather than just surface sensations. Despite advances over the past three decades, limitations in actuation technology still restrict the performance of kinesthetic haptic interfaces, particularly in achieving high transparency, high stiffness rendering, and large workspaces simultaneously. The field of haptics combines mechanical design, control theory, and perceptual psychology. An effective haptic device must generate appropriate forces with minimal latency, high precision, and across frequency ranges matching human perception. These devices must also operate safely in direct contact with users, creating additional constraints on their design and control systems. Kinesthetic haptic devices typically fall into two main categories: impedance-controlled and admittance-controlled systems. Impedance-controlled devices measure position and render force, providing low apparent inertia and smooth "free-space" motion but struggle with high stiffness values without stability issues. Admittance-controlled devices measure force and render position, naturally providing high stiffness but facing challenges in achieving low inertia and transparent operation. This

fundamental divide has resisted conventional solutions. A key limitation is the lack of ideal actuator technology. The ideal haptic actuator would offer high force/torque capability, high bandwidth, minimal inertia, zero backlash, inherent backdrivability, compact size, and safety. Conventional motors, hydraulic systems, and pneumatic actuators each have certain advantages but fail to meet all requirements. This has prompted research into hybrid approaches, composite actuation strategies, and new mechanical configurations to overcome individual actuator limitations.

1.1 Thesis Overview

The remainder of this dissertation is organized as follows: Chapter 2 provides background information and a review of related work, placing the research within the broader field. This chapter discusses various feedback methods for haptic devices and explores existing actuation approaches for kinesthetic interfaces. Chapter 3 presents the design, implementation, and evaluation of a handheld kinesthetic haptic device with coupled bidirectional input. This chapter includes a detailed system performance evaluation and reports findings from a user study comparing the device to a traditional rotary input interface. Chapter 4 introduces the series admittance actuation approach for improving kinesthetic haptic renderings. This chapter describes the frequency-partitioned control strategy, presents experimental results demonstrating performance improvements, and analyzes the limitations of the approach with respect to position saturation. Chapter 5 explores a series actuation approach for workspace expansion of impedance-based haptic devices. This chapter presents the actuation configuration, control methodologies, and performance evaluation results, with particular attention to stability, transparency, and practical implementation considerations. Chapter 6 summarizes the key contributions of the research and discusses directions for future work, including potential

applications in telepresence systems, virtual reality interfaces, and physical human-robot interaction. Appendix A presents additional work on layer jammers in a Simulated Environment Soft Haptic (S.E.S.H.) Glove, demonstrating an alternative approach to haptic feedback through controllable stiffness in a wearable form factor. Appendix B presents additional work on the effects of synchronous movement on human trust in robots, exploring the social and psycho physical aspects of robotics.

Throughout this dissertation, we demonstrate that series actuation approaches can significantly enhance the performance of kinesthetic haptic devices, addressing challenges in force rendering capability, transparency, and workspace limitations. The insights from this research have implications not only for haptic interface design but also for the broader field of physical human-machine interaction, where high-quality force exchange between users and mechanical systems is increasingly important.

2 BACKGROUND AND RELATED WORK

Our work is split into two different sections. The first section focuses on a novel input method for kinesthetic haptic devices whereas the second section focuses on actuation methods that drive kinesthetic haptic devices. We present some background on haptics in general, followed by a review of significant related work, including other novel input methods, as well as the focus of our current and future work, which is on actuation methods for haptic devices.

2.1 Background

Kinesthetic haptic devices are haptic devices that provide force feedback to the user in order to convey haptic information. There are two types of kinesthetic haptic devices, namely impedance-based and admittance-based haptic devices.

Impedance-based kinesthetic haptic devices are arguably the more popular kind of haptic device among kinesthetic haptic devices. The term "impedance" in this context refers to the mechanical resistance encountered by a user when interacting with the device, which can be modulated to simulate different forces, thereby enhancing the sense of realism in the interaction. They take user motion as input, compute the force they need to generate according to the haptic effect being displayed, and then output that force which the user feels as shown below in Figure 2.1. These types of devices are usually back-driveable, and are good at rendering free space and low impedances, but they struggle with rendering high impedances.

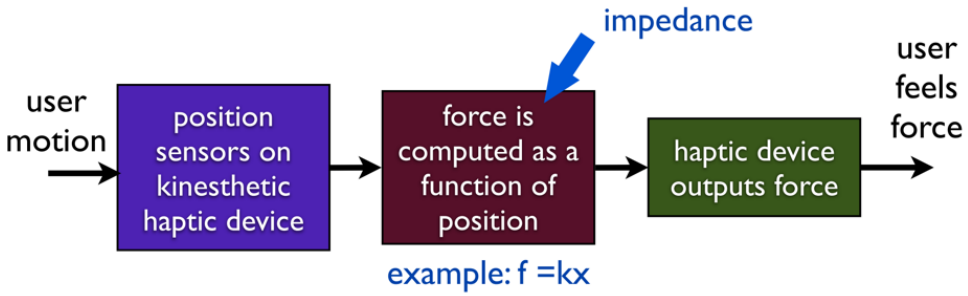

Figure 2.1: Block Diagram of an impedance-based haptic device(Image from Allison Okamura's Introduction to Haptics class)

Admittance-based kinesthetic haptic devices are a type of haptic technology engineered to interact with users by responding to the forces applied by the user. Unlike impedance-based haptic devices, which are driven by the motion input of the operator, admittance-based devices are driven by the force input from the operator. They take user force or torque as an input, compute the position that the device should move by, and then output this position which the user feels as shown in Firgure 2.2. This type of device is usually not backdrivable, is good at rendering high impedances but struggles with rendering low impedances and free space.

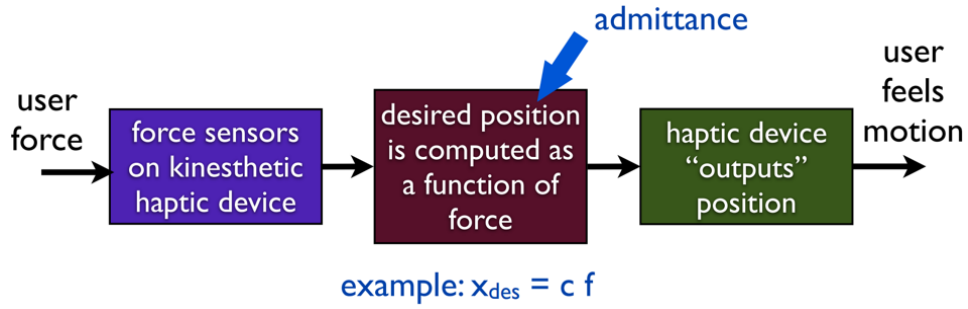

Figure 2.2: Block Diagram of an impedance-based haptic device(Image from Allison Okamura's Introduction to Haptics class)

2.2 Different feedback methods for haptic devices

In recent years, the domain of handheld haptic devices has witnessed significant advancements aimed at enhancing user interaction and feedback. Handheld devices like the ones by [1] and [2], make advances with form factors and actuation methods, but are more conventional in their way to provide force feedback to the user. Other devices like the *HAPmini*, designed to enrich the user's touch interaction through a simplistic structure with minimal mechanical complexity and actuators, while still delivering force and tactile feedback [3].

Furthermore, research on finger-worn wireless haptic devices like *Haplets* has demonstrated the value of providing rich haptic feedback to the fingertips during manipulation, with applications in texture, stiffness perception, and normal and shear force perception [4]. Additionally, a portable haptic guide device with omnidirectional driving gear has been proposed to signal route guidance commands to the end-user by delivering a sense of force to the thumb [5].

In the realm of bilateral haptic interaction, a novel device has been devised to render accurate force to a human operator for creating a virtual environment from a remote real environment. This device employs parallel mechanisms to facilitate force interaction in multiple degrees of freedom, addressing challenges in actuator and controller design due to non-constant Jacobian matrices [6].

A unique contribution to the field is the development of shape-changing haptic devices by [7]. The *Animotus* is a wirelessly-connected, 3D printed cube that acts as a haptic compass, altering its shape to guide the user in the right direction [7]. Another significant invention is the *S-BAN*, a new handheld haptic interface utilizing a parallel kinematic structure to deliver 2-DOF spatial information over a continuous workspace [8]. They further

explored the perception of shape-changing haptic interfaces, providing valuable insights through their work.

These are some of the conventional and unconventional novel methods of providing haptic feedback and taking input from the user. Most of these haptic devices are tailored to certain use cases and we have yet to invent a general purpose haptic device with the potential to become ubiquitous. In part of our work we design and inform a novel input method for a kinesthetic haptic interface and as such it is important to know relevant work in the field.

2.3 Actuation methods for Kinesthetic Haptic Devices

Haptic devices need actuators that can provide both high impedances and low impedances stably while providing high bandwidth as well. This would allow haptic devices to render a large range of impedances over a wide frequency range which would lead to more accurate haptic renderings. Impedance-controlled haptic devices are good at rendering low impedances but struggle to render high impedances. Admittance-controlled haptic devices are very good at presenting large impedances, but they are not very commonly used as compared to impedance-controlled haptic devices as they have a unique set of problems associated with them.

Admittance-controlled devices struggle with rendering low impedances because their actuators are inherently not backdrivable and thus, need a very high position control bandwidth to present low impedances in a stable manner. This is not possible as actuators have limited power, therefore actuators with high force or torque capabilities would not have a very high position control bandwidth and vice versa.

Attempts have been made toward actuator configurations that overcome these problems for both admittance controlled approaches like the

series elastic actuator[9], hybrid actuators[2, 10] or even the newer co actuation approaches [11] to name a few. However, it remains one of the open fundamental challenges in haptics to have an actuator that can have both high force or torque capabilities and a high position control bandwidth . These existing approaches have their own set of challenges that being complex mechanical design to integrate non-linear components and complicated control methods to deal with them.

Series elastic actuators use a compliant element between the operator and the actuator which allows for closed-loop force control by measuring the deflection of this compliant element. It is popular for wearable exoskeletons[12, 13] and robots[14]. Although they can produce large forces they fail to present high stiffnesses due to their compliant elements.

Hybrid actuators which introduced as a viable option which can render high stiffnesses and large forces for large force feedback systems as well as portable haptic devices[11] . These kind of actuation schemes often need complex control schemes or need complicated models of passive components to compensate for them. This makes them less accessible to use.

The newer co-actuation approach [11] is a type of admittance-based actuation approach that uses a clearance module with a non-collocated encoder which helps with free space rendering. The actuator tracks the position of the non collocated encoder while rendering free space and switches to an admittance based controller when rendering a stiffness. This approach does well with rendering free space and high stiffnesses. However, it would struggle with rendering low impedances due to the inherent problems with admittance controllers which this approach does not address.

In spite of prior efforts, there still exists a gap in finding the ideal actuator for haptic devices. Most of the research focus in the field of actuation has been on impedance-based haptic devices. The few efforts

to improve admittance-based actuation have yet to enable haptic devices that can achieve both high impedances as well as low impedances well.

For impedance-controlled haptic devices, most actuation methods do not address the gap of workspace limitations. There is some work done to try to address this gap, first by Harwin in his work[15] continued in [16], but they fail to provide a comprehensive analysis into their approach. Zinn came up with a distributed macro mini approach to address this issue for large workspace impedance based haptic devices [17], however, this approach greatly increases the mechanical design complexity of the haptic devices. Other attempts have been made to make large workspace haptic devices, but they attempt to make wearables which often have bulky setups and are compromise on performance[18] [19]. Literature in this area is limited, especially for compact, grounded interfaces using serial actuation configurations, and that is the gap we wish to address with chapter 5.

3 HANDHELD KINESTHETIC HAPTIC DEVICE WITH COUPLED BIDIRECTIONAL INPUT

3.1 Overview

This chapter describes work done on a handheld kinesthetic haptic device with a bidirectional coupled input as part of a NASA ULI project. To give a big picture perspective in short, our goal was to explore a new type of input method for shared control of a robotic arm and this chapter describes our work as such.

3.2 Introduction

Kinesthetic haptic devices offer a variety of ways to interact with users, from rendering virtual environments to providing guidance and feedback during teleoperation of robots. Traditionally, high-performance haptic devices have been grounded (e.g., the devices from Force Dimension [20] or Haption [21]), meaning that they are fixed in a location and generate haptic sensations by reacting against the environment. More recently, a variety of handheld haptic devices have been proposed that provide similar kinesthetic renderings by reacting against the user's hand or arm [1]. For example, Dills et al. [2] propose a high-performance one degree-of-freedom device employing hybrid actuation. Many of the other recent handheld devices provide haptic feedback to each finger individually either through finger-mounted devices [22, 23] or gloves [24, 25]. Notably, many of the recent handheld devices are designed for rendering virtual environments in gaming or virtual-reality applications. Alternatively, we are interested in one degree-of-freedom industrial applications and propose a new handheld haptic input device that is actuated using one hand through two mechanically-coupled triggers.

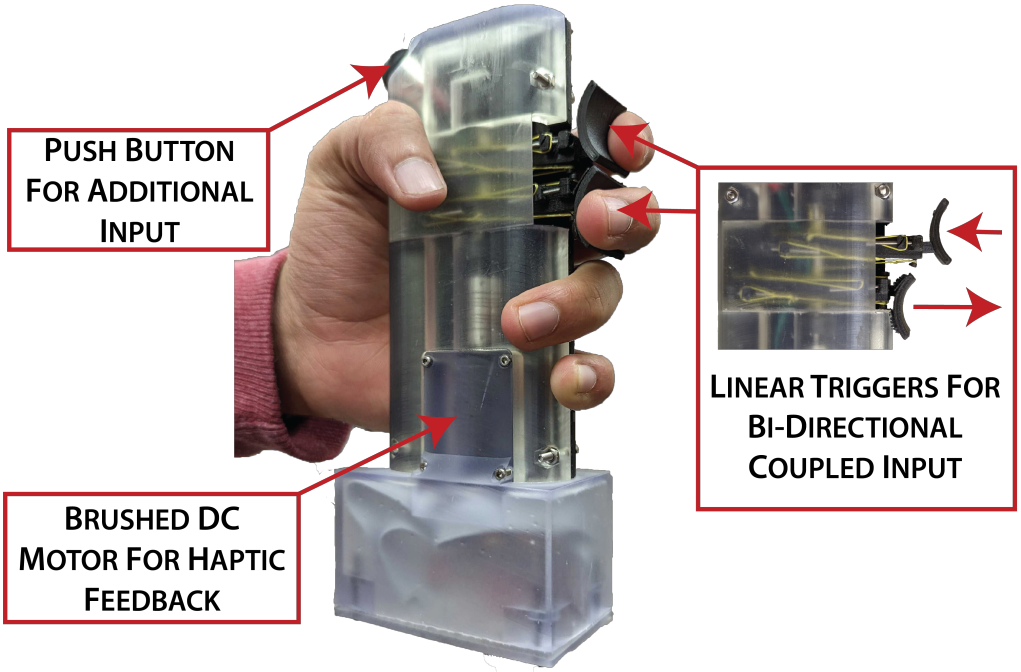

Figure 3.1: Our proposed handheld haptic device with two triggers that take input via finger flexion. The triggers are mechanically coupled (i.e., when one trigger is pushed in, the other pushes out).

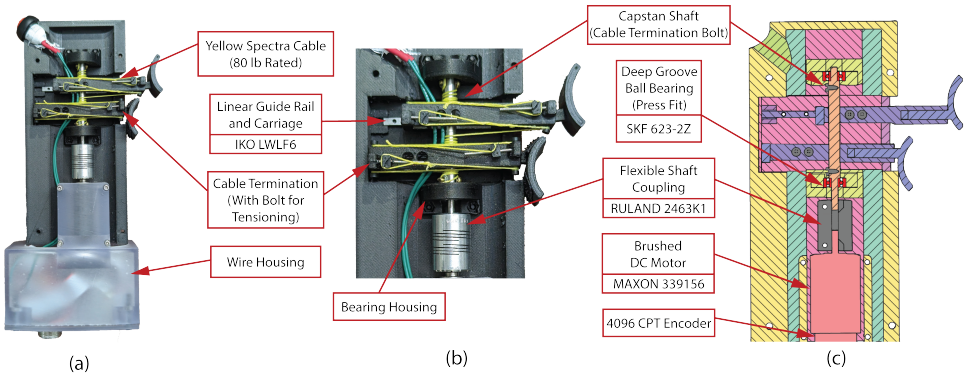

Figure 3.2: Internal (a) view, zoomed internal view (b), and cross-sectional view (c) of the device showcasing the drive-train and related design elements.

There are a variety of industrial applications that could benefit from a one degree-of-freedom haptic input device. For example, an operator could precisely control a single variable during an industrial process (e.g., flow rates, temperatures, feed rates, pressure during sanding) and the device could provide haptic cues or guidance as necessary (e.g., vibration, modulation of stiffness). In many applications, it would also be desirable for the input to be differential, meaning an operator may want to adjust a particular process variable from the current set point (e.g., go *faster* or *slower*). Finally, many industrial applications would benefit from a device that is one-handed, which frees the operators' other hand for secondary tasks (e.g., controlling a second input or feeling a surface during sanding). To address these desired qualities, we propose a one degree-of-freedom bidirectional input where the differential input is provided through two-mechanically coupled triggers, as shown in Figure 3.1. We were inspired by existing applications leveraging finger flexion, such as musical instruments (e.g., a trumpet), that allow for input in the natural direction of the finger. Specifically, we chose to investigate a mechanism leveraging adjacent finger flexion to utilize the innate structure of the human fingers, that is

more adept at pulling than pushing [26]. Additionally, the mechanically-coupled triggers allows for simple bidirectional inputs where the triggers correspond to opposite directions.

In this chapter, we propose a high-performance one degree-of-freedom (DOF) haptic device that is mobile and can be actuated using a single hand through two fingers. We first discuss our design requirements for realizing a usable and high-performance haptic device followed by describing our developed prototype. Through an experimental evaluation, we demonstrate that the prototype has many desirable characteristics for generating high-quality haptics, such as a high transparency and a high bandwidth. Finally, we investigate the performance of our prototype in terms of giving precise input via a user study comparing the device to a haptic knob, a form factor that is already widely used in industrial settings.

3.3 System Performance Evaluation

To evaluate the performance of our device, we conducted a series of experiments to evaluate (1) the rendering force and stiffness, (2) the friction (i.e. transparency), and (3) the rendering bandwidth of our prototype device. The experiments and their results are described in the following sections.

Maximum Rendering Force and Stiffness

To assess the device performance, we experimentally evaluated the maximum uncoupled stable rendering stiffness [27], [28]. We perform an experiment wherein we incrementally increase the stiffness rendered by the device in discrete steps and check for stability at each step. Stability is assessed by physically perturbing the finger triggers of the device through user touch and observing whether the system stabilizes. We can qualitatively asses stability by looking at the vibrations in the system i.e. if

the vibrations are increasing in amplitude, the system is deemed unstable. To reduce the bias of any single user interaction, we performed the testing with several cohorts. The average maximum stable rendering commanded stiffness was 1.06 N/mm while the maximum stable rendering commanded force was 15.9 N.

Friction tests to assess transparency

To evaluate the transparency [29], we performed an experiment to measure the friction of the drive train. Specifically, we applied a slowly increasing motor torque and identified the torque level at which the motor and drive-train initiated movement. This experiment was repeated at various motor positions to account for friction variation as a function of device configuration. The commanded motor torques varied from 0.177 to 1.029 mNm, with an average torque of 0.665 mNm. The equivalent (reflected) friction force at the finger interface, taking into account the drive-train reduction, varied from 0.05 to 0.343 N with an average frictional loss of 0.22 N. For comparison, other handheld haptic devices like the CLAW [1] and [30] report frictional losses (or a minimum transparency) of 0.5 N and 0.54 N respectively.

Rendering Bandwidth

The frequency range over which a haptic device can accurately display forces, with minimal magnitude and phase distortion, is referred to as the rendering bandwidth. A large rendering bandwidth is important for realistic user perception [31]. To achieve a large rendering bandwidth, it is important to design a stiff drive-train such that there are no structural vibration modes present within the desired bandwidth, typically up to 100 Hz for a high performance interface.

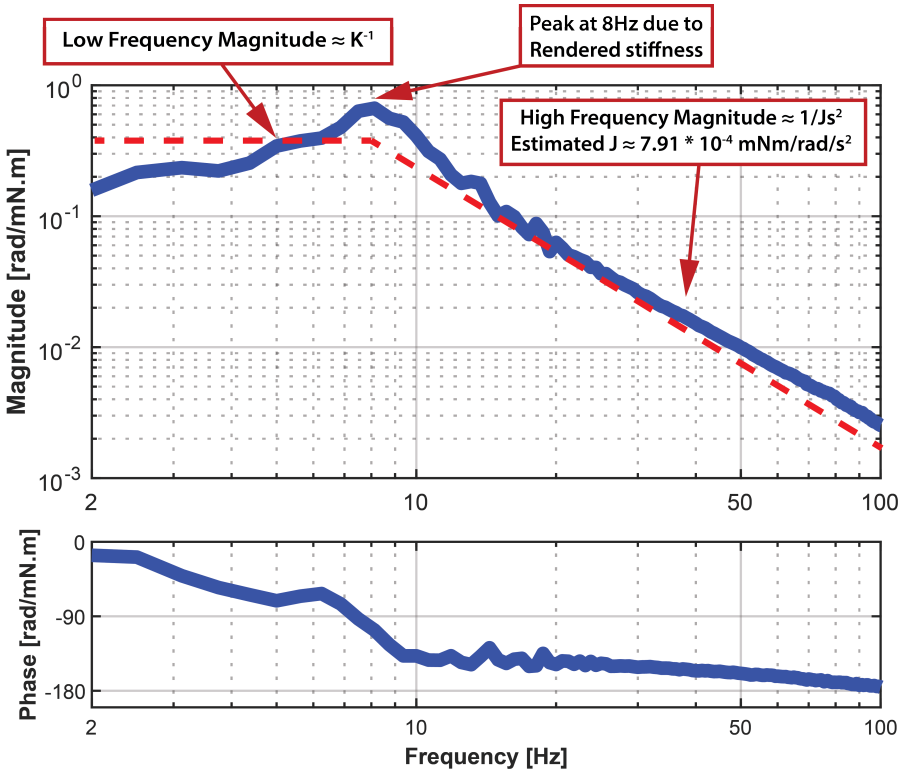

Figure 3.3: Frequency response of the proposed device. The only peak in the magnitude plot occurs due to the rendered stiffness.

To evaluate the rendering bandwidth, we measured the frequency response of the device drive-train. The frequency response was obtained by measuring the motor position output using the 4096 CPT encoder in response to an applied torque chirp signal. A virtual stiffness was overlaid on the torque chirp to maintain centering of the device. To provide a broad-spectrum evaluation, we performed an experiment to measure the frequency response across both low frequency and high frequencies. In the experiment, the disturbance chirp signal was varied from 0.1 - 100 Hz over a 30 second interval. The test was repeated 10 times. The results are shown in Figure 3.3.

As seen in Figure 3.3, the low frequency magnitude response is approximately flat up to 4 Hz, after which it increases as it approaches the resonance created by the introduction of the virtual centering spring. The flat portion of the curve is, as expected, approximately equal to the inverse of the rendered stiffness (0.5 rad/mNm). The high frequency magnitude response shows a peak at approximately 8 Hz, which corresponds to the induced resonance the results from the introduction of the virtual centering stiffness. Importantly, there is no evidence of drive-train flexible modes below 100 Hz. We can estimate the reflected inertia of the device from the high frequency magnitude of the frequency response which is approximately equal to 7.91×10^{-4} mNm/rad/s^2. A low value of reflected inertia infers highly transparent device.

3.4 User Study

To assess the efficacy of the proposed device, we conducted a user study. Specifically, our study aimed to assess the accuracy and perceived usability of the proposed device across a range of common one degree-of-freedom tasks.

Study Design

Our study compared our device (referred to as the *handheld* condition going forward) to a grounded rotary input (i.e., knob, see Figure 3.4) in a within-subjects design where the order of conditions (i.e., the device used for each task) was counterbalanced. We chose the knob as a baseline based on its prevalence in haptics (e.g., DC motors) and society (e.g., control panels, thermostats). Input devices like knobs are typically used to give more precise inputs as suggested by prior studies [32] and standards [33]. In this preliminary evaluation, we focused on using the inputs for two differential control applications: reaching target locations and tracking

trajectories. Accordingly, both input devices were programmed to render a static haptic stiffness around a center point, similar to a joystick.

Participants

Our study involved 11 participants (6 male, 5 female), aged 18–23 ($M = 19.27$, $SD = 1.60$) recruited from the university campus. All participants were right handed. None of the participants identified as having extensive experience with haptics. Participants were paid $15 an hour.

Procedure

After providing informed consent, participants were briefed on the structure of the experiment. The participants then completed a targeting task for each condition followed by a tracking task for each condition. The details of the tasks are presented in the next section. After completing each condition, participants filled out the NASA TLX [34] and the System Usability Scale (SUS) questionnaire [35]. The order of the conditions was counterbalanced across participants. For each task, the participants trained with the input device before collecting test data. Following the two tasks, participants completed a brief demographics survey and completed questions on qualitative data about the devices answering questions about their comfort levels with each device for both tasks. The study procedure lasted approximately one hour. The study was administered under a protocol approved by the university Institutional Review Board (IRB).

Apparatus

The knob condition used a Maxon motor (model no. 320165) with a rotary handle attached to the shaft. An encoder attached to the motor was used to measure the user's input. Both conditions were operated as differential inputs using a haptic overlay. For both the tasks, both input devices were

programmed to render a static stiffness of 7.5 mNm/rad for the knob and 7.4 mNm/mm for the handheld haptic device which centered the knob and the triggers of the device respectively. A stiffness value that was deemed comfortable for the task was chosen through testing by the authors. This stiffness is what provides the force feedback to the user through the motors in each device, the farther the user moves from the center point of each device, the greater the force. The knob was mapped to move the object on the screen left and right by rotating the knob in those directions. Whereas, the handheld device was mapped to move the object left and right by pushing each trigger in(the upper trigger to move right and lower to move left).

Tasks & Measurements

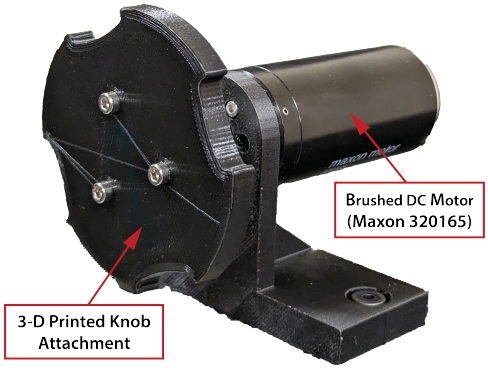

Figure 3.4: Knob used as the comparison input device in our study.

Targeting Task

We assessed the targeting performance of each condition through a Fitt's law experiment. In the targeting task, shown in Figure 3.5, participants used the input device to move a cursor to a designated goal location. The position and size of the goal varied between tests. Participants were in-

structed to reach the target as fast as possible. When possible, the design of the Fitt's law experiment followed the ISO standard proposed by Mckenzie [36]. In each trial, participants pressed a key to begin and the trial was stopped once the target was reached (defined as when the cursor was within the target for two seconds). For each condition, participants completed 30 training trials and 60 test trials. From each trial, we calculated the index of difficulty (ID) and used it to calculate the throughput (TP) of the input device.

$$\begin{aligned} ID &= \log_2(\frac{A}{W} + 1) \\ TP &= \frac{ID}{MT} \end{aligned} \tag{3.1}$$

where A is the amplitude of movement to the target, W is the width of the target, and MT is the time to reach the target. A higher throughput corresponds to better device performance for targeting tasks.

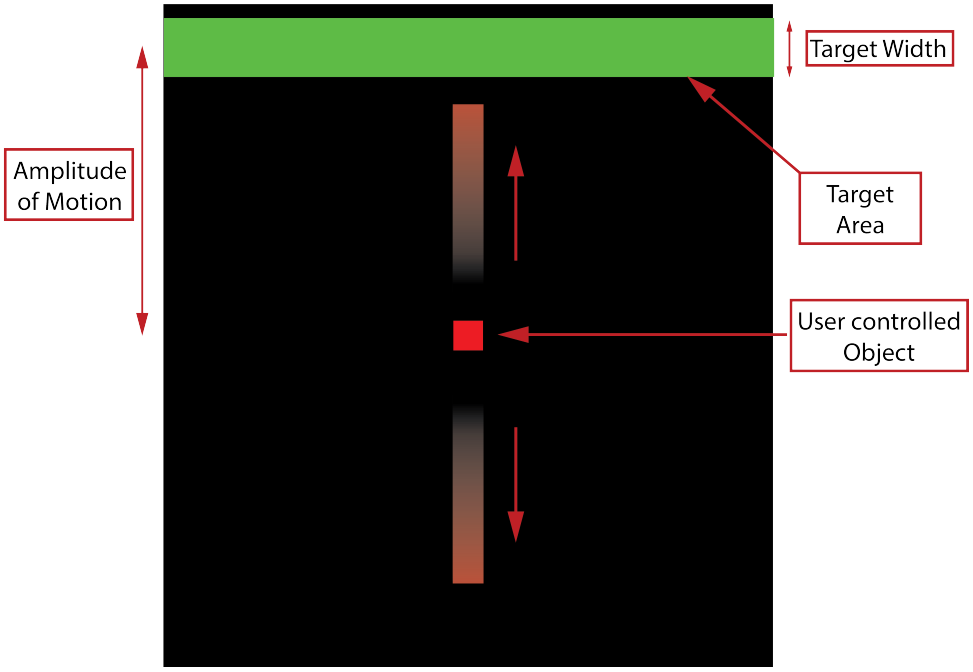

Figure 3.5: Targeting task following ISO 9421-9 to calculate throughput of device.

Tracking Task

We assessed the tracking performance for each condition through a series of sinusoid tracking tests. As shown in Figure 3.6, participants used the input device to follow the desired trajectory and we tracked the absolute value of error between the reference trajectory and participant cursor at each time-step. The frequency and amplitude of the trajectory were varied during the trials. Participants were instructed to follow the trajectory as closely as possible. To enable direct comparisons of performance across the conditions, we selected two different amplitudes and two different frequencies for the sinusoidal trajectory. The two frequencies, 0.3 Hz and 1 Hz (referred to as the *low frequency* and *high frequency*), were selected within the bandwidth of human control [37]. In the tracking task, each

participant performed 16 training trials (i.e., 4 trials of each combination of amplitude and frequency) before completing four test trials. The four trials were completed without any break (e.g., the second sinusoid started immediately upon the completion of the first sinusoid). The order of the effects were randomly generated and different between the training and testing trials. Each sinusoid consisted of 4 full periods of oscillation for the low frequency trajectories and 8 full periods of oscillations for the high frequency trajectories.

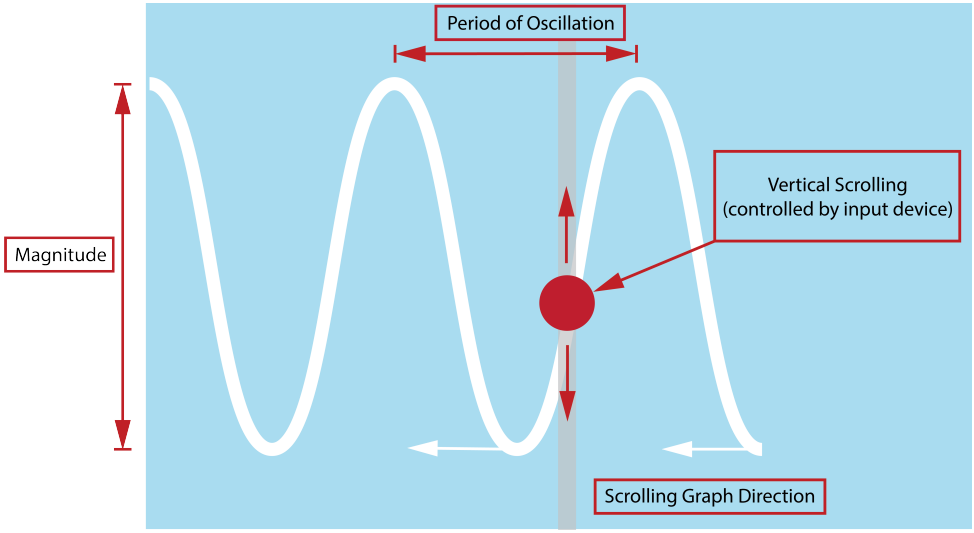

Figure 3.6: Task to assess device performance for tracking.

Results

The results for the targeting task were analyzed using a paired two-tailed t-test. We found a significant effect on throughput for the handheld device ($M = 1.65$, $SD = 0.70$) compared to the knob ($M = 2.05$, $SD = 0.60$, $t(10) = 11.48$, $p < 0.05$, $d = 0.59$) with the knob having a higher throughput.

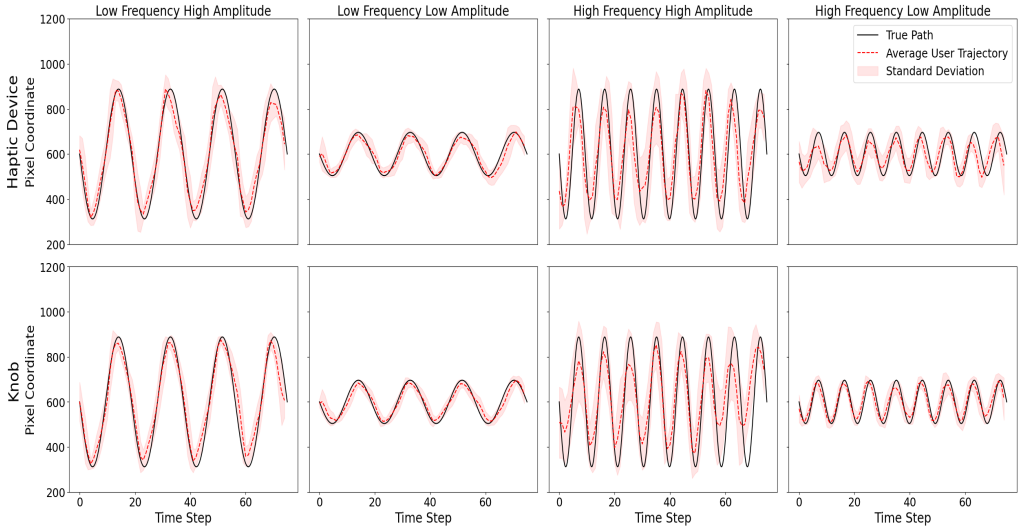

Figure 3.7: Average errors and standard deviations for trajectory tracking with the handheld haptic device and the knob.

The raw NASA TLX score for this task was 30.45 on average for the knob and 38.48 on average for the handheld haptic device. We perform a paired two-tailed T-test on the TLX scores and find that the haptic device($M = 38.48$, $SD = 16.36$) has significantly higher scores than those for the knob ($M = 30.45$, $SD = 16.36$, $t(10) = 2.28$, $p < 0.05$), .

The error results of the tracking task were analyzed using a three-way repeated measures ANOVA with device (haptic device, knob), frequency (high, low), and amplitude (high, low) as factors. The results are shown in Table 3.1. We find no significant effect of the device on the user error for this task. We do, however, find a significant effect of the amplitude ($F(1, 8) = 83.85$, $p < 0.001$) and the frequency ($F(1, 8) = 15.57$, $p < 0.001$) of the path on the user error. The average raw NASA TLX score for this task was 42.12 ($M = 42.12$, $SD = 17.42$.) for the knob and 42.42 ($M = 42.42$, $SD = 16.56$) for the handheld haptic device. We perform a paired two-tailed t-test on the TLX scores and find no significant difference ($t(10) =$

0.55, p = 0.58) between the scores of this task for both devices.

Table 3.1: Three-way ANOVA Results

Independent Variables	F Value	Num of DF	Den DF	PR>F
Device	0.798	1.0	8.0	0.398
Frequency	19.671	1.0	8.0	<**0.05**
Amplitude	62.447	1.0	8.0	<**0.001**
Device x Frequency	1.182	1.0	8.0	0.309
Device x Amplitude	0.011	1.0	8.0	0.920
Frequency x Amplitude	6.056	1.0	8.0	**0.039**
Device x Frequency x Amplitude	0.001	1.0	8.0	0.976

Since the results of the ANOVA do not show any significant relation to the device used, we do not perform any post hoc analysis on this data. The raw average error values per segment are as shown in the Table 3.2 below.

Table 3.2: Average Error Per Segment

Trajectory Segment	Device	Mean Error	Standard Deviation
Low Frequency Low Amplitude	Handheld Haptic Device	33.12	15.52
	Knob	29.19	10.76
Low Frequency High Amplitude	Handheld Haptic Device	81.10	25.26
	Knob	78.18	31.86
High Frequency Low Amplitude	Handheld Haptic Device	51.04	13.04
	Knob	38.17	14.85
High Frequency High Amplitude	Handheld Haptic Device	124.93	31.75
	Knob	113.57	55.67

The SUS score for our proposed handheld haptic device was 86.60 ($M = 86.60$, $SD = 3.88$) while that of the knob was 87.24 ($M = 87.24$, $SD = 2.57$). This falls in the excellent category in the SUS scale for both devices. We perform a two-tailed paired T-test on the SUS scores as well and find no statistically significant difference between the scores of the two devices ($t(10) : 0.90$, $p = 0.37$).

3.5 Discussion

There are several key takeaways from the user study. In the targeting task, we observed that our handheld haptic device did not perform as well as the knob in terms of throughput. Some participants appeared to struggle with the spatial mapping with the handheld haptic device (i.e., which trigger moves the cursor up or down on the screen) and would move the object in the wrong direction before correcting themselves. This effect was not observed when participants used the knob which was both more familiar to participants and grounded to the table in an orientation that was spatially consistent with the task. In the future, we are interested to explore whether the performance with the proposed device could be improved through additional training. The amount of training trials in our experiment was limited to prevent participant fatigue.

In the tracking task, the knob generally had lower average errors than our handheld haptic device for all frequencies and amplitudes. However, the average error varied by less than 13 pixels between the two devices. As seen in Figure 3.7, much of the difference in performance can be attributed to overshoot by the handheld haptic device, which was not observed when participants used the knob. Looking closely at the high-frequency high amplitude segment of the data in Figure 3.7, we can see that users commonly undershoot the desired motion when using the knob as compared to our haptic device. However, we see higher overshoots with the haptic device for high-frequency high amplitude trajectories as well. We can infer from these observations that the handheld haptic device may be more suited to tasks where reaching the peaks of the trajectory is more important than controlling the overshoot. The overshoot might also suggest that the haptic overlay was not optimal for the handheld haptic device. In the future, we are interested in exploring the impact of the overlay on user performance.

In terms of usability, both the proposed device and the knob scored in the excellent category for the SUS [35] and the difference between the

average usability scores for the devices was only 0.64 percent. Users who play video games frequently (at least once per week) expressed a high degree of satisfcation with the form factor of the handheld haptic device while users who had little or no experience with gaming found the device to be fatiguing.

3.6 Conclusion

In this chapter, we designed and evaluated a handheld haptic device that incorporates a bidirectional coupled finger flexion interface. Through experimental validation, we demonstrated that the proposed device can render high-performance haptic effects, as measured by its transparency and rendering bandwidth. Through a user study, we showed that participants rated the proposed device as highly usable and assessed the device with a series of targeting and tracking tasks. While the performance of the device was inferior to that of a haptic knob in some instances, the overall assessment was positive. The results suggest a range of modifications to be considered in future work including improvements to the ergonomic form factor, exploration of alternative haptic effects, and evaluation of these modifications on the overall device and user performance. Specifically, we are interested to test the device in simulated and realistic scenarios. Examples include industrial process control [38] and shared autonomy for collaborative robots [39].

4 A SERIES ADMITTANCE ACTUATION APPROACH TO IMPROVE KINESTHETIC HAPTIC RENDERINGS

4.1 Overview

This chapter describes a frequency partitioned admittance actuation approach which has the potential to expand the rendering capability of admittance based haptic devices by extending the admittance control's position control bandwidth. The actuation approach combines a high bandwidth, low amplitude actuator in series with a low bandwidth, large amplitude actuator. Summing the actuator velocities of these two leads to an actuator with both a large amplitude displacement and a high position control bandwidth. We describe the actuation and control approach and experimentally validate the approach with a one degree of freedom testbed. We experimentally demonstrate improvements in rendering through a measurable reduction in the minimum stable rendered inertia, the primary metric by which admittance-based systems are assessed, and an increase in the frequency range over which force rendering is accurate, known as the rendering bandwidth, as compared to a baseline admittance-based actuated system. Finally, we investigate the consequences of potential position saturation of the high frequency actuation during operation, on both rendering stability and rendering output impedance. The limitations section of this chapter has been contributed by a co-author of this work Patrick Dills.

4.2 Introduction

Admittance-based haptic devices, which typically employ high gear reductions to achieve high forces and high power, excel at rendering very high virtual impedances, such as high stiffness virtual walls, due to their

naturally high output impedance. Low impedance rendering, or transparency, is obtained through the use of closed-loop feedback, where interaction forces between the human user and device interface are measured and an admittance control law, in combination with a high-gain position feedback loop, drive the haptic interface to render the desired virtual admittance (i.e. high admittance for transparency). However, above the closed-loop bandwidth of the admittance-based system's position controller, the output impedance of the device cannot be modified, and transparency (or high admittance) is not achievable. To improve haptic rendering performance, it has been shown that increasing the bandwidth of the admittance-based system's position controller can increase transparency. In particular, this can increase the range of stable canonical impedances by allowing for lower values of virtual mass, stiffness, and damping than is achievable with lower bandwidths [40, 41]. While attempts have been made to develop actuation methods that can render both very high and very low impedances [2, 10, 11, 42, 43], none have achieved the high dynamic stiffness characteristics of admittance-based systems along with the low-impedance transparency required for high-performance haptic applications. In this work, we present a new approach that seeks to extend the rendering range of admittance-based haptic interfaces through a series combination of admittance-type actuators that extends the actuator's bandwidth capabilities while maintaining its high force and large range of motion capabilities. As shown in Fig. 4.1, our proposed frequency partitioned series admittance actuation approach attempts to increase the position control bandwidth of the actuator by splitting the low frequency and high frequency position error between two different actuators. Our proposed approach is introduced in Section 4.3 and is experimentally validated in Section 4.4. Finally, we present an analysis of the approach limitations in Section 4.5.

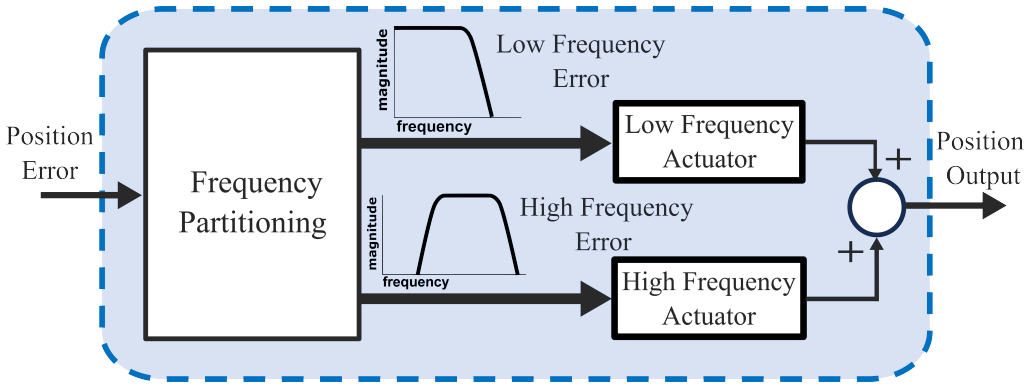

Figure 4.1: Conceptual diagram of frequency partitioned series admittance actuation approach.

4.3 Series Admittance Actuation Approach

The rendering range of admittance-controlled haptic interfaces is limited by the performance of their admittance controller's inner position-control loop. Specifically, the minimum stable rendered inertia, m_{min}, the primary metric by which admittance-based systems are assessed, has been shown to be inversely proportional to the position control's bandwidth (or cutoff frequency, ω_c) while the frequency range over which force rendering is accurate, known as the rendering bandwidth, ω_r, has been shown to be proportional to the position control's bandwidth [40]:

$$m_{min} \cong \frac{b}{\omega_c} \text{ and } \omega_r \cong \frac{3}{4}\omega_c$$

where b is a viscous damping term that approximates the impedance of the human operator, coupled to the haptic interface. As such, high-performance admittance-based haptic interfaces must be designed to facilitate high-bandwidth position control. This presents a challenge for high-power haptic interfaces given that the physics of position-controlled

actuators is such that the bandwidth generally scales inversely with actuator power and workspace size (i.e. higher actuator inertia and finite stable gains lead to lower overall bandwidths). In seeking a solution, it is useful to consider the motion requirements for human-robot physical interactions. Studies [44, 45, 46, 47] that have sought to characterize and model physical human-robot interaction have noted that the amplitude of volitional human motion (i.e. upper limb) remains relatively constant below 2 - 5 Hertz whereas above 5 Hertz, the motion amplitude decreases approximately with the inverse square of frequency. Similar trends have been reported for power and force output. While studies characterizing human motions during physical interaction are limited and the human element can't be reduced to a simple set of numbers it is reasonable to assume that the requirements for a haptic system will follow similar trends. This observation suggests an actuation partitioning approach that aligns the magnitude and speed of the actuation capabilities with the desired frequency content. As described above, the bandwidth of high dynamic stiffness admittance-based actuation is, in general, correlated with and approximately proportional to the workspace size. In other words, larger actuators generally have lower bandwidth capabilities while smaller workspace actuators generally have higher bandwidth capabilities.

Proposed Approach

While the actuator-size to bandwidth correlation is described as a limitation of larger admittance-based systems, if one considers an approach that incorporates two or more redundant admittance-based actuators (per manipulator degree-of-freedom), then the bandwidth-size correlation suggests that a larger actuator can be used for large, low-frequency motions and forces while a smaller, higher-bandwidth actuator, can provide high-frequency motions, albeit at smaller amplitudes. In the proposed approach, referred to here as series admittance actuation, a high frequency,

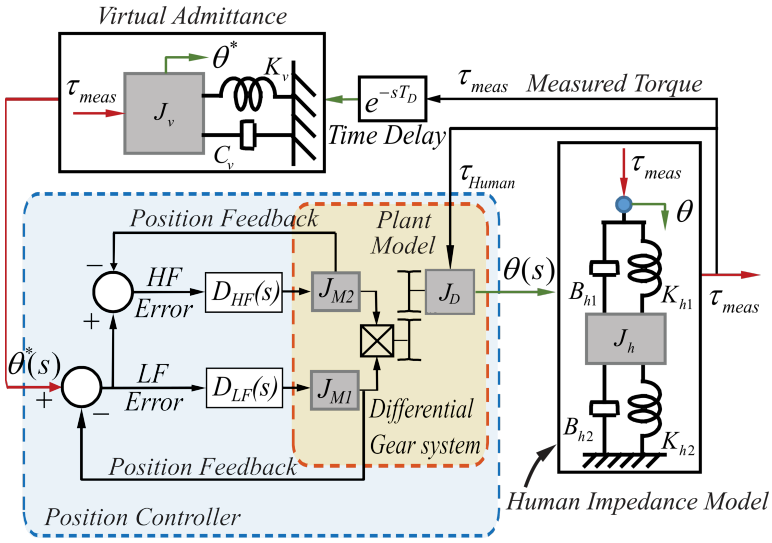

Figure 4.2: Conceptual Block Diagram of series admittance actuation approach. $D_{LF}(s)$ and $D_{HF}(s)$ represent the position controllers for the high-frequency and the low frequency actuator respectively. J_{M1} and J_{M2} represent the inertia of the individual low-frequency and high frequency actuators.

low amplitude actuator (referred to as the high frequency actuator for brevity) is connected in series with a low frequency, high amplitude actuator (referred to as the low frequency actuator) (see Fig. 4.2). The high frequency actuator has a limited displacement amplitude but a high position control bandwidth, whereas the low frequency actuator has a high displacement capability but has a limited position control bandwidth. Arranging the two actuators in series allows each actuators velocity to sum resulting in a single device capable of both high motion amplitudes as well as high positional bandwidth. The implication in haptics being that a higher position control bandwidth allows admittance-controlled devices to expand their range of stable rendering impedance and improve the accuracy of the impedances that are rendered. While actuator rendering control and partitioning can be affected through state feedback methods,

including explicit pre-filtering of the reference position input into low and high frequencies, or the PQ and design method [48] we instead, propose a simple and intuitive approach, shown in Fig. 4.2, that uses the dynamics of the actuators themselves for the frequency partitioning. Specifically, desired position or velocity commands are first commanded to the large actuator. The control errors, which consist of the high-frequency position or velocity components that the large actuator is incapable of providing, are used as the reference input to the smaller, high frequency actuator. The high frequency actuator compensates for the slow dynamics of the low frequency actuator and other errors, due to disturbances or unmodeled nonlinearities, resulting in a combined actuator with high position control bandwidth as well as a high amplitude of motion and enables kinesthetic haptic performance beyond what is obtainable by traditional admittance-controlled actuators.

4.4 Performance Evaluation

To evaluate the actuation approach, we developed a one degree of freedom actuation testbed (see Figure 4.3). Note, that the actuation testbed was developed as a concept demonstrator and was not intended as a platform to evaluate specific actuation technologies for either the low or high frequency actuators. Instead, the testbed was developed to validate the frequency partitioning concept and explore control methods and possible limitations. As such, the testbed incorporated a high-frequency actuator that is not ideally suited to the proposed approach but which was readily available in the author's lab and provided a platform to explore the proposed concept prior to development of hardware tailored to the proposed approach. The testbed haptic rendering is controlled through an admittance feedback controller, consisting of a position controller in combination with an admittance-based rendering law (see Fig. 4.4). As

described in the previous section, the position controller's desired input is first commanded to the low frequency actuator control and the resulting control errors are subsequently used as the reference input to the smaller, high frequency actuator. In this case, we implemented a lead compensator to regulate the low frequency actuator position. The high-frequency actuator control consists of an inner velocity control loop (implemented on the ultrasonic motors hardware controller) surrounded by proportional feedback outer position control loop. To emulate the limited displacement of the envisioned high frequency actuation, the testbed includes a software-imposed position limit on the high frequency actuator displacement. Both controllers were tuned to achieve as high a position-controlled bandwidth as practical. As seen from the experimentally obtained frequency response of the individual actuators (see Fig. 4.5), the resulting bandwidths of the low and high frequency actuators were approximately 8 Hz and 30 Hz, respectively.

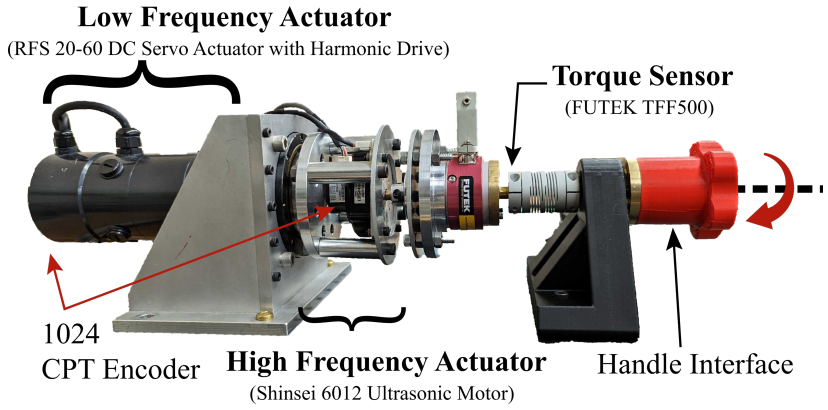

Figure 4.3: Series Admittance Actuation Test Bed

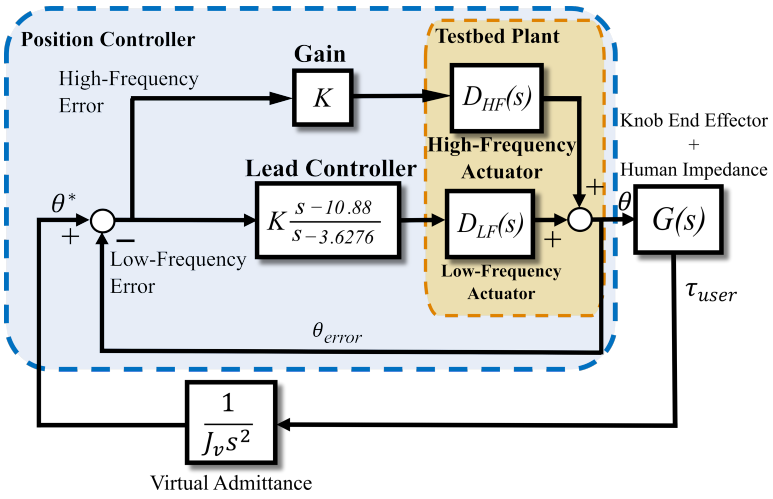

Figure 4.4: Block Diagram of Series Admittance Actuation Testbed Where K represent the gains of the respective position controllers, and Jv represents the virtual admittance rendered.

Minimum Stable Mass Assessment

Admittance-based haptic devices typically struggle with rendering low impedances and, in particular, can not render inertia levels below a threshold, referred to as their minimum stable rendered inertia, mmin, below which the rendering control becomes unstable. The minimum stable inertia is a proxy for the transparency of an admittance-based system and, as such, is commonly used as a primary metric by which admittance-based systems are assessed.

To measure the minimum stable rendered inertia, we must detect the threshold inertia value below which the rendering algorithm becomes unstable. The stability of admittance-based haptic devices is strongly affected by the coupled impedance of the human operator. Unlike impedance-based devices, where uncoupled stability is the more conservative measure of stability, for admittance-based devices, the coupled stability is the conservative measure of stability. To obtain consistent stability measurements,

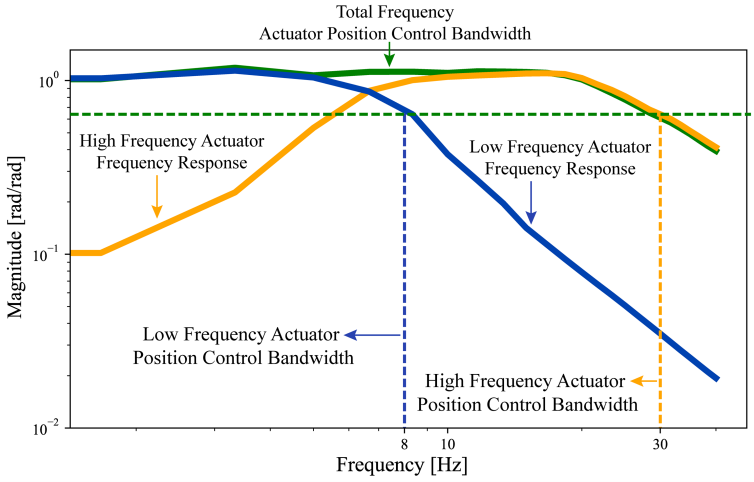

Figure 4.5: Measured position control frequency response of the low and high-frequency actuators. The position control bandwidth of low-frequency actuator and the high-frequency actuator can be observed to be 8 Hz and 30 Hz respectively

it is important to incorporate the effects of a human user's impedance. While stability experiments have typically been performed using human subjects (operating the haptic interface) [40, 41], these experiments can produce varying results, due to the wide variation of possible human impedance, which can vary due to posture, grip orientation, and grip pinch forces. To improve the consistency of our stability measurements, we developed a human impedance emulator, shown in Figure 4.6. For high performance admittance-based haptic interfaces, stability is primarily determined by the loop gain in the vicinity of 10 Hz or above [40], where the open loop phase is approximately -180 degrees. In this frequency range, the human impedance models proposed [49, 50] can be approximated as a linear damper [40]. For the experiments performed here, we selected a damping value of approximately 0.2 N-m/rad/sec, which is approximately equal to the average value for human subjects reported in [51]. The emulator produces the damping impedance through back-EMF forces of

a shorted DC brush motor (see Fig. 4.6). The minimum stable rendered inertia was obtained experimentally by physically coupling the series admittance testbed (Fig. 4.3) to the human impedance emulator (Fig. 4.6). To measure the minimum inertia, the programmed rendered inertia value was systematically reduced until instability was observed. The minimum stable rendered inertia of the series admittance actuator testbed (0.0025 Kg.m2) was found to be approximately 50% less than the minimum stable rendered inertia of the system using the low-frequency actuator alone (0.0057 Kg.m2). The reduction in inertia is consistent with the relationship established between the minimum stable rendered inertia and admittance position control bandwidth given in equation defined in section 4.3 and [40].

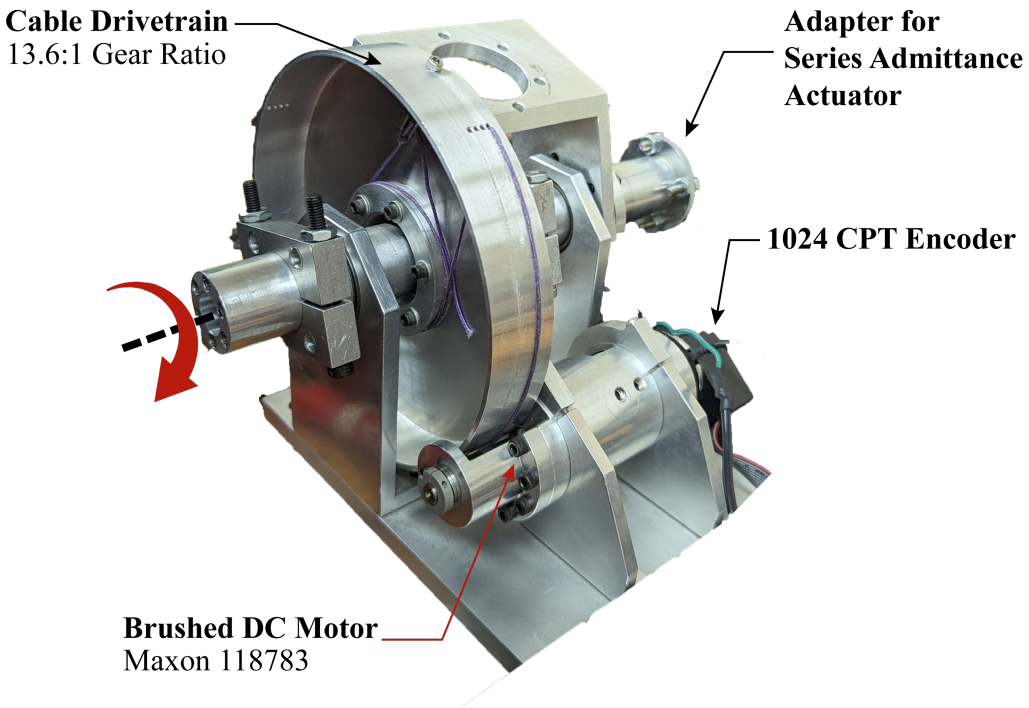

Figure 4.6: Human Impedance Emulator

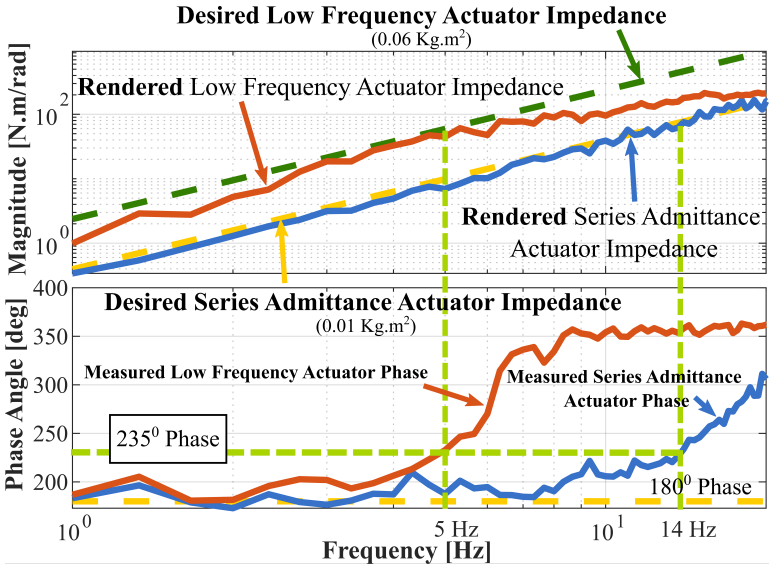

Figure 4.7: Impedance Frequency Response of Series Admittance Actuator testbed showing the output impedance and rendering bandwidth

Impedance Frequency Response and Rendering Bandwidth Measurement

In the performance evaluation of impedance-type and admittance-type haptic devices, transparency, or output impedance more generally, is an important performance characteristic, as it directly measures the ability of the device to render the desired impedance as a function of frequency. Due to the high output impedance of the admittance-based approach, particularly above the closed loop bandwidth of the position controller, it is not practical to obtain output impedance measurements through the controlled motion of the haptic interface, such as might be done for an impedance-based device. Is this case, output impedance measurements (see Fig. 4.7) are obtained by applying torques through the human impedance emulator described in section 4.4.1. Output impedance measurements were obtained for the series admittance testbed and, for comparison, for the low

frequency actuator alone. As seen in Fig. 4.7, both the series admittance actuator and the low frequency actuation stably rendered that desired inertia (of 0.01 kg-m2 and 0.06 kg-m2 respectively) below their respective position control bandwidths. Overall, the series admittance actuation rendering was more accurate, both in terms of magnitude and phase distortion, due to the error-correcting of the high frequency actuation. Importantly, the rendering bandwidth, which defines the frequency range over which the rendering accurately replicates the desired impedance [27], is significantly larger for the series admittance actuation (approximately 14 Hz) than for the low frequency actuation alone (approximately 5 Hz).

4.5 Limitations of Series Admittance Actuation

While the proposed series admittance actuation approach has demonstrated advantages in terms of improved rendering accuracy and bandwidth, design constraints inherent to the proposed actuation method present limitations to its performance. Primary among these limitations is the assumed small displacement range of the high frequency actuator (as compared to the low frequency actuator), which results from its higher bandwidth characteristics. During operation, position saturation of high frequency actuation limits both rendering stability and rendering output impedance.

To gain insight into the potential effects of high frequency actuator saturation, we can simplify the dynamic model given in Fig. 4.2. These simplifications include (1) an assumption that the high-frequency actuator has an infinite position control bandwidth (to remove the effect of phase loss above the closed-loop bandwidth), (2) an assumption that the disturbance forces from the human user are negligible (due to the high output impedance of the admittance position controller), and (3) an assumption that the human users output impedance can be modeled using

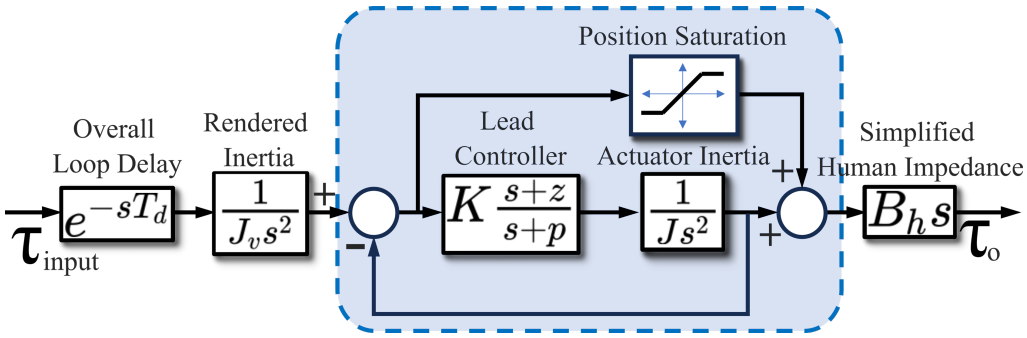

Figure 4.8: Simplified open loop block diagram of the SAA actuation approach expressed in a cascaded form. τ_{input} and τ_o represent the input and output torques respectively. J_v represents the virtual inertia rendered. K represents the gain of the lead controller. J represents the inertia of the actuator and B_h represents the simplified damping provided by the human.

a simple linear damper (for the same reasons given to justify the human impedance emulator discussed in section 4.4.1). These simplifications allow for the series admittance actuators open loop transfer function to be expressed in a simple cascaded form as shown in Fig. 4.8. To facilitate analysis we can further simplify the model of the high frequency actuator by approximating the actuator saturation through a variable gain, derived from the describing function [52] for a saturation gain which is a real valued nonlinearity with unity gain below the saturation amplitude (see Fig. 4.9). As high frequency actuator amplitude increases the describing functions gain reduces asymptotically to zero.

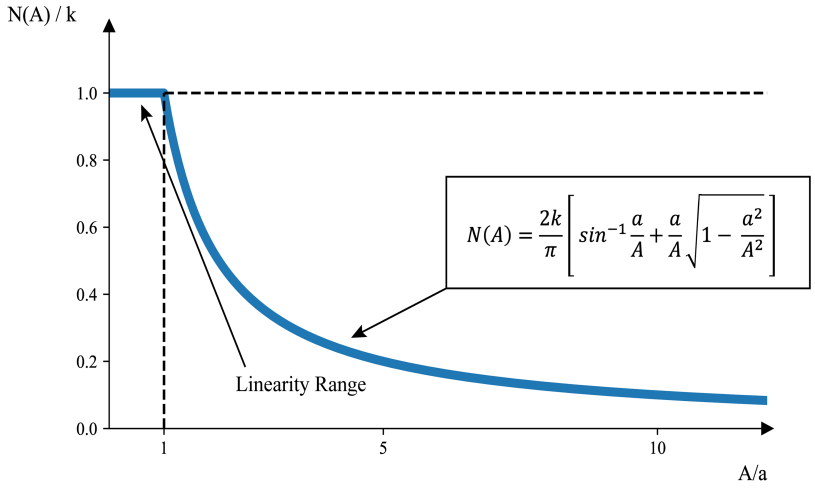

Figure 4.9: Describing function of saturation where k represents the saturation gain, 'a' represents the saturation amplitude limit and 'A' represents the actual amplitude of oscillations.

Stability Analysis with Position Saturation

Position saturation of the high frequency actuator can limit the performance of the series admittance actuation approach when high frequency position control commands exceed the position limits of the high frequency actuator. As a consequence, the series admittance actuation approach can become unstable when the user inputs rapid movements which exceed the capability of the high frequency actuator.

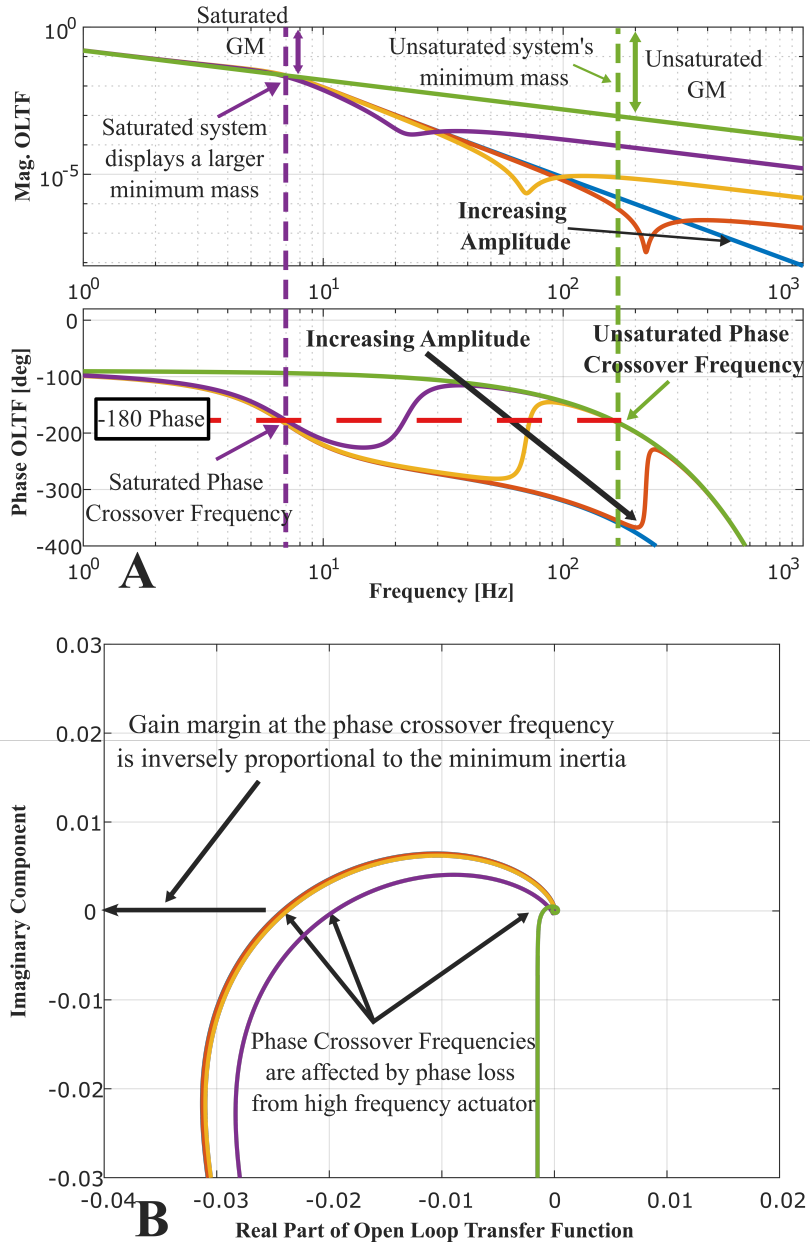

Figure 4.10: A) The systems open loop transfer function with the effects of position saturation shown as oscillation amplitude increases past the high frequency actuators position saturation point. It also shows that the minimum stable mass that can be rendered is inversely proportional to the gain margin. B) The same information shown in a Nyquist contour emphasizing the possibility of an encirclement and instability due to high frequency actuator position saturation.

We can gain insight into the effects of actuator saturation on stability by examining the open loop transfer function's frequency response for different amplitudes of oscillation (see Fig. 4.10). As seen in Fig. 4.10 A, significant phase loss above the bandwidth of the low frequency actuator occurs when the oscillation amplitudes exceed the saturation limits of the high frequency actuator. As the amplitude oscillations become very large (relative to the saturation threshold), the high frequency actuator has little to no effect on the stability of the system and the open-loop system frequency response approaches that of the low frequency actuator alone. As a result, the system's minimum stable inertia decreases to that of the system with low frequency actuation only, resulting in oscillations and potential instability. As seen in the Nyquist plot (see Fig. 4.10 B) of the open-loop system, position saturation reduces the gain margin of the unity virtual mass system which is inversely proportional to the minimum mass that the system can render stably. This effect is most prominent if the phase loss due to position saturation of the high frequency actuator is greater than 90 degrees. When the phase loss in the position controller is less than 90 degrees, an encirclement due to saturation is unlikely and the system will remain stable (ignoring other destabilizing effects, such as time delay in the control loop).

Effect of Position Saturation on Output impedance

Position saturation can also adversely affect the output impedance of the series admittance actuator. As identified in the previous section, the system will remain stable (while rendering a virtual mass) when the phase loss due to position saturation remains below 90 degrees. However, the presence of high frequency position saturation can distort the rendered impedance while still maintaining stability. We can gain insight into the effects of actuator saturation by examining the output impedance of the system, using the assumed system model simplifications described at the

beginning of this section (see Fig. 4.8). Assuming the simplified model shown in Fig. 4.11 A, we can evaluate the frequency response of the output impedance (see Fig. 4.11 B). As seen in Fig. 4.11 B, high frequency actuator saturation results in distortion of the output impedance (in both magnitude and phase) above the position control bandwidth of the low frequency actuator. At high frequencies and as the oscillation amplitudes become large the output impedance approaches the open loop output impedance of the device itself. Phase distortion due to position saturation is especially evident at frequencies near the position control bandwidth of the low frequency actuator. This phase distortion will adversely affect the rendering. For phase distortion greater than 45 degrees (shown as 0 degrees in Fig. 4.11 B), the rendering will no longer be perceived as a pure inertia [40]. The frequency at which the phase distortion exceeds 45 degrees is referred to as the rendering bandwidth [53, 54]. It follows from this analysis that high frequency actuator's position saturation can adversely affect the perceived rendering (i.e. output impedance) and the rendering stability. As such, the high frequency actuator's range of motion (i.e. position saturation threshold) must be carefully considered in any implementation of a series admittance actuated system.

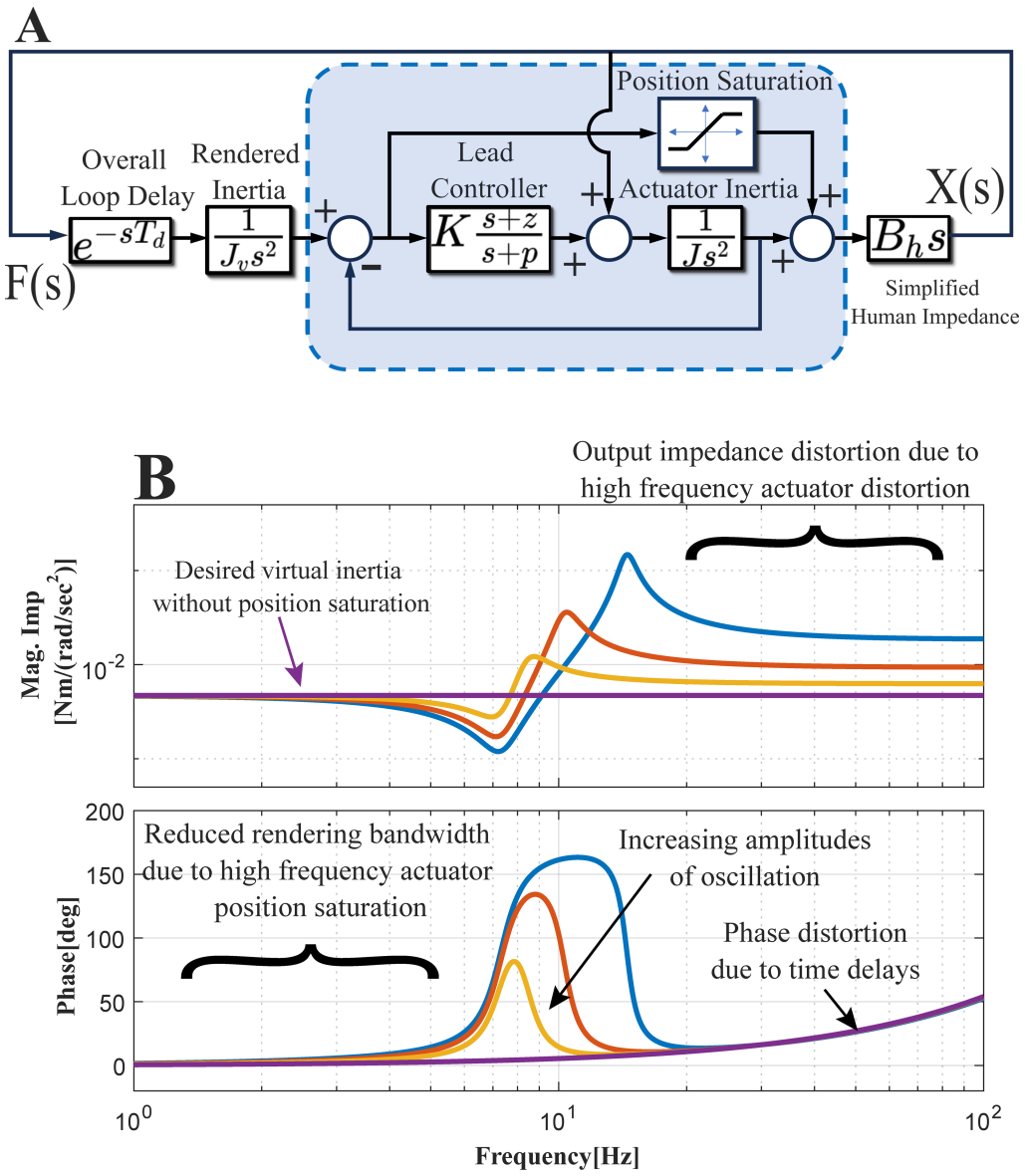

Figure 4.11: A) Block Diagram representing the output impedance in relation to the acceleration of the system including the humans disturbance and position saturation of the high frequency actuator. B) Impedance frequency responses of the system plotted across amplitudes of motion that are determined to be stable (show less than 90 degrees of phase loss from high frequency actuator saturation).

4.6 Conclusion

Our series admittance actuation approach brings the position control bandwidth needed to render lower masses to admittance controlled haptic devices. Our series admittance actuation approach does so through a frequency partitioned position error between two different actuators which are connected in series. The actuation approach also enables stable haptic renderings over a wide range of frequencies as well as more accurate haptic renderings at lower frequencies as well. Our actuation approach allows for a simple control structure as well as a simple mechanical design in comparison to other actuation approaches with the same goal. We see a 50% reduction in the minimum mass that can be rendered by an admittance controlled haptic device using our actuation approach due to the increase in position control bandwidth. Future work would include a more representative one-degree of freedom testbed and a deeper analysis to understand the benefits and limitations of this approach. A Multi degree of freedom test setup would also allow us to explore the scalability of our proposed actuation approach.

5 A SERIES ACTUATION APPROACH FOR WORKSPACE EXPANSION OF IMPEDANCE BASED HAPTIC DEVICES

5.1 Overview

The development of high-performance haptic interfaces faces fundamental trade-offs between workspace volume and force rendering capabilities. In this chapter, I present a series actuation framework designed to overcome this challenge by expanding the operational workspace of impedance-type haptic devices while maintaining their high-fidelity rendering characteristics.

Most impedance based kinesthetic haptic devices are either limited in performance i.e. cannot produce high stiffness [55][23], or are limited in their workspace capabilities. This limitation in workspace is often a result of their drivetrains, which allow for an increase in the impedance that these devices can render, but limit their workspace.Large workspace haptic devices which are very limited in the impedences that they can render or cannot be transparent enough in case of admittance based haptic devices. Our goal in this chapter is to explore a potential solution to this workspace problem through a proposed series actuation approach. We test the proposed series actuation approach with two different control approaches in this chapter and assess the stability, transparency and limitations through experiments and pilot studies.

5.2 Introduction

Typical impedance-based haptic devices face significant limitations in achieving both large workspaces and high-fidelity, high-impedance force rendering. High-performance systems, such as the Phantom Premium series [56], demonstrate good force feedback capabilities (maximum torque

values at 515 mNm and maximum force values at 37.5 N), yet remain constrained to relatively small operational volumes (typically less than 381 x 267 x 191 mm^3). This workspace limitation primarily stems from the mechanical drivetrain configurations employed to achieve the necessary torque amplification and back-drivability characteristics essential for transparent haptic rendering [57].

Conversely, large-workspace haptic systems, including cable-driven mechanisms [58, 59, 60] and extended serial-link manipulators [61], sacrifice force rendering capability to achieve broader operational ranges or are very complex mechanically [17]. These devices typically exhibit low rendered stiffness values, substantially limiting their ability to convey rigid virtual surfaces and precise force constraints [62]. Alternative approaches utilizing admittance-based architectures present additional challenges, including inherent transparency limitations arising from their device dynamics and elevated apparent inertia characteristics[63][64].

The concept of series actuation for haptic interfaces remains relatively unexplored, with only limited preliminary investigations reported in the literature [15][16]. Harwin et al. [15] initially proposed a dual-actuator configuration for enhanced workspace coverage, though they propose this approach, they fail to thoroughly explore the control limitations and haptic performance quantitatively. To address this gap in the limited literature, we present an investigation of series actuation strategies for high-performance impedance-type haptic rendering. As shown in Figure 3.3, our proposed series actuation approach attempts to expand the workspace of the primary impedance based actuator by adding a secondary actuator at the base of the primary i.e. any movement in the secondary actuator would move the primary actuator as well. In the next section, I give a more detailed explanation of the actuation and control approach.

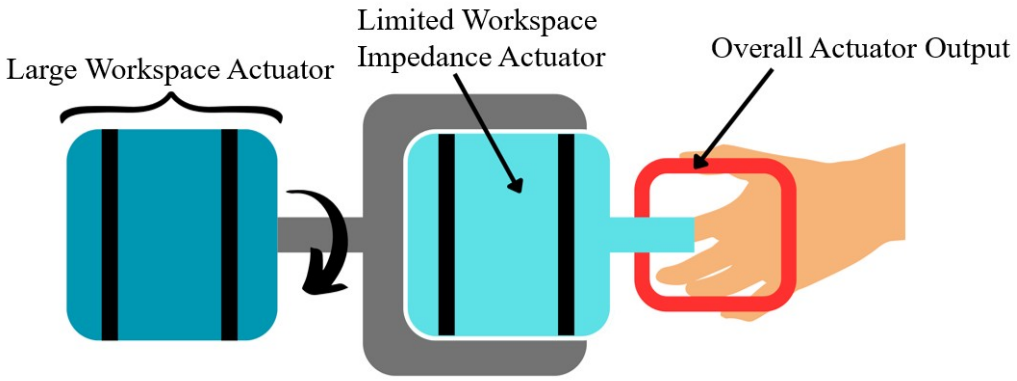

Figure 5.1: Actuator Configuration for Workspace Expansion through a Series Actuation Approach

5.3 Series Actuation Approach for Workspace Expansion

Impedance-based haptic devices excel at rendering low impedances, providing users with a sensation of free movement and low inertia interactions. However, these devices face significant challenges when attempting to render high impedances or stiff virtual environments. This fundamental limitation stems from the inherent mechanical and control characteristics of impedance-controlled systems, where the maximum achievable stiffness is constrained by factors including actuator torque capacity, structural compliance, sensor resolution, and control loop bandwidth [27, 65].

One of the most prevalent engineering solutions to address the limited force-rendering capabilities for haptic devices is the implementation of cable-driven drivetrains positioned at the actuator output. These mechanisms provide torque multiplication, enabling the rendering of higher impedances than would be possible with direct-drive configura-

tions [66, 67]. The mechanical advantage gained through such transmission systems, however, introduces a significant drawback: a reduction in the actuator's effective workspace. Traditional gearboxes are not often used for haptic devices due to issues with backlash and high reflected inertia. Cables drive transmissions, which are often used for these haptic devices, limit workspace due to limited length of the cable. It is not possible to simply increase the size of these cable transmissions as they have issues with scaling such as, low stiffness and higher compliance intruding more modes into the system.

The Series Actuation Approach proposed in this work directly addresses this workspace limitation through a novel architectural configuration. Our method involves coupling a limited-workspace, high-performance impedance type haptic device (hereafter referred to as the "primary actuator") in series with a large-workspace positioning system (designated as the "secondary actuator"). This hierarchical arrangement leverages the complementary characteristics of both subsystems to create a unified haptic interface with expanded capabilities.

The primary actuator in our configuration is optimized for high-bandwidth force rendering with good transparency characteristics. Typically implemented as a cable-driven or direct-drive mechanism with high-resolution encoders and precision bearings, this subsystem ensures high-fidelity haptic rendering within its limited operational range. The mechanical design prioritizes minimal friction, backlash, and inertia to maintain the device's ability to render low impedances effectively while also achieving substantial maximum stiffness values.

Complementing this, the secondary actuator serves as a positioning stage responsible for dynamically relocating the primary actuator's workspace throughout a much larger operational volume. While this secondary system may have a lower operational bandwidth with higher output impedance, its primary function is positional rather than haptic. The

fundamental objective of our Series Actuation Approach is to substantially expand the effective workspace of the primary actuator by continuously repositioning it via the secondary actuator. This dynamic repositioning is implemented such that the user always remains within the operational range of the high-fidelity primary system, regardless of their position within the expanded workspace. Critically, this configuration must maintain the output impedance characteristics of the primary actuator, ensuring that the user experiences consistent haptic rendering quality throughout the expanded workspace.

The control architecture for this series-actuated system presents unique challenges, particularly regarding the coordination between primary and secondary subsystems. In this investigation, we implement and evaluate multiple control methodologies to determine optimal approaches for maintaining rendering fidelity while enabling seamless workspace expansion. These control strategies include position-based control schemes, where the secondary actuator follows the primary system's position with appropriate offsets. Each control methodology presents distinct advantages and limitations regarding stability margins, transparency metrics, and transition smoothness between workspace regions. Through systematic experimental evaluation and user studies, we characterize the performance envelope of each approach and identify the most promising directions for future refinement of series-actuated haptic interfaces. The implementation details, experimental validation procedures, and quantitative performance assessments of our Series Actuation Approach are presented in subsequent sections, providing comprehensive evidence for the viability of this solution to the longstanding workspace limitation problem in high-fidelity haptic interfaces.

Hardware Implementation

A 1 degree of freedom prototype is developed to explore different control methods with this actuation approach. The prototype system comprises of a primary actuator, which is a one degree of freedom impedance based haptic device i.e. a brushed DC motor(Maxon 118783) with a 6:1 cable drive gearhead. This primary actuator is in series with a secondary actuator at it's base(as shown in Figure 5.2) which is a brushed DC motor with a 50:1 gearhead. This secondary actuator has a high output impedance and acts as a servo. Both actuators have rotary encoders on them and are controlled using a Speedgoat FPGA system and the control loops run at a frequency of 1000 Hz.

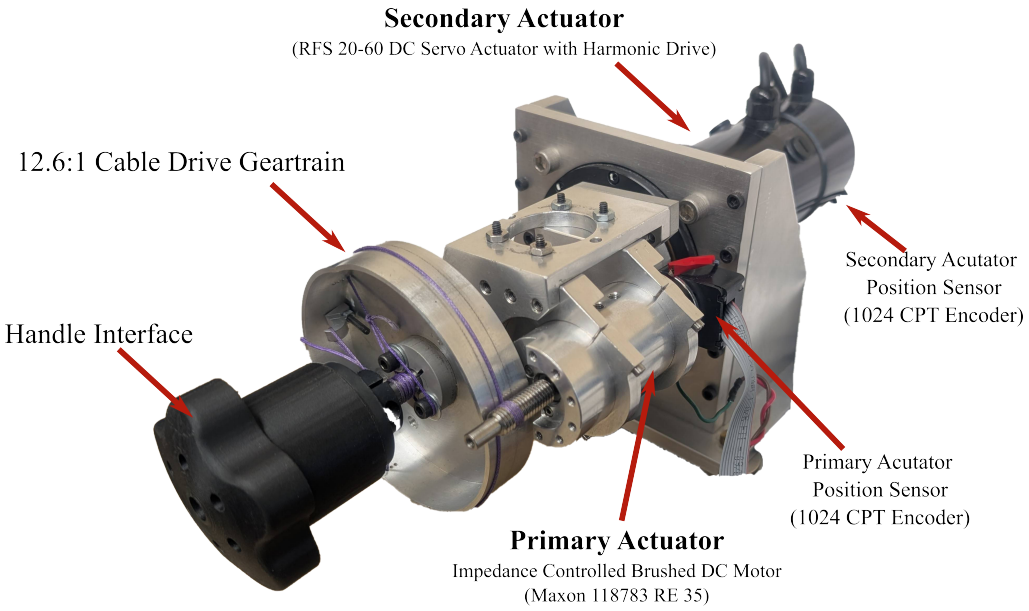

Figure 5.2: Prototype Actuator using Series Actuation scheme to expand actuator workspace

Proposed Control Approaches

The naive approach to this problem is to just have a position controller on the secondary motor that follows the position of the primary motor. We implemented this approach using a lead controller on the secondary motor as shown in Figure 5.3. Ideally, if a high bandwidth position controller was available, this simple approach should work for expanding the workspace; however, in practice it performs poorly because of actuator saturation in the secondary motor, making this method unsuitable for quick movements that need rapid acceleration and deceleration which leads to significant tracking errors causing frequent 'wiggles' during fast transitions.

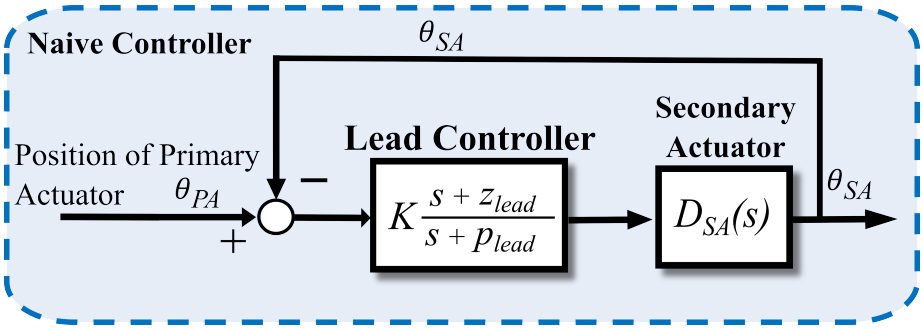

Figure 5.3: Block Diagram of Naive Controller Implementation for secondary actuator

Harwin and colleagues, in their work with the "Flying Phantom" at the University of Reading, used a PD controller with a deadzone to reduce unnecessary movements of the secondary actuator to achieve "high-bandwidth, low impedance interaction over the full range of horizontal movement". The Flying Phantom attached a Phantom Premium haptic device to a larger positioning system to expand the workspace while keeping the high-quality force feedback capabilities of the primary device aiming to provide both large movement area and good haptic feedback.

We tried Harwin's approach, but found a major problem: the quick

accelerations and decelerations of the secondary motor caused noticeable jerks at the end effector that reduced the quality of force rendering. These mechanical jerks were especially problematic when switching between stopped and moving states, creating unwanted force artifacts that worsened the haptic experience. We tried to fix these issues by adding velocity feedforward components as suggested in Harwin's approach to compensate for velocity-related forces and improve tracking, but our testing showed that these changes still produced poor rendering quality, particularly when simulating free-space environments where minimal resistance is important.

To solve these problems, we developed a different control strategy using an optimal control framework. We implemented a Linear Quadratic Regulator (LQR) controller designed to track both the velocity and position of the primary actuator, as shown in Figure 5.4. Through testing, we found that a weighting ratio of 2:1 for velocity to position tracking provided the best balance between position accuracy and smooth motion blending precise positioning with smooth velocity control. We carefully tuned the controller gains to prevent the secondary actuator from saturating while maximizing tracking performance, which significantly improved haptic quality across the expanded workspace.

For all our tests, we kept the control approach for the primary actuator the same across all secondary controller implementations to ensure fair comparison and isolate the effects of the secondary control design. This consistency allowed us to directly compare each approach based on transparency, stability, and overall user experience.

5.4 Performance Evaluation

Impedance-based haptic devices are very good at rendering low resistance and free-space motion, but struggle when rendering high stiffness. This

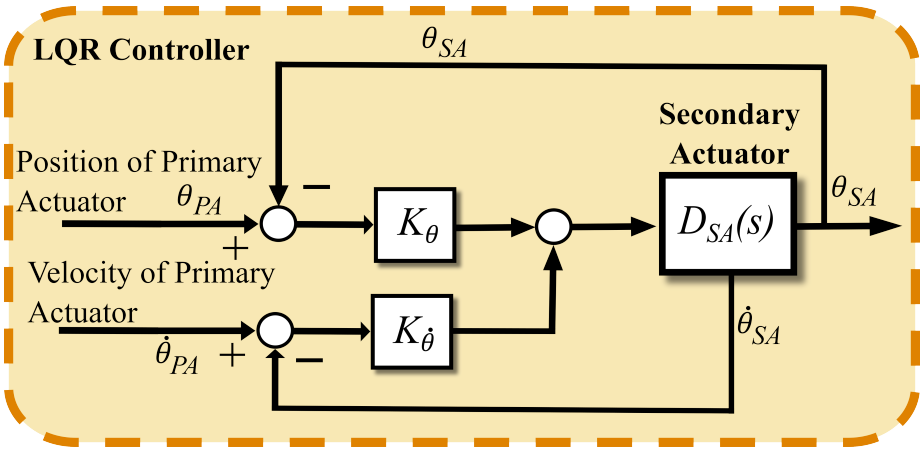

Figure 5.4: Block Diagram of LQR Approach Implementation on the Secondary Actuator

guided how we tested our system. We focused on two main performance metrics. First, we measured the maximum stable stiffness that our combined system could render compared to using just the primary actuator. This shows whether expanding the workspace reduces the device's ability to simulate rigid objects. We tested both coupled stability (when a user is interacting with the device) and uncoupled stability (when the device operates on its own). Second, we examined how well the system simulates free-space motion with minimal resistance. This is important for making movements feel natural across the expanded workspace, especially during large and fast movements. By comparing these metrics between the standalone primary actuator and our series-actuated setup (with both naive and LQR control approaches), we could directly assess whether our approach maintains the original device's performance while providing a larger workspace.

For any automated tests to evaluate our series actuation approach, we use a modified version of the test setup as described earlier (see Figure 5.5). A force torque sensor is added as shown below and the test device

has been modified to interface with our haptic device. The test device is used as a position source to give inputs to our Series Actuated haptic device.

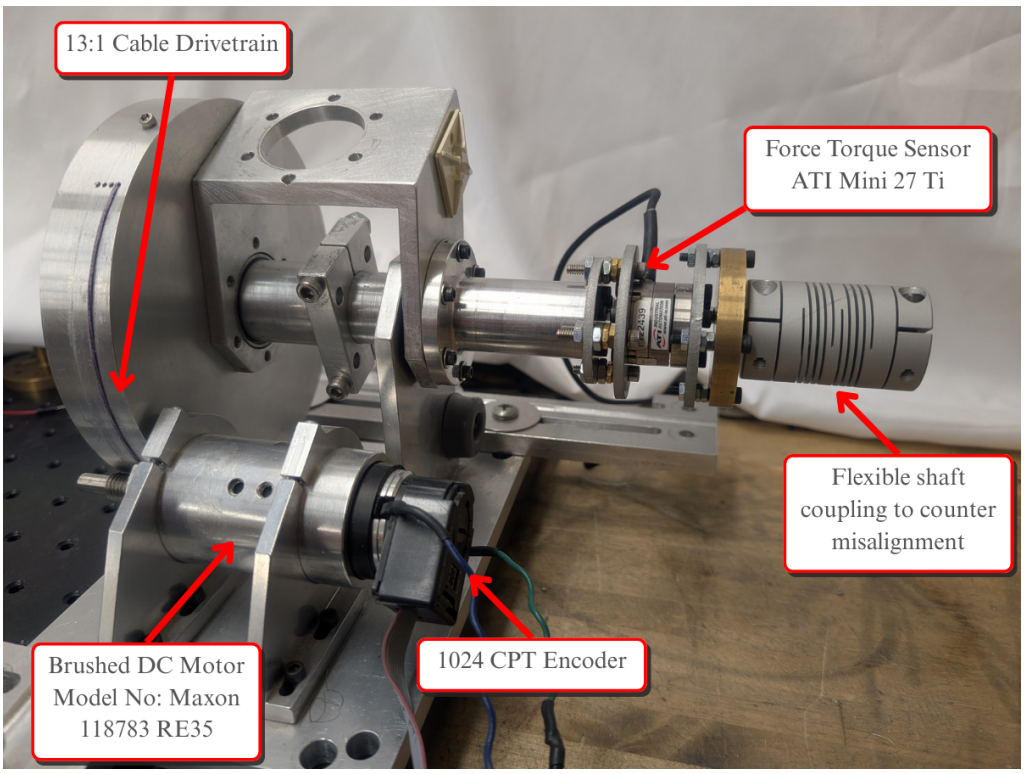

Figure 5.5: External position source for validation and testing of haptic devices

Maximum Stable Stiffness

The most conservative stability test for impedance-based haptic devices is uncoupled stability—when no user is touching the device. We tested this by programming a stiffness into the device and then disturbing it to see if it returns to a stable position or starts oscillating. We did this for three setups:

the primary actuator alone, the series actuation with naive control, and the series actuation with LQR control. Our results showed an interesting pattern. The LQR control approach had the highest maximum stable stiffness (853 mNm/rad), followed by the naive approach (195 mNm/rad), and lastly the standalone primary actuator (130 mNm/rad). We then

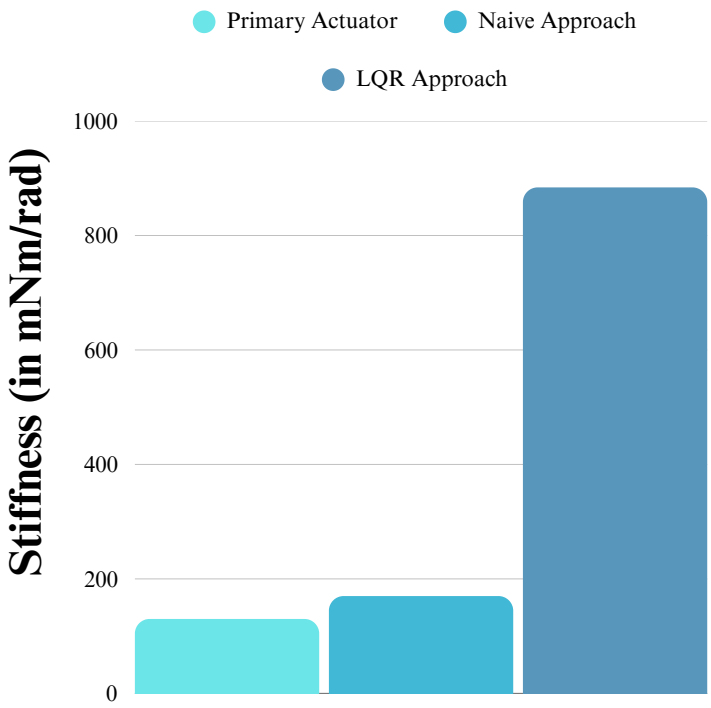

Figure 5.6: Maximum Stable Stiffness for the Bilateral Uncoupled Stability condition

tested the maximum stable stiffness with a user interacting with the system by simulating a virtual wall with all three setups. Testing was done both manually and using a Human Impedance Emulator as a consistent external input. The emulator, shown in Figure 5.5, was fitted with a force-torque sensor and attached to our haptic device as shown in Figure 5.9. This setup

generated a steady pattern of positions while the haptic device rendered a wall, allowing us to observe stability consistently. Interestingly, the results with user interaction showed the opposite trend from our first test. The primary actuator alone achieved the highest maximum stable stiffness (3000 mNm/rad), followed by the naive approach (2100 mNm/rad) and the LQR approach (1800 mNm/rad). We need to investigate further to understand and prove why this happens, but we think it is because the velocity feedback term from the LQR controller is adding damping to the system.

Enhanced Stability through Time Domain Passivity Control

To address stability limitations when rendering high-stiffness haptic walls, we implemented a Time Domain Passivity Controller (TDPC) as a complementary control element for both the LQR and naive control approaches. The TDPC framework continuously monitors energy exchange within the secondary actuator subsystem and dynamically modifies control parameters to maintain passivity. As illustrated in Figure **??**, the architecture incorporates a passivity observer that quantifies energy flow within the controlled system. When this observer detects negative energy readings—indicating that the direction of the applied torque and the measured velocity is different, which means controller is going unstable. In case this detected negative energy is more than a predetermined threshold, the passivity controller is triggered. The passivity controller, is a method for adaptive gain scheduling. It adds the minimum amount of damping needed by the system to dissipate the negative energy. It is equivalent to temporarily increasing the damping term in a PID controller.

To optimize system performance across different interaction scenarios, we selectively activated the TDPC only during haptic wall rendering. We observed that continuous activation during transparency conditions

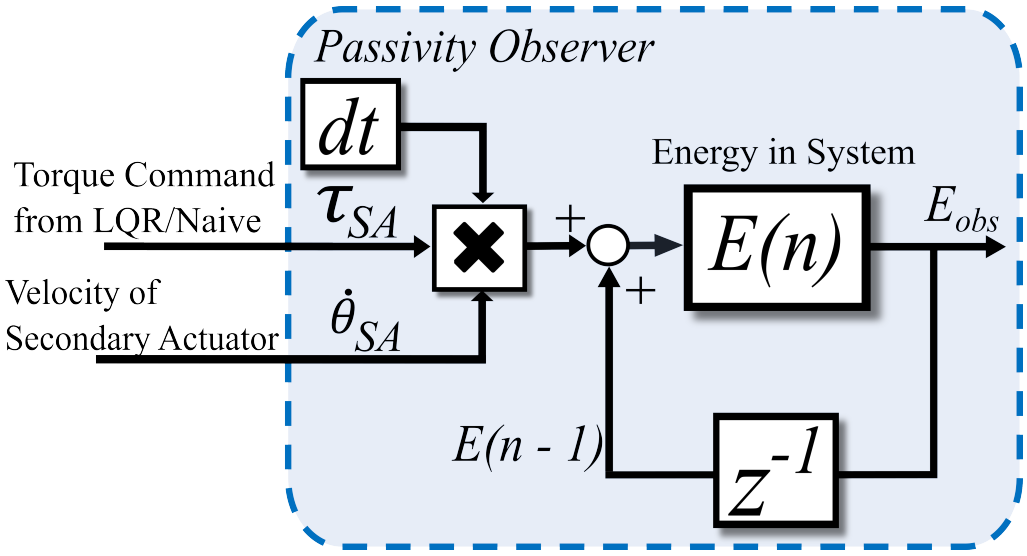

Figure 5.7: Passivity Observer measures the energy injected into the system at every timestep

resulted in excessive damping that compromised the secondary actuator's tracking performance, making it unacceptably sluggish for free-space movement simulation. With TDPC integration, both control approaches demonstrated substantially improved stability characteristics. Maximum stable stiffness values increased to approximately 3000 mNm/rad for both LQR and naive control implementations, as shown in Figure 5.9, approaching the performance envelope of the standalone primary actuator. The TDPC effectively stabilizes the secondary actuator during high-stiffness wall interactions without compromising the perceived stiffness at the end-effector. To validate that the rendered impedance remains unaffected by the TDPC intervention, we conducted an experiment using a previously unstable stiffness value implemented with the LQR control approach augmented by TDPC. Using our external position source to systematically excite the haptic device, we measured force-displacement characteristics.

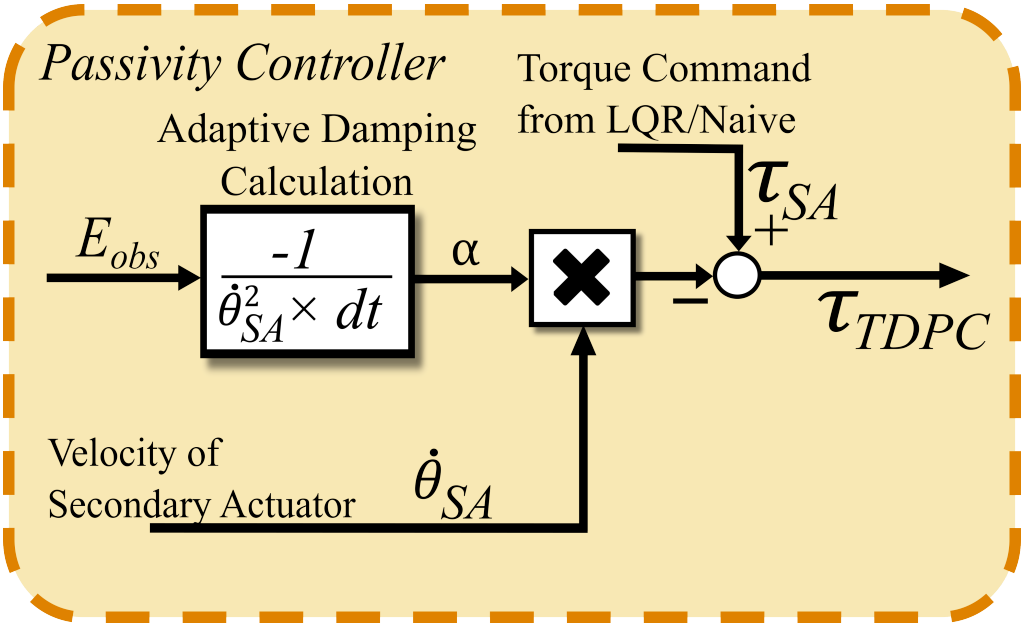

Figure 5.8: Passivity controller adds minimum amount of damping to the system needed to dissipate the negative energy

As demonstrated in Figure 5.10, the virtual wall maintains its programmed stiffness characteristics despite the additional passivity control layer, confirming that the stability enhancement occurs without compromising rendering fidelity.

Transparency Assessment

In evaluating haptic interfaces, transparency—the ability of a device to accurately render desired impedance characteristics across frequency ranges—represents a critical performance metric. Impedance-type haptic systems inherently exhibit low output impedance, making them particularly effective at simulating free-space environments with minimal resistance. Since our primary actuator is an impedance-based device with

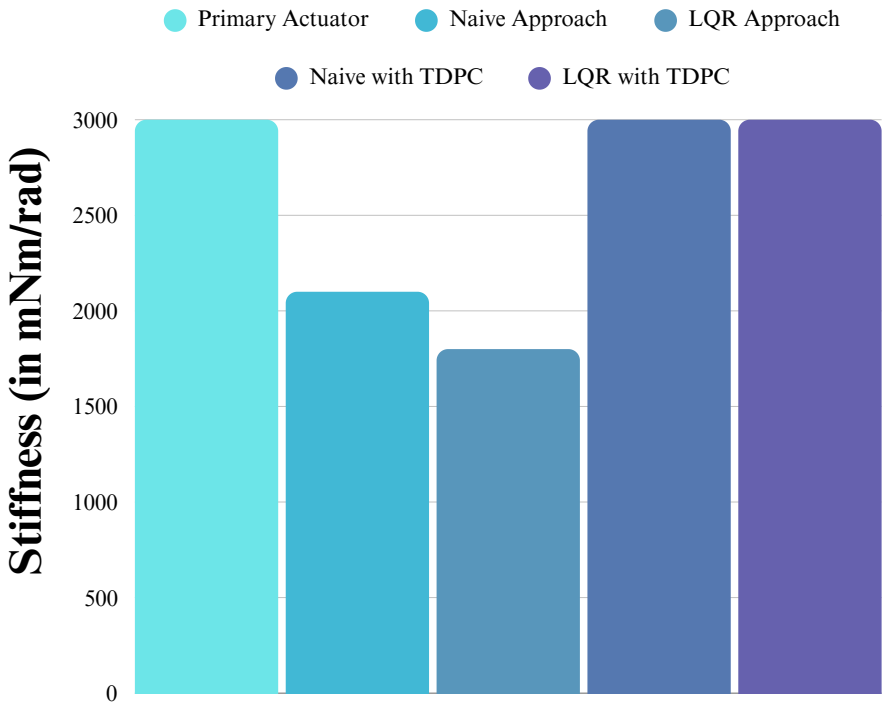

Figure 5.9: Maximum stable stiffness for the unilateral coupled stability condition(haptic wall)

naturally low output impedance, our evaluation focuses on whether the series actuation approach preserves this desirable characteristic despite the addition of the secondary actuator subsystem.

To systematically evaluate transparency preservation, we conducted two complementary experimental assessments. The first examination focused on time-domain transparency characteristics. We configured the system to render free-space conditions using three distinct configurations: the standalone primary actuator, the naive control approach, and the LQR control approach. An external position source generated and applied a sinusoidal trajectory with 1 radian amplitude as a standardized input

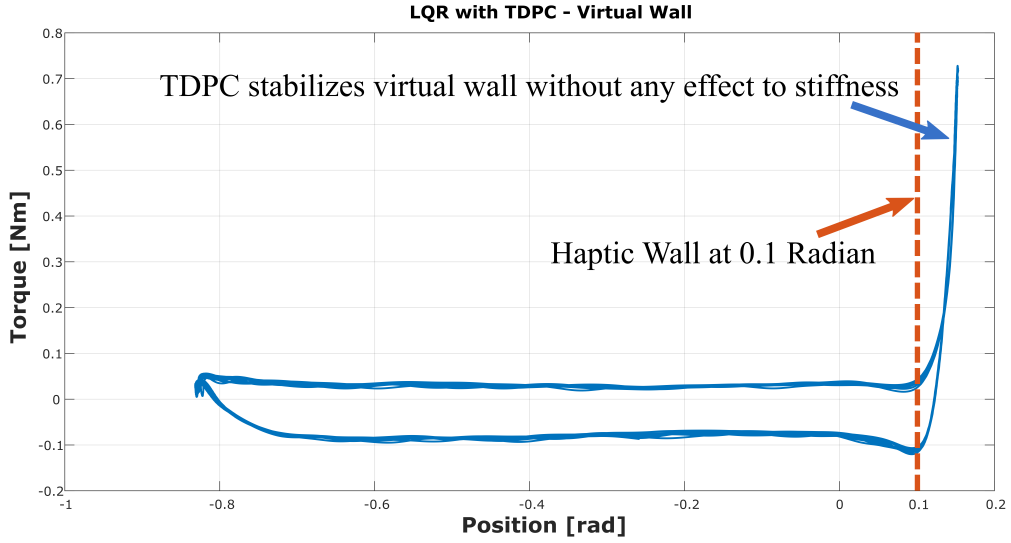

Figure 5.10: Time Domain data showing a haptic wall at a previously unstable stiffness, now stabilized through Time Domain Passivity Control without affecting wall stiffness

to the haptic device. As illustrated in Figure 5.11, all three approaches demonstrated comparable output characteristics at the end-effector. The residual torque observed in the time-domain response primarily originates from mechanical friction in the drivetrain rather than from differences in control architecture.

Our second experimental protocol examined frequency-domain transparency through impedance characterization across a spectrum of input frequencies. The external position source generated a frequency-swept chirp signal (0.1 Hz to 15 Hz) which was applied as input to the haptic device while rendering free-space conditions. This procedure was replicated for all three control configurations. Figure 5.12 presents the resulting frequency response data, showing minimal variation in magnitude and phase characteristics across the three implementations. The response pro-

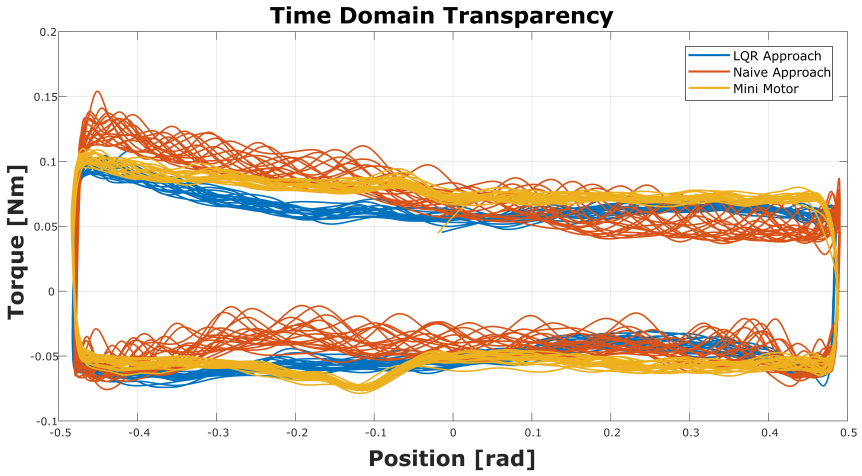

Figure 5.11: Time Domain data showing the torques felt by the user in transparency condition across approaches

file reveals damper-like behavior at lower frequencies—attributable to drivetrain friction—transitioning to inertia-dominated characteristics at higher frequencies, which aligns with theoretical expectations.

It is important to acknowledge certain methodological limitations in this analysis. The relationship between input position and output torque exhibits significant nonlinearity, as demonstrated in Figure 5.13, where a low-frequency sinusoidal position input produces distinctly non-sinusoidal torque output. This nonlinearity indicates that the phase data presented in Figure 5.12 should be interpreted with caution, as phase characteristics provide crucial insights into the qualitative feel of a haptic device. Further refined testing and analysis will be necessary to comprehensively characterize transparency across the frequency spectrum.

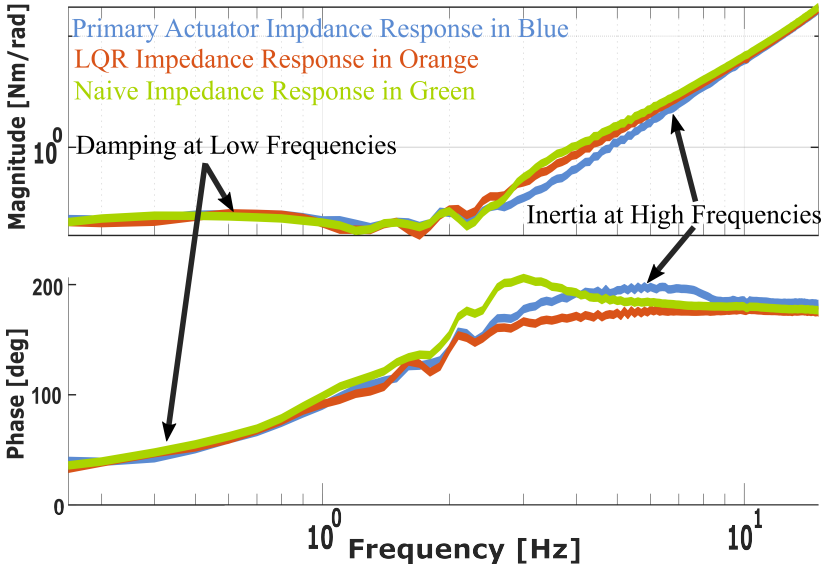

Figure 5.12: Impedance Frequency Response of Series Admittance Actuator testbed showing the output impedance across approaches

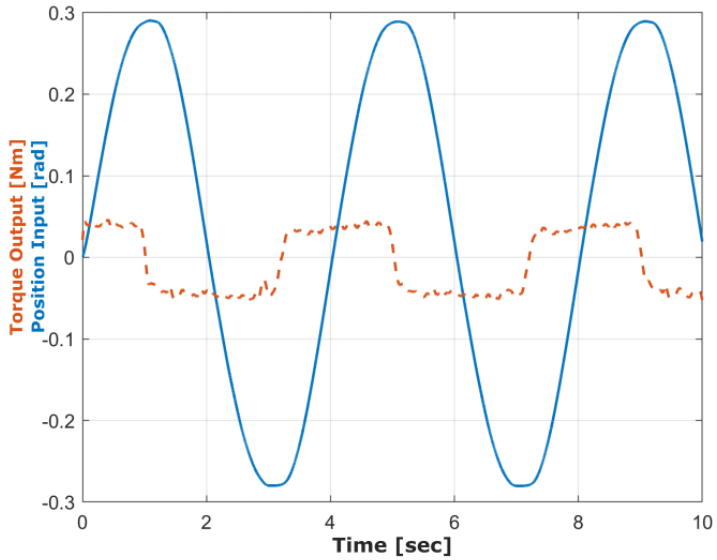

Figure 5.13: Low Frequency Sine Wave position input to haptic device showing non linearity

5.5 Conclusion

This chapter presented a series actuation approach to expand the workspace of impedance-based haptic devices. Our 1-DOF prototype combined a limited-workspace primary actuator with a larger secondary positioning system to increase operational range while maintaining performance. Testing multiple control strategies showed that the LQR approach with 2:1 velocity-to-position tracking ratio performed better than the basic position-following method, which had tracking errors during transitions. Adding Time Domain Passivity Control improved stability, allowing stiffness values up to 3000 mNm/rad when coupled with a user, similar to the standalone primary actuator. Time and frequency domain tests confirmed that the series approach maintains the low-impedance characteristics of the primary device, with minimal differences in output impedance between configurations, especially in free-space rendering. We observed limitations including nonlinear impedance responses and tuning challenges. More analysis is needed to understand the conflicting stability performance between uncoupled and coupled configurations. The causes of these results require further investigation. Future work should address these issues and test multi-DOF implementations. Additional research could explore adaptive control methods and user studies to evaluate performance in complex scenarios. This approach provides a practical solution to expand workspace in haptic interfaces without compromising rendering quality, with potential applications in simulation, teleoperation, and virtual reality.

6 THESIS CONTRIBUTIONS

The contributions of this dissertation include theoretical frameworks, hardware implementations, and experimental validation of new actuation approaches. Specifically, the key contributions include:

1. A frequency-partitioned series admittance actuation approach that combines a high-bandwidth, low-amplitude actuator with a low-bandwidth, large-amplitude actuator to extend rendering capability in admittance-based systems.

2. A series actuation framework for workspace expansion in impedance-type haptic devices that maintains rendering quality across an extended operational volume.

3. Development and evaluation of a handheld haptic device with a bidirectional coupled input mechanism, demonstrating comparable performance to traditional grounded interfaces in certain tasks.

4. Analytical models that characterize the stability boundaries and performance limitations of series actuation approaches, particularly regarding position saturation effects and their impact on system behavior.

5. Experimental validation of the proposed approaches through systematic performance evaluation, showing improvements in metrics including minimum stable rendered inertia, rendering bandwidth, maximum stable stiffness, and workspace volume.

These contributions advance the state of the art in haptic actuation, providing both practical implementations and theoretical frameworks that can guide future developments in the field.

7 CONCLUSIONS AND FUTURE WORK

7.1 Recommended Future Work

In chapter 4, we provide a proof of concept for our series admittance actuator through our series admittance testbed. We also evaluate the performance of our actuation approach and asses some of the limitations. However, our current testbed is limited in capability and is not representative of our vision of the series admittance actuator. The high-frequency actuator that we use in the testbed is limited in terms of both its torque capacity and its position control bandwidth, which limits the capability of our actuation approach. The current high-frequency actuator does not have position saturation limitations, which would be present in a representative actuator. The main objective of our future work would be to first design and build a more representative actuator with a high frequency actuator with a more representative force/torque capability as well as a higher position control bandwidth. A possible choice for this high-frequency actuator may be a piezo stack, which is known to have high force capabilities and high position control bandwidths but low amplitudes. The choices for the high-frequency actuator, however, need to be thoroughly explored with a thoughtful and analytical approach to what we need the capabilities of the high-frequency actuator to be. An option that we could explore would be to design a high frequency actuator by picking a high frequency, high amplitude and low torque actuator and adding a custom designed cable driven gearhead to it, in case an appropriate option cannot be found for the high frequency actuator.

The next steps would naturally involve using the new one degree of freedom testbed to test the capability of the actuation approach in the context of haptics. In our work so far, we have only considered rendering inertia for simplicity; however, rendering a combination of springs,

masses, and dampers and performing tests like the impedance frequency response or stability analysis would provide insight into the working of our approach. The effect of saturation of the high-frequency actuator would also be interesting to observe. A better analytical understanding of our approach may also be part of the future work which is aided by the new testbed. We may test more complicated position controllers like observer based LQR control which may provide benefits and improve the performance of our actuator. We also want to explore using the series admittance actuator for force control which would make it more relevant for physical human robot interaction. This would be a natural choice of application as force control would also benefit from the increased position control bandwidth that our approach provides. Again, building a new one-degree-of-freedom actuator would allow us to show the true benefits and limitations of our series admittance actuation approach; it would allow us to perform more representative tests, gain a better understanding of our approach, and be an important contribution as well.

Another obvious avenue to explore would be multi degree of freedom implementations of this approach. There may be phenomena that are may be more apparent when implementing this actuation configuration for multi DOF systems.

In chapter 5, we do some preliminary experimental research into a series actuation configuration for Workspace expansion, however, more work needs to be done, both analytical and experimental. Analytical models will help understand exactly why the dynamic system behaves this way. Wide-band haptic actuation, integrating kinesthetic and vibrotactile actuation into one combined actuator might be a avenue to explore that could extend this approach.

A LAYER JAMMERS IN A SIMULATED ENVIRONMENT SOFT HAPTIC (S.E.S.H.) GLOVE

While the main dissertation focuses on series actuation for improving traditional haptic devices, this appendix explores an alternative approach to haptic feedback that shares the goal of enhancing force rendering capabilities. The haptics field needs wearable devices that can provide varied impedances and transition between high transparency and high stiffness. These devices are useful in VR/AR and telerobotics applications where compact size and body conformity matter. This appendix examines layer jamming technology from soft robotics as an approach for creating variable-stiffness haptic interfaces. Unlike the series actuation methods in the main text, which address limitations in rigid haptic devices, layer jamming uses controllable friction between stacked layers to achieve variable stiffness without complex mechanisms. This approach offers advantages including flexibility, low weight, simpler manufacturing, and better body conformity. This appendix describes the design and testing of layer jamming elements in a soft haptic glove. We analyze how design parameters affect jamming force and establish guidelines for predictable performance. This work shows how soft robotics principles can address haptic rendering challenges through different methods than those presented in the main dissertation.

A.1 Overview

The field of haptics is constantly seeking better wearable kinesthetic haptic devices. Devices that can render a wider range of impedances and transition from high transparency to high stiffnesses while also being compliant. Such kinesthetic haptic devices are desirable for VR/AR as well as teler-

obotic systems. We draw inspiration from the field of soft robotics and present a layer jamming based approach to wearable haptic devices. In this chapter, we explore vacuum-based layer jammers, characterize their jamming force versus key characteristics, and explore the design rules regulating their performance. We present a theoretical analysis, comparing the behavior of our layer jammers to results from classical beam theory, and we select one motif from which to build a demonstration device. We present a haptic glove consisting of layer jammers that provide kinesthetic haptic feedback. We demonstrate our proposed soft haptic glove through a Unity-based virtual environment, in which a user can grasp objects through our jamming glove which resists user motion.

A.2 Introduction

Wearable kinesthetic haptic devices have been used in various human-robot interaction applications. Many kinesthetic haptic devices are attached to a fixed point in the environment (i.e. grounded) [68] to apply forces to a user. Recently, wearable devices have emerged that are attached only to a user (ungrounded) [69]. Ungrounded devices, such as haptic gloves, provide sensory feedback either to individual fingers or to the hand as a whole (gripping/vibrating) but cannot provide ground force resistance (e.g., simulating pushing against a wall) as they are not mounted to a grounding surface. These devices have found use in teleoperation [70] and medical rehabilitation [71]. Using haptic devices for virtual reality [72] is especially promising.

Within these haptic devices, the method of actuation has proven crucial to performance and effectiveness. An early haptic device, SPIDAR-MF [73] used DC Servo Motors, which can have safety risks, complex design or form factor, and low transparency (the ability to be deflected with low force when not actuated so the device appears “transparent” to a user).

Other examples include magnetorheological fluid [74] and pneumatic pistons [75] which have controllable force but suffer from large system volume. Other approaches explore hydraulic artificial muscles [76] and dielectric elastomers [77] which offer creative approaches towards actuation, but drawbacks include electrical safety, high cost, and difficulty of fabrication. Another approach is using actively controlled brakes which can provide resistive loads in both grounded [78] and ungrounded devices [79, 80]. Typically, devices with passive actuators such as brakes have a high inertia and low transparency or need to use complex control methods to compensate for the non-linearities of the brake.

The emerging field of soft robotics presents potential options for actuation, braking, and sensing in wearable haptics. Soft robots can be built from intrinsically soft materials such as low-modulus elastomers [81] or from traditional materials in novel form factors to exhibit overall flexible behavior [82]. We utilize the former approach in this work (Fig. A.1).

This field gives us actuators that can provide resistive loads while also having a low reflected inertia. One compelling technology for haptics is jamming, in which a media of discrete components moves freely within an enclosed membrane, but "jams" in place when exposed to vacuum. Jamming media can be categorized into zero-, one-, and two-dimensional systems. Zero-dimensional jammers contain granular media (approximating zero dimensional points). When the enclosing membrane is pressed against an object, the grains freely displace, conforming to the shape of the object [83]. When vacuum is applied, the granular media is "jammed", locking the object in its grasp until vacuum is released. One-dimensional jammers contain a bundle of flexible but inextensible fibers aligned lengthwise. The enclosed bundle of fibers is able to bend freely, wrapping around objects [84]. Vacuum jamming locks the fibers in place, yielding a high-modulus rod of the desired shape. Two-dimensional jammers, as developed in our 2017 work [85] and in Narang's 2018 work [86], contain

Figure A.1: The Simulated Environment Soft Haptics (S.E.S.H.) glove prototype featuring five layer jammers mounted to the palm side of a work glove.

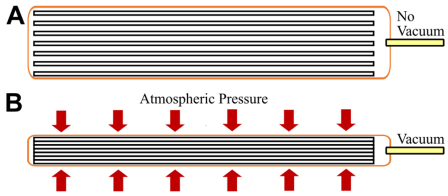

Figure A.2: Illustration of layer jamming: (A) Without vacuum applied, the layers can slide freely relative to one another; (B) With vacuum applied, the atmospheric pressure creates normal force between layers, causing frictional coupling.

flexible sheets. In these systems, stacked layers of 2D sheets such as paper or fabric (Fig. A.2A) are able to bend and slide relative to one another before they are jammed in place (Fig. A.2B) upon exposure to vacuum.

In all of these systems, a low-modulus system deforms to a desired

shape, then is jammed via exposure to vacuum, resulting in an increase in impedance. Jamming systems can be used in robotic grippers to cause force closure [83], in soft robots to vary modulus in actuators, and in wearable devices to simulate virtual environments [87]. There has been work with soft robotic gloves for virtual reality medical applications [88], and teleoperation [89]. Joint impedance with layer jamming has been investigated [87] but quantitative analysis of underlying variables governing performance has yet to be undertaken. We present a layer jammer, characterizing key variables and exploring the design rules governing their performance. We use this jammer in a demonstration of a Simulated Environment Soft Haptic (S.E.S.H.) glove. We believe that this work provides a foundation for robust predictive design to obtain desired performance in future VR/AR haptic devices.

There is a need in the wearable haptics community for a new method of force reflection, which allows the user to immerse themselves in a new reality without the use of complex, bulky, expensive brake systems.

We present a characterization of layer jammers and a design for a haptic feedback glove that can simulate environments as a demonstration of these jammers.

The key contributions of our work are as follows:

- Systematic analysis of design rules governing layer jamming for haptics, relating these rules to first principles found in beam theory.
- Characterization of the jammers for parameters: braking force, free space rendering transparency and effect of wear on braking force, and development of a system to measure these parameters.
- Demonstration of a jammer design and fabrication method using readily available, low-cost components yielding a range of jammers with predictable performance.

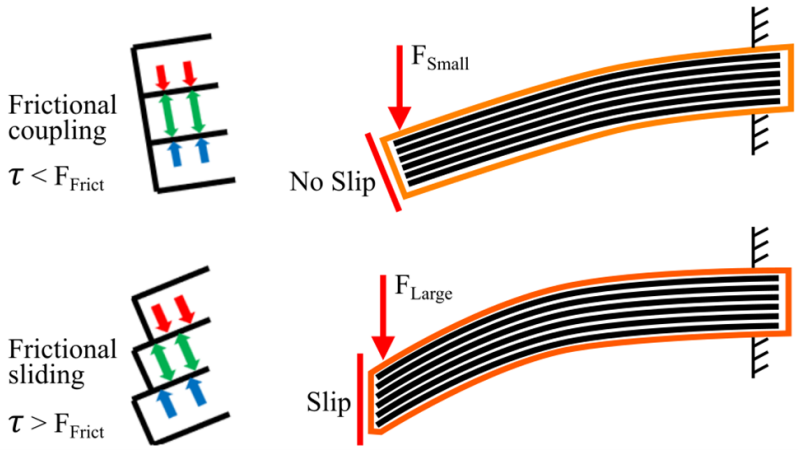

Figure A.3: Close-up of a single layer jammer showing the stacked sheets of paper enclosed in PVC membrane with vacuum tubing connection.

- Demonstration of a prototype haptic glove integrated with a virtual reality simulation.

A.3 Method

The SESH glove consists of a modified work-glove, instrumented with five jammers and one bend sensor. The system uses an Arduino microcontroller to communicate with a Unity-based virtual environment. Layer jammers are a lightweight and low-cost way to achieve a soft brake, well suited for force reflection in haptic devices (Fig. A.3).

The jammer presented in this work can be fabricated of simple materials in under ten minutes at a cost of less than 20 cents. Printer paper was selected as it provides a high ratio of jammed to unjammed slipping force. Materials with higher friction (sand paper) retain friction force even when no vacuum is applied, reducing transparency. 1 mil PVC is selected as it shows little resistance to force. Both materials are inexpensive and readily available.

Jammer Design

The following steps describe our fabrication method for our 40-sheet jammer, with sheets of 104 mm $\times$ 30 mm. Other configurations described in this work were fabricated using a similar procedure.

Assembly Procedure

1. Cut 40 sheets of 20 lb. printer paper (Boise Inc. Boise ID, USA) to 104 mm by 30 mm.

2. Cut two sheets of PVC thermoplastic (1 mil shrink-wrap bag) large enough to enclose the sheets in step 1 (~115 mm $\times$ 40 mm) and place the paper sheets between the sized PVC sheets.

3. With a film sealer (Yeler PFS-100, Runyii, China), seal the long edges and one short edge of the assembly from step b.

4. Instrument the remaining open edge with 3 mm OD tubing. Seal the edge with a silicone gasket of Ecoflex 00-30 (Smooth-On, Macungie PA. USA). Sandwich the assembly between two layers of acrylic and screw together with M2 screws.

Without external pressure applied to the jammer, there is little friction between the sheets, thus they move freely relative to one another (Fig. A.2A), allowing the jammer to bend with little resistance, similar to a 40-sheet magazine. When vacuum is applied to the jammer, the sheets are pressed against one another from outside atmospheric air pressure. The pressure creates a normal force between the sheets (Fig. A.2B), making the jammer appear stiff under external load.

During jamming, external load causes little deformation of the stiff jammer (Fig. A.4A) as the individual sheets resist slip due to frictional coupling ($F < F_{slip}$) where F is as shown in Fig. **??**, and F_{slip} is the force

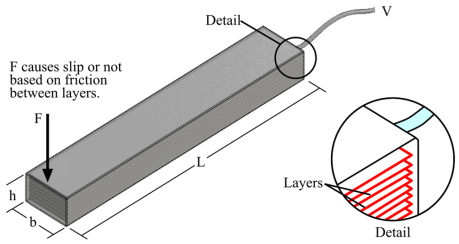

Figure A.4: Jammer mechanics: (A) With vacuum applied and external load below the slipping threshold, the jammer maintains rigidity; (B) When external load exceeds the slipping threshold, the layers slip relative to one another.

required to overcome friction, causing the pages to slip relative to one another. When the applied load is sufficiently large to overcome the frictional coupling ($F = F_{slip}$), the sheets inside the jammer will slip (Fig. A.4B) relative to one another.

Variables used in analysis of jammer mechanics: F is the applied force, L is the distance from the base, b is the width, and h is the thickness of the jammer. We call this transition the slipping point of a jammer. In this state, the layers slip to a new stiff state and will remain in that state until a new force causes frictional slip or until vacuum is released. Using classic Euler-Bernoulli beam theory from mechanics of materials, we explore the contributions that system parameters have on the slipping point, using variables as shown:

$$\sigma_{slip} = \frac{mc}{I} \tag{A.1}$$

Where σ_{slip} is the point at which slip occurs, and c is the distance from the neutral axis. For a rectangular cross section:

$$c = \frac{h}{2} \tag{A.2}$$

Moment at the base due to a force F is:

$$m = F \times L \tag{A.3}$$

And for a rectangular cross section, second moment of inertia is:

$$I = \frac{bh^3}{12} \tag{A.4}$$

Combining Eq. (1), Eq. (2), Eq. (3), and Eq. (4):

$$F_{slip} = \frac{\sigma_{slip} b h^2}{6L} \tag{A.5}$$

Where σ_{slip} is determined by the friction properties between layers, and vacuum applied.

Jammer Testing

To validate the correlation between our jammers and beam theory, we performed an experimental investigation using a testing assembly shown in Fig. A.5. This assembly contained a vertical translation stage, (item 1 in Fig. A.5), with a clamp to hold a jammer. This jammer (item 2 in Fig. A.5) was translated onto a scale (item 4 in Fig. A.5) which was used to measure F_{slip}.

Test 1

We evaluated jammers with sheet counts from 20 sheets to 50 sheets, each 104 mm by 30 mm, to evaluate the effect of sheet count (similar to h in eq. 5). We evaluated each jammer in its jammed state (vacuum applied) to determine F_{slip}. In order to evaluate transparency (the reflected inertia when no vacuum is applied) we evaluated each actuator in a free (no vacuum state). We evaluated quantity three of each jammer using the following procedure:

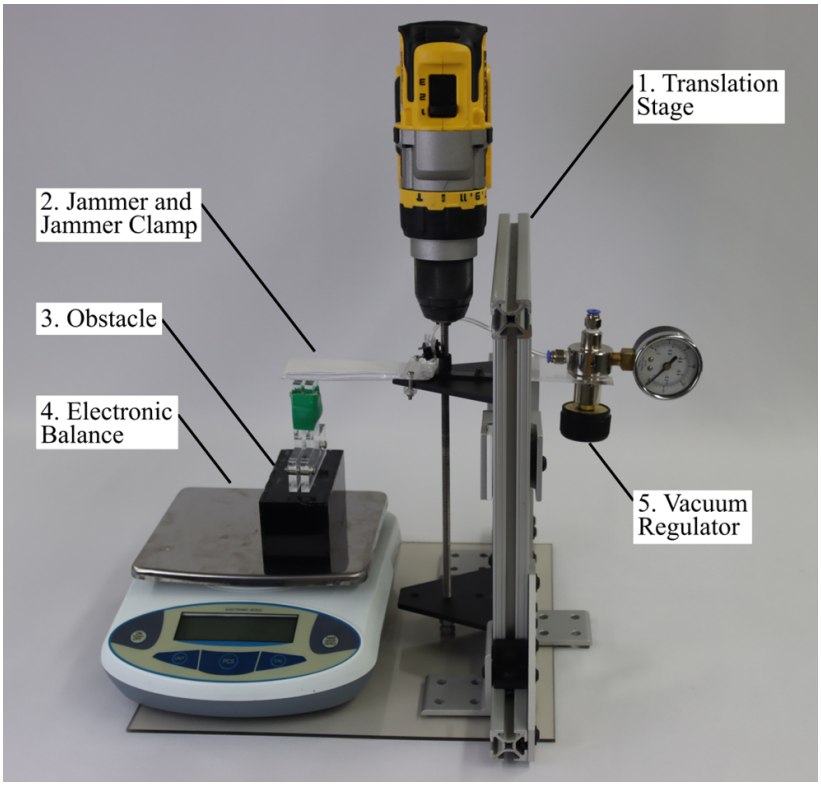

Figure A.5: Experimental setup for jammer testing: (1) Vertical translation stage, (2) Jammer in clamp, (3) Obstacle on scale, (4) Digital scale for measuring force.

Test Procedure

1. If the jammer is new, apply vacuum, apply force F until slip occurs. Release vacuum and repeat this procedure ten times as break-in cycles.

2. With vacuum applied, lower the jammer onto the obstacle until slip. Record this value (F_{slip}) from the scale.

3. Raise the jammer. Release vacuum. Re-apply vacuum.

4. Perform the lowering and raising procedure described above three times for each jammer in each configuration.

Test 2

We evaluated the effect of width (b in eq. 5) on slipping force of jammers. In this evaluation, we used jammers with 40 sheets, 104 mm by b mm, varying b from 20 mm to 45 mm. For each of these evaluations, we tested three jammers of each configuration and tested each three times using the procedure described above.

Test 3

We evaluated distance from the base of the jammer (L in Eq. 5) using jammers with 40 sheets of 154 mm by 30 mm. Rather than fabricate jammers of various lengths, we used the same configuration for each and varied the point of load application (L = 50 mm, 100 mm, and 150 mm). This method was selected as we believe that it is likely that jammers will have loads applied in regions other than at the distal tip. We evaluated three jammers in each point of application and tested each three times using the procedure described above.

Test 4

To evaluate the effect that vacuum level has on slip force, (anticipated to be proportional to σ_{slip} in eq. 5), we evaluated three jammers, with 40 sheets of 104 mm by 30 mm, varying vacuum from -80 kPa to -20 kPa (gauge). We tested each using the test procedure described above.

Test 5

To test repeatability, we tested a jammer using the procedure described above for twenty cycles to find the relationship between cycle count and

slip force. Jammer performance varied during the first eight cycles. Thus, we determined that ten "break in" cycles were required prior to use. This is the point at which a crease is formed in the individual sheets of the jammer, ensuring repeatable results.

Glove Design

We developed a simulated environment soft haptics (S.E.S.H.) glove to demonstrate layer jammers' capabilities in a variety of applications. This glove was to take advantage of relationships discovered to allow a user to feel a computer-generated environment. We defined our design guidelines as shown in Table A.1.

Table A.1: Design Rules

Design Rules For Jammers	**Description**
Gesture Recognition	Sensing the motion of fingers
Transparency	Friction and interior force should be less than the user's detection threshold on force magnitude.
Force Reflection	Apply resistant force on fingers sufficiently large to simulate stiff objects (4N)
Wearability	The method of mounting the glove to the user's hand

The SESH glove (Fig. A.1) consisted of five jammers (each with 40 sheets of 30 mm $\times$ 104 mm) mounted to custom attachment hardware and sewn to a glove. The mounting hardware in the palm of the glove consisted

of an acrylic plate which houses the jammer bases, allowing pivotal rotation for the thumb. This plate mounting style allows the jammers to act as cantilevers with jamming direction in the plane of actuation of each finger. A flex sensor (Adafruit, New York, NY. USA) is sewn to the dorsal surface of the glove's index finger to track finger flexion.

The flex sensor is connected to an Arduino Uno microcontroller, which is connected to custom software to interpret sensor data (Fig. A.6). The software is connected to a vacuum regulator which applies vacuum on demand to emulate resistance in gripping. The glove uses palm-mounted layer-jammers connected to the vacuum regulator to reflect resistant force to simulate objects.

To simulate an environment, the SESH glove is connected to a computer program which allows the user to see the simulated environment that they are feeling with the glove. To create this program, we used Unity 2024 game engine (Unity Technologies, San Francisco, CA. USA) to develop custom software which receives data from the integrated sensor on the glove and visualizes it to a hand model. As shown in Fig. A.7, the animation shows the user navigating the environment that the glove is reproducing (See supplementary video).

Glove Testing

For evaluation, the S.E.S.H. glove was instrumented with a force transducer (Force Sensitive Resistor, Interlink Electronics, Camarillo, CA. USA) at the distal end of the index finger, between the glove and the wearer's finger. This allowed us to measure the force between the distal tip of the index finger and the jammer. Vacuum was applied to the jammer, the wearer flexed the index finger, and force required for slip was measured. This procedure was conducted twelve times.

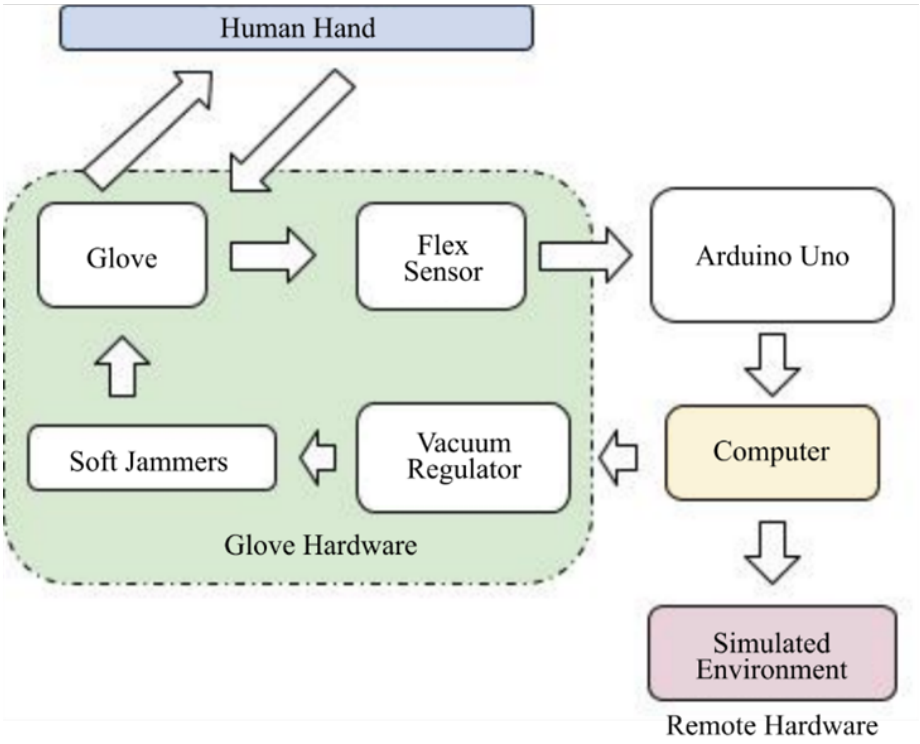

Figure A.6: System diagram of the SESH glove: Flex sensor data is processed by the Arduino, which controls the vacuum regulator based on Unity environment interactions.

A.4 Results

Analyzing Jammers

Using the processes described in Methods, results are presented (Fig. A.8) showing the effects of varying parameters of jammers. The trend line for sheet count vs slip force (Fig. A.8A) is second order. As F_{slip} is expected to increase with the square of thickness (eq. 5), correlating with beam theory. Unjammed slip force is also presented in Fig. A.8A and does not rise above 0.2 N for any configuration tested. This yields a transparency ratio (F_{slip} for jammed/unjammed) from 2× for ten sheets for 28.4× for

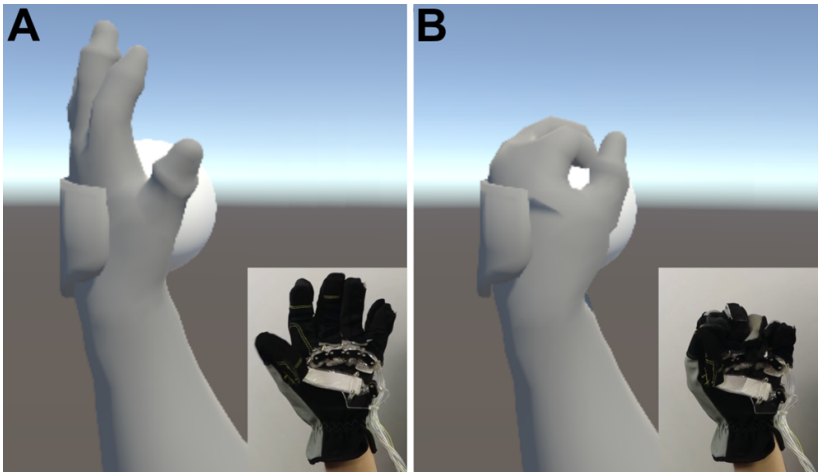

Figure A.7: Screenshot of the Unity virtual environment showing a user interacting with virtual objects using the SESH glove.

fifty sheets.

Initial cycle testing on new (never used) jammers had a higher slip force than those that had undergone numerous cycles. Our testing demonstrated that slip force decreased for eight cycles, then remained relatively constant (Fig. A.9). Thus, we conducted ten "break in" cycles prior to experimenting with any jammers. During break in, a physical crease has been formed in the papers in the layer jammer.

Analyzing Glove

The force sensing resistor test yielded slip force of 3.96 N $\pm$ 0.5 N. With 44 sheets at 104 mm $\times$ 30 mm, This is within 3% of the 3.86 N predicted by the second order trendline and is highlighted in Fig. A.8A with a red square and range bar.

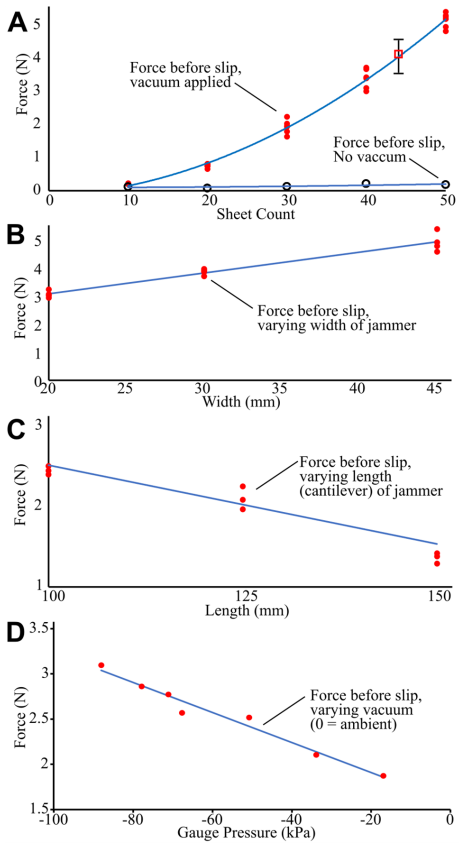

Figure A.8: Results of parameter testing: (A) Effect of sheet count on slip force showing quadratic relationship; (B) Effect of jammer width on slip force; (C) Effect of load application point on slip force; (D) Effect of vacuum level on slip force.

A.5 Discussion

We have presented a vacuum based layer-jammer as well as a layer jamming gripper for use in haptic devices. We characterized the jammers, analyzing the effect of design parameters (Sheet count, width, length, and vacuum gauge pressure) on overall slip force (max force that can be applied prior to jammer slipping). Using the resulting device, we presented a Simulated Environment Soft Haptic (S.E.S.H.) glove and used it

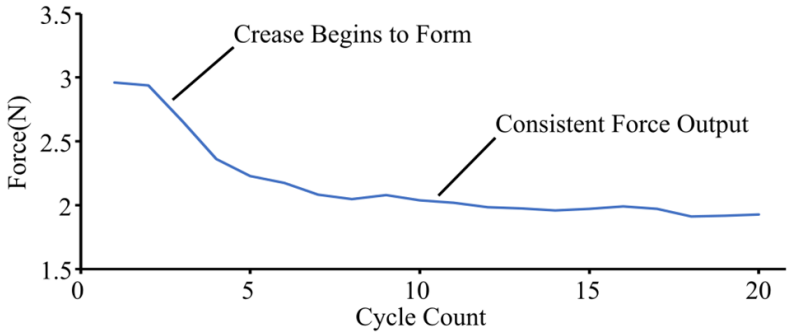

Figure A.9: Effect of repeated cycling on jammer slip force, showing initial decrease over the first eight cycles before stabilizing.

in a Unity 2024 based virtual reality environment, simulating grabbing a ball. The jammers provided four Newtons of blocking force in the finger-sized configurations tested. When vacuum was released, force dropped to near zero, for realistic transparency. Maximum slip force F_{slip} can be adjusted by varying the key parameters evaluated. This work enables future jammers to be designed with quantitative metrics known a-priori, varying parameters during the design stage to yield devices with desired performance characteristics. Future work will be needed to characterize other materials in jamming (using jamming layers of other materials such as fabric, polyimide or other plastics, or paper with different surface properties), and multi-dimensional actuation (for out-of-plane actuation). These jammers also have the potential to provide non discrete levels of stiffness by combining multiple jammers into one actuator and varying the pressure levels of vacuum. Further exploration of these jammers in this context will pave the way to make these jammers an attractive option for a soft haptic actuator. These jammers provide a low-cost, low-impedance actuator option for compliant and wearable haptic devices.

B EFFECTS OF SYNCHRONOUS MOVEMENT ON HUMAN TRUST IN ROBOTS

Robot-human trust is becoming an important concern as robots become integrated into human spaces. We tested a method grounded in psychological theory to increase human-robot trust—synchronous motion. Human participants completed a goal-oriented ball-moving task with a robotic arm to sound cues that were synchronous or asynchronous with the robot's pacing. Participants were instructed to follow sound cues without information about synchrony. We found that participants in the synchrony condition trusted the robot to complete a new task that was comparable to the task they completed, significantly more than the asynchrony condition. However, this effect did not extend to harder tasks. The participants in the synchrony condition also believed that the robot had more influence on the outcomes of the new task compared to the asynchrony condition. On average, participants' trust increased with the robotic arm after completing the task, regardless of condition. We report findings from a thematic analysis that demonstrate that participants in the synchrony condition found synchrony to be beneficial, while participants in the asynchrony condition found it cognitively taxing to be out-of-sync. Results from this work may be used to improve human-robot interactions in various contexts.

B.1 Introduction

Robots are becoming more common in industrial settings, restaurants, homes, educational institutions, and healthcare. However, because humans lack a complete understanding of how robots function, they may be unsure about the utility of robots in joint action tasks. As humans learn the behaviors of robots, they may develop greater trust in them and a greater understanding of how robots can collaborate with humans. Research in

Figure B.1: Experimental setup for the human-robot ball-moving task. The image shows a Kinova Mico 6-DOF robotic arm positioned between a stand with colored balls (left) and a shared collection box (right). During the experiment, participants stood opposite the robot and moved toy balls from their stand into the shared box while listening to timed sound cues. In the synchrony condition, participants and the robot moved balls at the same speed, while in the asynchrony condition, they moved at different speeds. This setup was designed to investigate how movement synchrony between humans and robots influences trust and risk-taking behavior in human-robot interaction.

computer science, psychology, and engineering has explored different strategies for improving trust in non-human agents, such as personification [90], increasing the predictability of behavior [91], and improving safety through computer vision [92]. These methods often require intensive developments to the robotic system or require a human-like robot with a face or body. We tested a new method based in psychological theory to increase human-robot trust that has not been well examined, and that may be more scalable, namely, motor synchrony.

Extant research shows that when people move in synchrony—moving in the same rhythm and in the same way—it increases trust [93], liking [94], connection [95], and predictability [96] of the other person's move-

ment. The causal impacts of synchrony have been well documented, from children swinging together on a swing [97], to people tapping their fingers in unison [98]. The benefits of synchronous movement on trust have not been well established in human-robot collaborations. We examined the effects of synchronous versus asynchronous movement in human-robot interaction and made the following predictions. 1. Synchronous movement with a robotic arm will increase trust in the robot and robotics in general. 2. Increased trust will transfer to a new task that involves risk.

B.2 Related Works

Human-Human Synchrony

Humans have engaged in activities that involve synchronous movement across time, culture, and environment. Synchrony occurs naturally when people dance, engage in religious ritual, walk or swing in unison, and march in protest. The ubiquity of this practice has led many researchers to examine the beneficial effects of synchrony, especially on processes of social connection [99]. In 1912, Émile Durkheim originally proposed that shared group activities, like synchrony, create a "collective effervescence" that leads individuals to feel united in their emotions [100]. Indeed, Wiltermuth and Heath [101] found that both motor and vocal synchrony increased cooperation, cohesion, and trust within small groups. In several dyad and small group studies, researchers found that synchronized bodily movement increased measures of prosocial attitudes and behaviors [102, 103], feelings of affiliation [98], social bonding [104], cooperation [105], increased social cohesion [94], feelings of closeness and liking [95], and trust [93, 106] toward group members. Notably, human interpersonal synchrony has been shown to increase trust in a virtual interaction, and with a virtual agent [93, 106]. We predict that similar effects occur in human-robot interactions.

Human-Robot Synchrony

Several past studies have examined human robot synchronous action [107]; however, none have adequately examined the causal effects of synchronous versus asynchronous action on trust. Hasnain and colleagues programmed a Nao robot to either move its arm at a fixed oscillatory frequency without adapting to a human participant or to adapt such that it moved in synchrony with the participant's arm [108]. They found that when entrainment was uni-directional (meaning that the participant could fall into synchrony with the robot, but the robot moved at a fixed pace), participants adapted their movement to be synchronous with the robot

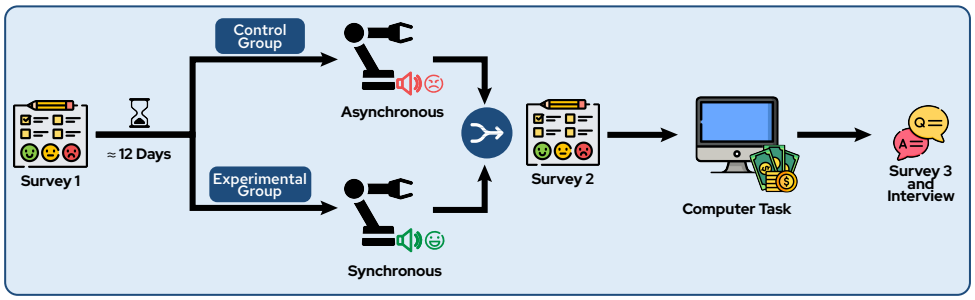

Figure B.2: Experimental design flowchart for the human-robot synchrony study. The diagram illustrates the experimental procedure beginning with an initial survey, followed by an approximately 12-day interval before lab participation. Participants were randomly assigned to either the asynchrony condition (performing asynchronous movements with the robot, indicated by a negative emotion icon) or the synchrony condition (performing synchronous movements with the robot, indicated by a positive emotion icon). After the interaction task, participants completed a second survey, followed by a computer-based risk assessment task involving monetary decisions, and concluded with a final survey and interview. This design allowed for measurement of how movement synchrony affects trust development in human-robot interactions.

[108]. In bi-directional interactions, they found that participants came into synchrony with the robot more easily, and the robot and human's movement met halfway between their original frequencies [108]. Overall, their work and other studies found that participants have a natural inclination to synchronize even with no instruction to do so [109].

In another study, Michalowski and colleagues programmed a small robot with a cute appearance to move rhythmically to external sound in a public space [110]. Their qualitative results revealed that more children danced with the robot when it was moving synchronously to music than when it was not [110]. Their quantitative results were not significant but trended in the same direction [110]. Further, in several studies, Marin and colleagues demonstrated that human participants coordinated their movements to robots uni-directionally, particularly the more human-like and less industrial they were [111]. Mörtl and colleagues programmed a robotic arm to move synchronously with human participants and found qualitative evidence of a pleasant experience, although they did not test the causal effects of synchrony on human perceptions [112].

In studies testing the causal effects of synchrony, participants viewed videos of interactions between a human actor and a service robot that either moved synchronously in the direction of the actor's movements, moved in the opposite direction, or did not move at all [113]. They found that participants felt closer to the robot and liked it more in the synchrony condition, followed by the opposite movement condition, and finally the no movement condition (Lehmann, 2015). In another causal study, a robot adapted its movement to be coordinated with a human participant or remained at a constant speed; participants preferred to work with the robot that coordinated its movements to the human [114].

These results reveal that in various ways, human synchronous interactions with robots are similar to synchrony in human-human interactions (i.e., automatic and pleasant). However, there is a gap in understanding

the causal impact of synchrony on trust in human-robot interactions. We tested whether synchronous action in human-robot pairs resulted in positive outcomes as has been found in human-human pairs. Specifically, we examined whether synchronous action compared to asynchronous action increased trust in a robotic arm. We deliberately chose asynchrony as a valid control for two reasons. 1) We were interested in industrial or teamwork settings where a robot (or cobot) and human would move together to complete a goal-oriented task which eliminates a "no movement" condition. 2) In settings where robots are completing complex tasks, they often do not move at one constant speed and a variable speed may be perceived as more natural, which eliminates a "constant speed" condition.

B.3 Method

Participants

We recruited 32 students from a large university via flyers and emails to participate in a human-robot interaction study. The final sample included 29 participants with 41% identifying as White, 24% as East Asian, 10% as South Asian, 7% as Latiné, 7% multiracial, and the remaining 11% as Black, Arab American, and Puerto Rican. 62% identified as women, 34.5% as men, and 3.5% as non-binary. 72% of the sample were undergraduate students, and 28% were graduate students. The mean age was 21 (18 - 35, SD = 4.32).

Study Design

Quantitative

We conducted a mixed design experiment with two conditions (synchronous and asynchronous). Trust was measured at two time points—before and after a ball-moving task—allowing for between-group and within-

group comparisons. Statistical analyses included repeated measures ANOVA to examine within-subject effects and independent samples t-tests to compare between-group differences.

Qualitative

Interview and free-response survey data were used to conduct a thematic analysis using the standard six-step approach and applying inductive coding [115, 116].

Experimental Procedure

Participants were screened to confirm no extensive experience with robots. After prescreening, they received Survey 1 via email and completed it from home via Qualtrics (see GitHub repository). The survey assessed their past experience with robots (adapted from Sanders and colleagues [117]), propensity to take risks ($\alpha = .92$), (General Risk Propensity Scale; [118]), self-confidence ($\alpha = .82$), [119]), trust in robotic technology ($\alpha = .86$) (adapted from the Propensity to trust Technology Scale [120]), baseline trust in robotic arms ($\alpha = .80$) (adapted from the Generalized Attitudes Towards Robots Scale or GAToRS [121]) and demographics. After an average of 12 days (min = 7, max = 32), participants came into the lab to complete the experiment. A time delay was used to prevent participants from learning the aims of the study. Participants were randomly assigned to the synchrony and asynchrony conditions.

Participants in both conditions were instructed to stand across from a Kinova robotic arm, which was situated on a large desk (see Fig. 1). Toy balls were placed on a stand to the right of the robot and a second stand was placed to the left of the participant. A long, shared box was placed on the other side of the robotic arm and the participant. The robot used was a 6 - DOF Kinova Mico co-bot arm and was programmed using ROS

to pick and place toy balls from a platform on the left of the arm to the shared box.

Participants took part in a brief training protocol in which they were instructed to listen to sound cues which directed them to move nine toy balls one by one, from the stand into the shared box. Their movements were designed to match the programmed movements of the robotic arm in form; however, participants were not told this. Participants were told that they would hear their own sound cues which would direct their timing, and the robotic arm would receive it's own sound cues. Participants in the asynchrony condition moved each of the nine toy balls at a different speed than the robotic arm. Participants in the synchrony condition moved toy balls at the same speed as the robotic arm. One sound file was created for each group. The sound file used for the asynchrony condition was the same as the sound file used for the synchrony condition except that the sound cues for each ball were made to be in a different order to make the movements with the robotic arm out-of-sync (see GitHub repository for video demonstration). Participants were recorded during the task. All other components of the study were the same for both groups.

After completing the ball-moving task with the robotic arm, participants completed Survey 2, which measured the following constructs: adapted version of the Trust of Automated Systems Test or TOAST ($\alpha = .78$), [122], adapted version of the Multi-Dimensional Measure of Trust or MDMT ($\alpha = .90$), [123], adapted version of The Robotic Social Attribute Scale or ROSAS ($\alpha = .64$), [124], the GAToRs ($\alpha = .84$), [121], and other measures (see GitHub repository for full survey).

Participants then engaged in a computer task that measured their willingness to risk money based on their trust in the robotic arm's success on a task. Participants were told that the robotic arm previously completed additional ball-moving tasks that were categorized as easy, medium, or hard. Easy tasks resembled the ball-moving task they performed with the

robot. Medium tasks were categorized as containing two physical obstacles in the robotic arm's path of movement and hard, three obstacles (see Demo on GitHub). Participants were presented with six choices ranging from 0% trust to 100% and 30 trials (10 of each difficulty). Participants were given feedback on trial 9 that the robotic arm succeeded at a hard task and feedback at trial 18 that the robotic arm failed at a hard task. Feedback was given to assess trust recovery after failure. Following the computer task, participants answered questions about how synchronous they believed they were with the robotic arm in the ball-moving task ($\alpha = .95$), how much they enjoyed the task ($\alpha = .89$), and various questions about who or what they believed influenced or controlled the success of the robot. Synchrony questions were asked to confirm that our intervention was successful for participants in the synchrony, but not the asynchrony condition. Because synchrony tends to be more enjoyable than asynchrony [98], participants were asked how much they enjoyed the ball-moving task.

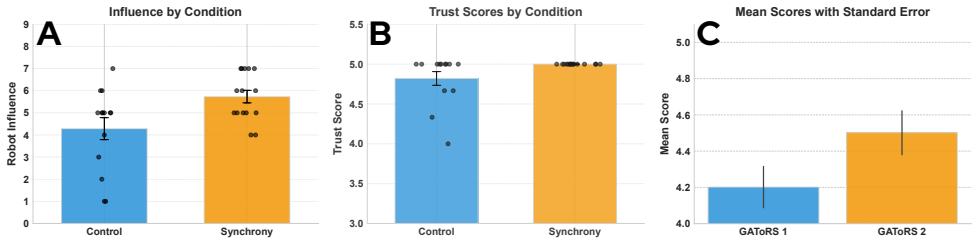

Figure B.3: A: The relationship between condition and the amount of influence participants believed the robotic arm had on the outcome of the computer task. B: The relationship between condition and the amount of trust participants had in the robotic arm to succeed during the computer task. C: Mean scores on GAToRS (trust scale) before and after completing the ball-moving task. Error bars correspond to $\pm$ 1 standard error of the point estimate for the slope of the regression line. Data points are jittered along the x-axis to enhance visibility.

Qualitative Procedure

Finally, participants were interviewed about their impressions of the robot, the robot's speed, the experiment overall, working with the robot, how they made decisions in the computer task, and what they thought the study was about (see GitHub repository). The thematic analysis was informed by a background in social psychology and research in human synchronous interactions. Data familiarization included conducting interviews with participants, transcribing their verbal comments, and two weeks of reading through and annotating transcripts. Subsequently, codes and candidate themes were generated and visualized in spreadsheets. We computed the frequency of keywords and phrases to help visualize patterns of difference across the synchrony and asynchrony conditions. Themes were reviewed and an abbreviated report of the findings is provided. None of the participants believed the experiment tested synchrony, despite how frequently participants discussed being in or out of synchrony with the robotic arm. Code and survey materials are available at `https://github.com/MarjiMi/robot_synchrony`

B.4 Results

Quantitative Analyses

Assumption and Manipulation Checks

Before testing our predictions, we confirmed that there was no significant difference in trust between the synchrony and asynchrony conditions in Survey 1 (before the experiment began). Likewise, groups did not differ significantly in confidence in themselves, risk taking tendency, and enjoyment of the experimental task. Further, we tested the effectiveness of our experimental manipulation and found that participants in the synchrony condition (m = 4.24, sd = 1.29) believed they were moving in synchrony

with the robot significantly more than participants in the asynchrony condition (m = 2.4, sd = 1.33).

Generalized Trust

When examining generalized trust (GAToRS), participants in the synchrony condition did not indicate higher trust in the robot compared to those in the asynchrony condition, following the ball-moving task. Further, conditions did not differ significantly in their increased trust in the robot following the ball-moving task. When examining all participants, we found a significant increase in generalized trust after the ball-moving task, regardless of condition (b = .30, SE = .14, t(28) = 2.185, p = .037) (see Figure 3C).

Behavioral Trust

In the computer task, participants in the synchrony condition rated easy obstacles with significantly more trust (m = 5, sd = 0) than the asynchrony condition (m = 4.82, sd = .32) (before feedback about success and failure was given) (b = .18, SE = .08, t(26) = 2.162, p = .04) (see Figure 3A). However, we note that the data show significant ceiling effects, which may have reduced the strength of the effect. All other computer task trust model tests were not significant, although they were in the predicted direction. That is, participants in the synchrony condition trusted the robot more than those in the asynchrony condition in the computer task, but not significantly.

Robot Influence

Participants in the synchrony condition believed that the robotic arm had significantly more influence on the outcome of the computer task compared to the asynchrony condition (b = 1.45, SE = .56, t(26) = 2.575, p

= .015) (see Figure 3B). Further, participants in the synchrony condition believed that the outcome of the computer task was due to the robotic arm more than the asynchrony condition; however, the effect did not reach significance (b = 1.07, SE = .59, t(26) = 1.796, p = .084).

Qualitative Analyses

The thematic analysis resulted in three themes related to synchronous or asynchronous, goal-oriented, human interactions with a robotic arm (see Table 1).

Synchrony creates a positive experience

participants in the synchrony condition described the interaction positively when in sync with the robot. They described synchronous interactions with the robot as “comfortable” and “natural” and connected the idea of teamwork to a synchronous interaction much more frequently than in the asynchrony condition. However, some participants noticed that the synchronous interaction was uni-directional which made one participant feel less connected to the robot stating: "I didn’t feel connected to the arm...I don’t think it was following me but only what it was pre-programed to do" - P42 (synchrony).

Asynchrony is cognitively taxing

participants in the asynchrony condition sometimes described the robot’s pacing as distracting or as creating uncertainty about their own movements. Because participants were instructed to follow a specific pace signaled to them audibly, they may have experienced heightened cognitive load when paying attention to the robotic arm’s different pacing, and their own pacing. One participant noted, "It was sometimes faster and slower than me, which was not cool" - P15 (asynchrony).

Non-human capabilities matter

participants in both conditions referred to the robotic arm's capabilities both by comparing it to a human's capabilities or by noting that they needed to adjust their movement to accommodate the robot's inability to match their pace (uni-directional synchrony). Despite there being no instruction or need to synchronize to complete the task, participants in the synchrony condition described a desire to adjust to the robotic arm's pace to enhance synchrony.

Other themes not directly related to synchrony included an overall fascination about the robot with many calling the experience cool and interesting. A few participants also described the interaction as weird, or that it created a sense of weariness about whether the task would end successfully. However, many noted that this feeling decreased and they felt better over time as the robot successfully completed the task. This result maps onto quantitative findings which revealed that on average, all participants' trust in the robot increased after the task.

B.5 Discussion

We tested the effects of human-robot synchronous action compared to asynchronous action in a ball-moving task. Participants also rated their trust level in the robot's ability to complete a task similar to the one they just performed (easy), as well as medium and hard tasks with financial rewards at risk. Participants in the synchrony condition trusted the robotic arm to complete comparable tasks more than the asynchrony condition. However, this effect did not transfer to medium or hard tasks. This suggests that synchrony narrowly increases trust in a robotic teammate for the specific task at hand rather than new tasks that may be more challenging. Future research may examine if synchrony improves trust in robots to complete different tasks of similar difficulty.

We found that participants trusted the robotic arm more after completing the ball-moving task compared to before (regardless of condition). This suggests that mere exposure to successful teamwork tasks with a robotic arm improves trust, while synchrony may narrowly enhance that effect.

Participants in the synchrony condition also believed the robotic arm had more influence over the outcome of the easy, medium, and hard tasks compared to the asynchrony condition. We outline three potential reasons for this effect that should be explored in future research. 1) It is possible that synchrony makes the robotic arm appear more influential or in control because the experience feels more seamless. That is, the participant can rely on the actions of the robot to complete the task and avoid the increased cognitive load of asynchronous movement. 2) Synchrony leads to increased connection with one's synchronous partner. This may create the perception that the robot has more agency, as a human would, over the outcome. 3) Finally, participants in the synchrony condition may have attended to the robotic arm more closely, leading to an increased awareness of its movements and the belief that the robot influenced the outcome of the tasks.

Our thematic analysis resulted in the theme that synchrony creates a positive experience, while asynchrony is cognitively taxing. Synchrony appeared to signal teamwork and comfort while asynchrony felt like a distraction or led participant's to be unsure about their own actions. The teamwork task generally led participants to consider the robot's human and non-human features. They considered the unique capabilities that the robot has, while noticing its limitations. In the synchrony condition, some participants felt the need to adjust their movements to be more precisely in sync with the robot despite no directive to do so. Although participants were directed to follow the pacing of sound cues only, they felt it was more useful to match the robot's pace versus only following the sound cues.

Synchrony appeared to signal teamwork which participants may have felt was beneficial for completing the task.

Limitations & Future Work

This research has limitations. The robotic arm did not actively synchronize with the human participant, leading some participants to adapt to the robot's capabilities. The robot's movements were slower than natural human movement and as a result, some participants stated that they felt robotic or stiff. There may be benefits to embodying robot movement for connection and trust with a robot; however, it will be important for future research to examine bi-directional synchronous human-robot movement at a natural human speed. This work may disentangle the confound of humans adapting to the robot's movements during synchronous interaction. Further, participants rated their trust in the robot to complete new actions via a virtual computer task. Future research may engage participants in a real follow-up task where participants can witness errors. Live errors may intensify changes in participant's trust in the robot.

Design Implications

Our findings can be applied to cobot-worker interactions in factories, wheelchair mounted robotic arms, service robots, and educational robot tutors. Simple and quick synchrony interventions may improve human-robot introductions to potentially support trust and comfortability.

Themes	Sub-categories	Quotes
Synchrony creates a positive experience	Synchrony feels comfortable	"Same speed and timing as me so I felt comfortable with it." - P60 (synchrony)
	Synchrony signals teamwork	"if I was moving too fast I tried to slow down to work as a team rather than us moving as two separate people or things." - P39 (synchrony)
Asynchrony is cognitively taxing	Asynchrony is a distraction	"The robotic arm feels like a distraction for me while I'm moving the balls." - P37 (asynchrony)
	Asynchrony creates uncertainty	"The speed of the robot made me self conscious like why are you doing it faster or slower." - P55 (asynchrony)
Non-human capabilities matter	Robot vs human capabilities	"My arm started to hurt a bit and I was thinking about how robots don't have to worry about that." - P45 (asynchrony) "Definitely on the slower side and would have been nice if it moved more to a human pace." - P46 (synchrony)
	Adjusting to the robot's ability	"I felt like I was going too fast at some points so I started slowing down to stay at the robots pace. I felt, working as a team, I had more control over my pace and so I made more effort to stay at the robots pace than it should have to make to speed up to match me." - P39 (synchrony)

Table B.1: Themes and example quotes generated from a thematic analysis. Participants were interviewed about their experiences working with the robotic arm.

BIBLIOGRAPHY

[1] Inrak Choi, Eyal Ofek, hrvoje Benko, Mike Sinclair, and Christian Holz. Claw: A multifunctional handheld haptic controller for grasping, touching, and triggering in virtual reality. In *CHI 2018*. ACM, April 2018. ISBN 978-1-4503-5620-6.

[2] Patrick Dills, Nick Colonnese, Priyanshu Agarwal, and Michael Zinn. A hybrid active-passive actuation and control approach for kinesthetic handheld haptics. In *2020 IEEE Haptics Symposium (HAPTICS)*, pages 690–697, 2020. doi: 10.1109/HAPTICS45997.2020.ras.HAP20.12.af578b0a.

[3] Hwan Kim and Kyung Hoon Hyun. Hapmini: 2d haptic feedback generation using single actuator device. *PLOS ONE*, 2023. doi: 10.1371/journal.pone.0285002.

[4] Pornthep Preechayasomboon and Eric Rombokas. Haplets: Finger-worn wireless and low-encumbrance vibrotactile haptic feedback for virtual and augmented reality. *Frontiers in Virtual Reality*, 2: 738613, 2021.

[5] Kazuki Abe Kenjiro Tadakuma Tetsuya Aizawa, Haruhiko Iizima and Riichiro Tadakuma. Study on portable haptic guide device with omnidirectional driving gear. *Advanced Robotics*, 35(5):320–336, 2021. doi: 10.1080/01691864.2021.1888796. URL `https://doi.org/10.1080/01691864.2021.1888796`.

[6] Meng-Kuan Cho, Sheng-Yuan Huang, and Chao-Chieh Lan. Design of a novel haptic device for bilateral teleoperations requiring accurate force interaction. In *2019 IEEE/ASME International Conference on Advanced Intelligent Mechatronics (AIM)*, pages 74–79, 2019. doi: 10.1109/AIM.2019.8868591.

[7] Adam J. Spiers and Aaron M. Dollar. Design and evaluation of shape-changing haptic interfaces for pedestrian navigation assistance. *IEEE Transactions on Haptics*, 10(1):17–28, 2017. doi: 10.1109/TOH.2016.2582481.

[8] Adam Spiers, Eric Young, and Katherine J. Kuchenbecker. The s-ban: Insights into the perception of shape-changing haptic interfaces via virtual pedestrian navigation. *ACM Trans. Comput.-Hum. Interact.*, 30(1), mar 2023. ISSN 1073-0516. doi: 10.1145/3555046. URL `https://doi.org/10.1145/3555046`.

[9] G.A. Pratt and M.M. Williamson. Series elastic actuators. In *Proceedings 1995 IEEE/RSJ International Conference on Intelligent Robots and Systems. Human Robot Interaction and Cooperative Robots*, volume 1, pages 399–406 vol.1, 1995. doi: 10.1109/IROS.1995.525827.

[10] C. Parthiban, P. Dills, I. Fufuengsin, N. Colonnese, P. Agarwal, and M. Zinn. A balanced hybrid active-passive actuation approach for high-performance haptics. In *2019 IEEE World Haptics Conference (WHC)*, pages 283–288. doi: 10.1109/WHC.2019.8816146.

[11] Ruihang Chu, Yuru Zhang, Hongdong Zhang, Weiliang Xu, Jee-Hwan Ryu, and Dangxiao Wang. Co-actuation: A method for achieving high stiffness and low inertia for haptic devices. *IEEE Transactions on Haptics*, 13(2):312–324, 2020. ISSN 1939-1412. doi: 10.1109/toh.2019.2944611. URL `https://dx.doi.org/10.1109/toh.2019.2944611`.

[12] Nikos C. Karavas, Nikos G. Tsagarakis, and Darwin G. Caldwell. Design, modeling and control of a series elastic actuator for an assistive knee exoskeleton. In *2012 4th IEEE RAS EMBS International Conference on Biomedical Robotics and Biomechatronics (BioRob)*, pages 1813–1819, 2012. doi: 10.1109/BioRob.2012.6290757.

[13] Daniel Ragonesi, Sunil Agrawal, Whitney Sample, and Tariq Rahman. Series elastic actuator control of a powered exoskeleton. In *2011 Annual International Conference of the IEEE Engineering in Medicine and Biology Society*, pages 3515–3518, 2011. doi: 10.1109/IEMBS.2011.6090583.

[14] Chan Lee and Sehoon Oh. Development, analysis, and control of series elastic actuator-driven robot leg. *Frontiers in Neurorobotics*, 13, 2019. ISSN 1662-5218. doi: 10.3389/fnbot.2019.00017. URL `https://www.frontiersin.org/articles/10.3389/fnbot.2019.00017`.

[15] A. L. Barrow and W. S. Harwin. High bandwidth, large workspace haptic interaction: Flying phantoms. In *2008 Symposium on Haptic Interfaces for Virtual Environment and Teleoperator Systems*, pages 295–302, 2008. doi: 10.1109/HAPTICS.2008.4479961.

[16] Alastair Barrow and William Harwin. Design and analysis of a haptic device design for large and fast movements. *Machines*, 4 (1), 2016. ISSN 2075-1702. doi: 10.3390/machines4010008. URL `https://www.mdpi.com/2075-1702/4/1/8`.

[17] Michael Zinn, Oussama Khatib, Bernard Roth, and J. Kenneth Salisbury. Large workspace haptic devices - a new actuation approach. In *2008 Symposium on Haptic Interfaces for Virtual Environment and Teleoperator Systems*, pages 185–192, 2008. doi: 10.1109/HAPTICS.2008.4479941.

[18] Ingo Kossyk, Jonas Dörr, and Konstantin Kondak. Design and evaluation of a wearable haptic interface for large workspaces. In *2010 IEEE/RSJ International Conference on Intelligent Robots and Systems*, pages 4674–4679. IEEE, 2010.

[19] Laroussi Bouguila, Masahiro Ishii, and Makoto Sato. A large workspace haptic device for human-scale virtual environments. In *First International Workshop on Haptic Human-computer Interaction*, pages 86–91, 2000.

[20] F. Sanfilippo, P. B.T. Weustink, and K. Y. Pettersen. A coupling library for the force dimension haptic devices and the 20-sim modelling and simulation environment. In *IECON 2015 - 41st Annual Conference of the IEEE Industrial Electronics Society*, pages 000168–000173, 2015. doi: 10.1109/IECON.2015.7392094.

[21] Rahaf Rahal, Giulia Matarese, Marco Gabiccini, Alessio Artoni, Domenico Prattichizzo, Paolo Robuffo Giordano, and Claudio Pacchierotti. Caring about the human operator: Haptic shared control for enhanced user comfort in robotic telemanipulation. *IEEE Transactions on Haptics*, 13(1):197–203, 2020. doi: 10.1109/TOH.2020.2969662.

[22] Inrak Choi, Heather Culbertson, Mark R. Miller, Alex Olwal, and Sean Follmer. Grabity: A wearable haptic interface for simulating weight and grasping in virtual reality. In *Proceedings of the 30th Annual ACM Symposium on User Interface Software and Technology*, UIST '17, page 119–130, New York, NY, USA, 2017. Association for Computing Machinery. ISBN 9781450349819. doi: 10.1145/3126594.3126599. URL https://doi.org/10.1145/3126594.3126599.

[23] Inrak Choi, Elliot W. Hawkes, David L. Christensen, Christopher J. Ploch, and Sean Follmer. Wolverine: A wearable haptic interface for grasping in virtual reality. In *2016 IEEE/RSJ International Conference on Intelligent Robots and Systems (IROS)*, pages 986–993, 2016. doi: 10.1109/IROS.2016.7759169.

[24] Emanuele Lindo Secco and Andualem Maereg Tadesse. A wearable exoskeleton for hand kinesthetic feedback in virtual reality. In *Wireless Mobile Communication and Healthcare: 8th EAI International Conference, MobiHealth 2019, Dublin, Ireland, November 14-15, 2019, Proceedings 8*, pages 186–200. Springer, 2020.

[25] Minglu Zhu, Zhongda Sun, Zixuan Zhang, Qiongfeng Shi, Tianyiyi He, Huicong Liu, Tao Chen, and Chengkuo Lee. Haptic-feedback smart glove as a creative human-machine interface (hmi) for virtual/augmented reality applications. *Science Advances*, 6(19): eaaz8693, 2020. doi: 10.1126/sciadv.aaz8693. URL https://www.science.org/doi/abs/10.1126/sciadv.aaz8693.

[26] Diana Cotoros, Cornel Druga, and Anca Stanciu. Statistical analysis of forces developed by fingers. In *2017 E-Health and Bioengineering Conference (EHB)*, pages 21–24, 2017. doi: 10.1109/EHB.2017.7995351.

[27] J.E. Colgate and J.M. Brown. Factors affecting the z-width of a haptic display. In *Proceedings of the 1994 IEEE International Conference on Robotics and Automation*, pages 3205–3210 vol.4, 1994. doi: 10.1109/ROBOT.1994.351077.

[28] Daniel Cleveland and Keyvan Hashtrudi-Zaad. The effect of discretization techniques on uncoupled stability of haptic simulation systems. In *2018 IEEE Haptics Symposium (HAPTICS)*, pages 66–71, 2018. doi: 10.1109/HAPTICS.2018.8357154.

[29] Dale A Lawrence, Lucy Y Pao, Mark A Salada, and Anne M Dougherty. Quantitative experimental analysis of transparency and stability in haptic interfaces. In *Proc. Fifth Annual Symposium on Haptic Interfaces for Virtual Environment and Teleoperator Systems*, pages 441–449, 1996.

[30] Yu Zhang, Dangxiao Wang, Ziqi Wang, Yueping Wang, Li Wen, and Yuru Zhang. A two-fingered force feedback glove using soft actuators. In *2018 IEEE Haptics Symposium (HAPTICS)*, pages 186–191, 2018. doi: 10.1109/HAPTICS.2018.8357174.

[31] K.J. Kuchenbecker, J. Fiene, and G. Niemeyer. Improving contact realism through event-based haptic feedback. *IEEE Transactions on Visualization and Computer Graphics*, 12(2):219–230, 2006. doi: 10.1109/TVCG.2006.32.

[32] Wendy A Rogers, Arthur D Fisk, Anne Collins McLaughlin, and Richard Pak. Touch a screen or turn a knob: Choosing the best device for the job. *Human factors*, 47(2):271–288, 2005.

[33] MIL-STD-1472D. MIL-STD-1472D:Human engineering design criteria for military systems, equipment, and facilities. Standard, Department of Defense, Washington, DC, 1989.

[34] Sandra G. Hart and Lowell E. Staveland. Development of nasa-tlx (task load index): Results of empirical and theoretical research. In Peter A. Hancock and Najmedin Meshkati, editors, *Human Mental Workload*, volume 52 of *Advances in Psychology*, pages 139–183. North-Holland, 1988. doi: https://doi.org/10.1016/S0166-4115(08)62386-9. URL `https://www.sciencedirect.com/science/article/pii/S0166411508623869`.

[35] James R Lewis. The system usability scale: past, present, and future. *International Journal of Human–Computer Interaction*, 34(7):577–590, 2018.

[36] I. Scott MacKenzie. *Fitts' Law*, chapter 17, pages 347–370. John Wiley & Sons, Ltd, 2018. ISBN 9781118976005. doi: https://doi.org/10.1002/9781118976005.ch17. URL https://onlinelibrary.wiley.com/doi/abs/10.1002/9781118976005.ch17.

[37] C Häger-Ross and M H Schieber. Quantifying the independence of human finger movements: comparisons of digits, hands, and movement frequencies. *J. Neurosci.*, 20(22):8542–8550, November 2000.

[38] Michael Tannous, Marco Miraglia, Francesco Inglese, Luca Giorgini, Filippo Ricciardi, Riccardo Pelliccia, Mario Milazzo, and Cesare Stefanini. Haptic-based touch detection for collaborative robots in welding applications. *Robotics and Computer-Integrated Manufacturing*, 64:101952, 2020. ISSN 0736-5845. doi: https://doi.org/10.1016/j.rcim.2020.101952. URL https://www.sciencedirect.com/science/article/pii/S0736584519302200.

[39] Michael Hagenow, Emmanuel Senft, Robert Radwin, Michael Gleicher, Bilge Mutlu, and Michael Zinn. Informing real-time corrections in corrective shared autonomy through expert demonstrations. 07 2021.

[40] Chembian Parthiban and Michael Zinn. Performance and stability limitations of admittance-based haptic interfaces. In *2018 IEEE Haptics Symposium (HAPTICS)*, pages 58–65. IEEE, 2018.

[41] Patrick Dills, Kaitlyn Gabardi, and Michael Zinn. Stability and rendering limitations of high-performance admittance based haptic interfaces. IEEE. doi: 10.1109/haptics52432.2022.9765573. URL https://dx.doi.org/10.1109/haptics52432.2022.9765573.

[42] M. Zinn, O. Khatib, B. Roth, and J. K. Salisbury. Large workspace haptic devices - a new actuation approach. In *2008 Symposium on Haptic Interfaces for Virtual Environment and Teleoperator Systems*, pages 185–192. ISBN 2324-7355. doi: 10.1109/HAPTICS.2008.4479941.

[43] Arvid QL Keemink, Herman van der Kooij, and Arno HA Stienen. Admittance control for physical human–robot interaction. *The International Journal of Robotics Research*, 37(11):1421–1444, 2018. doi: 10.1177/0278364918768950. URL https://journals.sagepub.com/doi/abs/10.1177/0278364918768950.

[44] R. V. Baratta, M. Solomonow, and B. H. Zhou. Frequency domain-based models of skeletal muscle. *Journal of Electromyography and Kinesiology*, 8(2):79–91, 1998. ISSN 1050-6411. doi: https://doi.org/10.1016/S1050-6411(97)00024-2. URL https://www.sciencedirect.com/science/article/pii/S1050641197000242.

[45] P. D. Neilson. Speed of response or bandwidth of voluntary system controlling elbow position in intact man. *Medical and biological engineering*, 10(4):450–459, 1972. ISSN 1741-0444. doi: 10.1007/BF02474193. URL https://doi.org/10.1007/BF02474193.

[46] G. I. Zahalak and S. J. Heyman. A quantitative evaluation of the frequency-response characteristics of active human skeletal muscle in vivo. *Journal of Biomechanical Engineering*, 101(1):28–37, 1979. ISSN 0148-0731. doi: 10.1115/1.3426220. URL https://doi.org/10.1115/1.3426220.

[47] Jeremy D. Wong, Tyler Cluff, and Arthur D. Kuo. The energetic basis for smooth human arm movements. *eLife*, 10:e68013, 2021. ISSN 2050-084X. doi: 10.7554/eLife.68013. URL https://doi.org/10.7554/eLife.68013.

[48] S. J. Schroeck, W. C. Messner, and R. J. McNab. On compensator design for linear time-invariant dual-input single-output systems. *IEEE/ASME Transactions on Mechatronics*, 6(1):50–57, 2001. ISSN 1941-014X. doi: 10.1109/3516.914391.

[49] John E. Speich, Liang Shao, and Michael Goldfarb. Modeling the human hand as it interacts with a telemanipulation system. *Mechatronics*, 15(9):1127–1142, 2005. ISSN 0957-4158. doi: https://doi.org/10.1016/j.mechatronics.2005.06.001. URL https://www.sciencedirect.com/science/article/pii/S095741580500070X.

[50] T. Flash and F. Mussa-Ivaldi. Human arm stiffness characteristics during the maintenance of posture. *Experimental Brain Research*, 82 (2), 1990. ISSN 0014-4819. doi: 10.1007/bf00231251. URL https://dx.doi.org/10.1007/bf00231251.

[51] Andreas; Resch Arnold; Matthiesen Sven; Gwosch Thomas Schröder, Tassilo; Lindenmann. Influence of coupling forces on the mechanical impedance of the hand-arm system during rotational vibration excitation around the xh-axis. *International journal of industrial ergonomics. 2023 Vol. 95 p. 103427-*, 2023. ISSN 0169-8141. doi: 10.1016/j.ergon.2023.103427.

[52] Jean-Jacques E. Slotine and Weiping Li. Applied nonlinear control.

[53] J. S. Mehling, J. E. Colgate, and M. A. Peshkin. Increasing the impedance range of a haptic display by adding electrical damping. IEEE. doi: 10.1109/whc.2005.79. URL https://dx.doi.org/10.1109/whc.2005.79.

[54] Nick Colonnese, Alexa F. Siu, Caroline M. Abbott, and Allison M. Okamura. Rendered and characterized closed-loop accuracy of impedance-type haptic displays. *IEEE Transactions on Haptics*, 8 (4):434–446, 2015. ISSN 1939-1412. doi: 10.1109/toh.2015.2457438. URL https://dx.doi.org/10.1109/toh.2015.2457438.

[55] Ben Levy, Megh Vipul Doshi, Keng-yu Lin, and Michael Wehner. Layer jammers in a simulated environment soft haptic (s.e.s.h.) glove. In *2024 IEEE Haptics Symposium (HAPTICS)*, pages 360–365, 2024. doi: 10.1109/HAPTICS59260.2024.10520848.

[56] Alejandro Jarillo Silva, Omar A. Domínguez Ramirez, Vicente Parra Vega, and Jesus P. Ordaz Oliver. Phantom omni haptic device: Kinematic and manipulability. In *2009 Electronics, Robotics and Automotive Mechanics Conference (CERMA)*, pages 193–198, 2009. doi: 10.1109/CERMA.2009.55.

[57] Stephen P Buerger and Neville Hogan. Novel actuation methods for high force haptics. *Advances in Haptics*, pages 1–29, 2010.

[58] *Performance Assessment of a 3D Cable-Driven Haptic Device*, volume Volume 12: Mechanics of Solids, Structures and Fluids of *ASME International Mechanical Engineering Congress and Exposition*, 10 2008. doi: 10.1115/IMECE2008-67261. URL https://doi.org/10.1115/IMECE2008-67261.

[59] Cong Bang Pham, Song Huat Yeo, Guilin Yang, and I-Ming Chen. Workspace analysis of fully restrained cable-driven manipulators. *Robotics and Autonomous Systems*, 57(9):901–912, 2009. ISSN 0921-8890. doi: https://doi.org/10.1016/j.robot.2009.06.004. URL https://www.sciencedirect.com/science/article/pii/S0921889009000827.

[60] Robert L. Williams Ii. Cable-suspended haptic interface. *International Journal of Virtual Reality*, 3(3):13–20, 1998. ISSN 1081-1451. doi: 10.20870/ijvr.1998.3.3.2627.

[61] Michael Fennel, Antonio Zea, Johannes Mangler, Arne Roennau, and Uwe D. Hanebeck. Haptic rendering of arbitrary serial manipulators for robot programming. *IEEE Control Systems Letters*, 6: 716–721, 2022. ISSN 2475-1456. doi: 10.1109/lcsys.2021.3086059.

[62] Yi Li, Sanyuan Zhang, and Xiuzi Ye. Data analysis on virtual stiffness in 6dofs haptic rendering system. *Neurocomputing*, 196:107–112, 2016. ISSN 0925-2312. doi: https://doi.org/10.1016/j.neucom.2015.11.098. URL https://www.sciencedirect.com/science/article/pii/S0925231216003143.

[63] Megh Vipul Doshi, Patrick Dills, and Michael Zinn. Improving kinesthetic haptic rendering through a frequency partitioned series admittance actuation approach. In *2024 IEEE Haptics Symposium (HAPTICS)*, pages 286–291, 2024. doi: 10.1109/HAPTICS59260.2024.10520871.

[64] Van Q, Piet Lammertse, Erwin Frederiksen, and Birgit Ruiter. The hapticmaster, a new high-performance haptic interface. 07 2002.

[65] R.J. Adams and B. Hannaford. Stable haptic interaction with virtual environments. *IEEE Transactions on Robotics and Automation*, 15(3): 465–474, 1999. doi: 10.1109/70.768179.

[66] Thomas H Massie, J Kenneth Salisbury, et al. The phantom haptic interface: A device for probing virtual objects. In *Proceedings of the ASME winter annual meeting, symposium on haptic interfaces for virtual environment and teleoperator systems*, volume 55, pages 295–300. Chicago, IL, 1994.

[67] Marc Ueberle, Nico Mock, and Martin Buss. Vishard10, a novel hyper-redundant haptic interface. In *12th International Symposium on Haptic Interfaces for Virtual Environment and Teleoperator Systems, 2004. HAPTICS'04. Proceedings.*, pages 58–65. IEEE, 2004.

[68] Y. Ueda, I. Yamano, and T. Maeno. Development of a grounded haptic device and a 5-fingered robot hand for dexterous teleoperation. In *2004 International Conference*, 2004.

[69] I. Choi, E. Ofek, H. Benko, M. Sinclair, and C. Holz. Claw: A multifunctional handheld haptic controller for grasping, touching, and triggering in virtual reality. In *Proceedings of the 2018 CHI Conference on Human Factors in Computing Systems*, pages 1–13, 2018. doi: 10.1145/3173574.3174228.

[70] S. Park, Y. Jung, and J. Bae. A tele-operation interface with a motion capture system and a haptic glove. In *2016 13th International Conference on Ubiquitous Robots and Ambient Intelligence (URAI)*, pages 544–549, 2016. doi: 10.1109/URAI.2016.7625774.

[71] M. Hoda, B. Hafidh, and A. El Saddik. Haptic glove for finger rehabilitation. In *2015 IEEE International Conference on Multimedia Expo Workshops (ICMEW)*, pages 1–6, 2015. doi: 10.1109/ICMEW.2015.7169803.

[72] I. Choi, H. Culbertson, M. R. Miller, A. Olwal, and S. Follmer. Grabity: A wearable haptic interface for simulating weight and grasping in virtual reality. In *Proceedings of the 30th Annual ACM Symposium on User Interface Software and Technology*, pages 119–130, 2017. doi: 10.1145/3126594.3126599.

[73] L. Liu, S. Miyake, K. Akahane, and M. Sato. Development of string-based multi-finger haptic interface spidar-mf. In *2013 23rd International Conference on Artificial Reality and Telexistence (ICAT)*, pages 67–71, 2013. doi: 10.1109/ICAT.2013.6728908.

[74] J. Blake and H. B. Gurocak. Haptic glove with mr brakes for virtual reality. *IEEE/ASME Transactions on Mechatronics*, 14(5):606–615, 2009. doi: 10.1109/TMECH.2008.2010934.

[75] M. Bouzit, G. Burdea, G. Popescu, and R. Boian. The rutgers master ii-new design force-feedback glove. *IEEE/ASME Transactions on Mechatronics*, 7(2):256–263, 2002. doi: 10.1109/TMECH.2002.1011262.

[76] D. Ryu et al. Micro hydraulic system using slim artificial muscles for a wearable haptic glove. In *2008 IEEE/RSJ International Conference on Intelligent Robots and Systems*, pages 3028–3033, 2008. doi: 10.1109/IROS.2008.4651159.

[77] R. Zhang, A. Kunz, P. Lochmatter, and G. Kovacs. Dielectric elastomer spring roll actuators for a portable force feedback device. In *2006 14th Symposium on Haptic Interfaces for Virtual Environment and Teleoperator Systems*, pages 347–353, 2006. doi: 10.1109/HAPTIC.2006.1627137.

[78] C. Parthiban, P. Dills, I. Fufuengsin, N. Colonnese, P. Agarwal, and M. Zinn. A balanced hybrid active-passive actuation approach for high-performance haptics. In *2019 IEEE World Haptics Conference (WHC)*, pages 283–288, 2019. doi: 10.1109/WHC.2019.8816146.

[79] M. Sinclair, E. Ofek, M. Gonzalez-Franco, and C. Holz. Capstancrunch: A haptic vr controller with user-supplied force feedback. In *Proceedings of the 32nd Annual ACM Symposium on User Interface Software and Technology*, pages 815–829, 2019. doi: 10.1145/3332165.3347891.

[80] P. Dills, N. Colonnese, P. Agarwal, and M. Zinn. A hybrid active-passive actuation and control approach for kinesthetic handheld haptics. In *2020 IEEE Haptics Symposium (HAPTICS)*, pages 690–697, 2020. doi: 10.1109/HAPTICS45997.2020.ras.HAP20.12.af578b0a.

[81] C. Laschi and M. Cianchetti. Soft robotics: new perspectives for robot bodyware and control. *Frontiers in Bioengineering and Biotechnology*, 2:3, 2014.

[82] J. A. Rogers, T. Someya, and Y. Huang. Materials and mechanics for stretchable electronics. *Science*, 327(5973):1603–1607, 2010. doi: 10.1126/science.1182383.

[83] J. R. Amend, E. Brown, N. Rodenberg, H. M. Jaeger, and H. Lipson. A positive pressure universal gripper based on the jamming of granular material. *IEEE Transactions on Robotics*, 28(2):341–350, 2012. doi: 10.1109/TRO.2011.2171093.

[84] M. Brancadoro, M. Manti, S. Tognarelli, and M. Cianchetti. Preliminary experimental study on variable stiffness structures based on fiber jamming for soft robots. In *2018 IEEE International Conference on Soft Robotics* (*RoboSoft*), pages 258–263, 2018. doi: 10.1109/ROBOSOFT.2018.8404929.

[85] K.-Y. Lin and S. K. Gupta. Soft fingers with controllable compliance to enable realization of low cost grippers. In *Biomimetic and Biohybrid Systems*, pages 544–550, 2017. doi: 10.1007/978-3-319-63537-8_48.

[86] Y. S. Narang, A. Degirmenci, J. J. Vlassak, and R. D. Howe. Transforming the dynamic response of robotic structures and systems through laminar jamming. *IEEE Robotics and Automation Letters*, 3 (2):688–695, 2018. doi: 10.1109/LRA.2017.2779802.

[87] Y. Zhang, D. Wang, Z. Wang, Y. Zhang, and J. Xiao. Passive force-feedback gloves with joint-based variable impedance using layer jamming. *IEEE Transactions on Haptics*, 12(3):269–280, 2019. doi: 10.1109/TOH.2019.2908636.

[88] W. V. I. Awantha, A. T. Wanasinghe, A. G. P. Kavindya, A. L. Kulasekera, and D. S. Chathuranga. A novel soft glove for hand tremor suppression: Evaluation of layer jamming actuator placement. In *2020 3rd IEEE International Conference on Soft Robotics* (*RoboSoft*), pages 440–445, 2020. doi: 10.1109/RoboSoft48309.2020.9115994.

[89] I. Zubrycki and G. Granosik. Novel haptic glove-based interface using jamming principle. In *2015 10th International Workshop on Robot Motion and Control* (*RoMoCo*), pages 46–51, 2015. doi: 10.1109/RoMoCo.2015.7219712.

[90] Yunus Terzioglu, Bilge Mutlu, and Erol Sahin. Designing social cues for collaborative robots: The role of gaze and breathing in human-robot collaboration. In *ACM/IEEE International Conference on Human-Robot Interaction*, pages 343–357. IEEE Computer Society, 3 2020. ISBN 9781450367462. doi: 10.1145/3319502.3374829.

[91] Sylvain Daronnat, Leif Azzopardi, Martin Halvey, and Mateusz Dubiel. Impact of agent reliability and predictability on trust in real time human-agent collaboration. In *Proceedings of the 8th International Conference on Human-Agent Interaction*, pages 131–139. ACM, 11 2020. ISBN 9781450380546. doi: 10.1145/3406499.3415063.

[92] Nicole Robinson, Brendan Tidd, Dylan Campbell, Dana Kulić, and Peter Corke. Robotic vision for human-robot interaction and collaboration: A survey and systematic review. *ACM Transactions on Human-Robot Interaction*, 12:1–66, 3 2023. ISSN 2573-9522. doi: 10.1145/3570731.

[93] Jacques Launay, Roger T. Dean, and Freya Bailes. Synchronization can influence trust following virtual interaction. *Experimental Psychology*, 60:53–63, 10 2013. ISSN 1618-3169. doi: 10.1027/1618-3169/a000173.

[94] Anja S. Göritz and Miriam Rennung. Interpersonal synchrony increases social cohesion, reduces work-related stress and prevents sickdays: a longitudinal field experiment. *Gruppe. Interaktion. Organisation. Zeitschrift für Angewandte Organisationspsychologie (GIO)*, 50:83–94, 3 2019. ISSN 2366-6145. doi: 10.1007/s11612-019-00450-8.

[95] Liam Cross, Martine Turgeon, and Gray Atherton. How moving together binds us together: The social consequences of interpersonal entrainment and group processes. *Open Psychology*, 1:273–302, 7 2019. doi: 10.1515/psych-2018-0018.

[96] Inbal Ravreby, Yoel Shilat, and Yaara Yeshurun. Liking as a balance between synchronization, complexity and novelty. *Scientific Reports*, 12:3181, 2 2022. ISSN 2045-2322. doi: 10.1038/s41598-022-06610-z.

[97] Tal-Chen Rabinowitch, Rechele Brooks, and Andrew N. Meltzoff. Children in sync: exploring how interpersonal synchrony experience induces cooperation between child peers. *Scientific Reports*, 14: 28130, 11 2024. ISSN 2045-2322. doi: 10.1038/s41598-024-78810-8.

[98] Michael J Hove and Jane L Risen. It's all in the timing: interpersonal synchrony increases affiliation. Technical report, 2009.

[99] Reneeta Mogan, Ronald Fischer, and Joseph A. Bulbulia. To be in synchrony or not? a meta-analysis of synchrony's effects on behavior, perception, cognition and affect. *Journal of Experimental Social Psychology*, 72:13–20, 9 2017. ISSN 00221031. doi: 10.1016/j.jesp.2017.03.009.

[100] Émile Durkheim. Les formes élémentaires de la vie religieuse, 1912.

[101] Scott S Wiltermuth and Chip Heath. Synchrony and cooperation. Technical report, 2009.

[102] Paul Reddish, Eddie M. W. Tong, Jonathan Jong, Jonathan A. Lanman, and Harvey Whitehouse. Collective synchrony increases prosociality towards non-performers and outgroup members. *British Journal of Social Psychology*, 55:722–738, 12 2016. ISSN 01446665. doi: 10.1111/bjso.12165. URL `https://bpspsychub-onlinelibrary-wiley-com.ezproxy.library.wisc.edu/doi/pdfdirect/10.1111/bjso.12165`.

[103] Miriam Rennung and Anja S. Göritz. Prosocial consequences of interpersonal synchrony. *Zeitschrift für Psychologie*, 224:168–189, 7 2016. ISSN 2190-8370. doi: 10.1027/2151-2604/a000252.

[104] Ellen M. Howard, Danielle Ropar, Roger Newport, and Bahar Tunçgenç. Social context facilitates visuomotor synchrony and bonding in children and adults. *Scientific Reports*, 11, 12 2021. ISSN 20452322. doi: 10.1038/s41598-021-02372-2.

[105] Arla Good, Becky Choma, and Frank A. Russo. Movement synchrony influences intergroup relations in a minimal groups paradigm. *Basic and Applied Social Psychology*, 39:231–238, 7 2017. ISSN 01973533. doi: 10.1080/01973533.2017.1337015.

[106] Ron Tamborini, Eric Novotny, Sujay Prabhu, Matthias Hofer, Clare Grall, Brian Klebig, Lindsay S. Hahn, Janine Slaker, Rabindra A. Ratan, and Gary Bente. The effect of behavioral synchrony with black or white virtual agents on outgroup trust. *Computers in Human Behavior*, 83:176–183, 6 2018. ISSN 07475632. doi: 10.1016/j.chb.2018.01.037.

[107] Darja Stoeva, Andreas Kriegler, and Margrit Gelautz. Body movement mirroring and synchrony in human–robot interaction. *ACM Transactions on Human-Robot Interaction*, 13:1–26, 12 2024. ISSN 2573-9522. doi: 10.1145/3682074.

[108] Syed Khursheed Hasnain, Ghiles Mostafaoui, Robin Salesse, Ludovic Marin, and Philippe Gaussier. Intuitive human robot interaction based on unintentional synchrony: A psycho-experimental study. In *2013 IEEE Third Joint International Conference on Development and Learning and Epigenetic Robotics (ICDL)*, pages 1–7. IEEE, 8 2013. ISBN 978-1-4799-1036-6. doi: 10.1109/DevLrn.2013.6652569.

[109] Eva Ansermin, Ghiles Mostafaoui, Xavier Sargentini, and Philippe Gaussier. Unintentional entrainment effect in a context of human robot interaction: An experimental study. In *2017 26th IEEE International Symposium on Robot and Human Interactive Communication (RO-MAN)*, pages 1108–1114. IEEE, 8 2017. ISBN 978-1-5386-3518-6. doi: 10.1109/ROMAN.2017.8172442.

[110] Marek P. Michalowski, Selma Sabanovic, and Hideki Kozima. A dancing robot for rhythmic social interaction. In *Proceedings of the ACM/IEEE international conference on Human-robot interaction*, pages 89–96. ACM, 3 2007. ISBN 9781595936172. doi: 10.1145/1228716.1228729.

[111] Ludovic Marin, Johann Issartel, and Thierry Chaminade. Interpersonal motor coordination. *Interaction Studies. Social Behaviour and Communication in Biological and Artificial Systems*, 10:479–504, 12 2009. ISSN 1572-0373. doi: 10.1075/is.10.3.09mar.

[112] Alexander Mörtl, Tamara Lorenz, and Sandra Hirche. Rhythm patterns interaction - synchronization behavior for human-robot joint action. *PLoS ONE*, 9:e95195, 4 2014. ISSN 1932-6203. doi: 10.1371/journal.pone.0095195.

[113] Hagen Lehmann, Joan Saez-Pons, Dag Sverre Syrdal, and Kerstin Dautenhahn. In good company? perception of movement synchrony of a non-anthropomorphic robot. *PLoS ONE*, 10, 5 2015. ISSN 19326203. doi: 10.1371/journal.pone.0127747.

[114] Qiming Shen, Kerstin Dautenhahn, Joe Saunders, and Hatice Kose. Can real-time, adaptive human–robot motor coordination improve humans' overall perception of a robot? *IEEE Transactions on Autonomous Mental Development*, 7:52–64, 3 2015. ISSN 1943-0604. doi: 10.1109/TAMD.2015.2398451.

[115] Virginia Braun and Victoria Clarke. Using thematic analysis in psychology. *Qualitative Research in Psychology*, 3:77–101, 1 2006. ISSN 1478-0887. doi: 10.1191/1478088706qp063oa.

[116] Muhammad Naeem, Wilson Ozuem, Kerry Howell, and Silvia Ranfagni. A step-by-step process of thematic analysis to develop a conceptual model in qualitative research. *International Journal of Qualitative Methods*, 22, 10 2023. ISSN 1609-4069. doi: 10.1177/16094069231205789.

[117] Tracy L. Sanders, Keith MacArthur, William Volante, Gabriella Hancock, Thomas MacGillivray, William Shugars, and P. A. Hancock. Trust and prior experience in human-robot interaction. *Proceedings of the Human Factors and Ergonomics Society Annual Meeting*, 61: 1809–1813, 9 2017. ISSN 1071-1813. doi: 10.1177/1541931213601934.

[118] Don C Zhang, Scott Highhouse, and Christopher D Nye. Development and validation of the general risk propensity scale (grips). *Journal of Behavioral Decision Making*, 32(2):152–167, 2019.

[119] Robert Hogan and Joyce Hogan. Hogan personality inventory. *Journal of Applied Psychology*, 1995.

[120] Sarah A. Jessup, Tamera R. Schneider, Gene M. Alarcon, Tyler J. Ryan, and August Capiola. *The Measurement of the Propensity to Trust Automation*, pages 476–489. 2019. doi: 10.1007/978-3-030-21565-1_32.

[121] Mika Koverola, Anton Kunnari, Jukka Sundvall, and Michael Laakasuo. General attitudes towards robots scale (gators): A new instrument for social surveys. *International Journal of Social Robotics*, 14:1559–1581, 9 2022. ISSN 1875-4791. doi: 10.1007/s12369-022-00880-3.

[122] Heather M. Wojton, Daniel Porter, Stephanie T. Lane, Chad Bieber, and Poornima Madhavan. Initial validation of the trust of automated systems test (toast). *Journal of Social Psychology*, 160:735–750, 11 2020. ISSN 19401183. doi: 10.1080/00224545.2020.1749020.

[123] Bertram F. Malle and Daniel Ullman. *A multidimensional conception and measure of human-robot trust*, pages 3–25. Elsevier, 1 2020. ISBN 9780128194720. doi: 10.1016/B978-0-12-819472-0.00001-0.

[124] Colleen M. Carpinella, Alisa B. Wyman, Michael A. Perez, and Steven J. Stroessner. The robotic social attributes scale (rosas): Development and validation. In *ACM/IEEE International Conference on Human-Robot Interaction*, volume Part F127194, pages 254–262. IEEE Computer Society, 3 2017. ISBN 9781450343367. doi: 10.1145/2909824.3020208.